

DIRECT COAL LIQUEFACTION: DISTINCTION BETWEEN REACTANTS  
AND CATALYSTS

ENE0 C. MORONI

U.S. department of Energy, FE-231 GTN, Washington, D.C. 20545

INTRODUCTION

An extensive research and development program on disposable catalysts and slurry catalysis was supported by the Fossil Energy Office of the U.S. Department of Energy (DOE) during the period 1978-82. Actually, prior to 1978, a project of similar nature was carried out for several years, at a low priority effort, at the U.S. Department of Interior, Bureau of Mines laboratories which is now known as the Pittsburgh Energy Technology Center (PETC).

Although numerous slurry-phase catalysts were tested in this program, two metals, iron and molybdenum, in their sulfided form, were singled out as the most promising candidates for scale-up processing.

In 1982, Gray and Neuworth (1) and in 1983, Davidson (2) have made comprehensive reviews on the role of iron sulfides on coal liquefaction, and, up to the present, there has been a continuing level of activity in this area. Iron and molybdenum sulfides catalysts were amply covered in a very recent comprehensive and critical review on catalysis in direct coal by Derbyshire (3). This excellent review provides a current state of knowledge of all form of catalysis which are potentially of interest from a practical standpoint, in addition to give valuable new directions for research in this area.

Garg and Givens (4) have shown evidences of synergism for an Iron-Molybdenum catalyst in which mixed catalyst has a definite advantage over each individual metal preforming. Similarly Gatsis (5) uncovered a distinct synergism occurring for an Iron-Vanadium catalyst which permits the partial replacement of the expensive Vanadium with the low cost Iron, with no loss of the catalytic activity level.

The aforementioned references report that iron sulfides catalysts exhibit consistently lower hydrogenation activity than either the molybdenum or the vanadium sulfides. Various explanations were attributed to the low catalytic activity of the iron sulfides, such as the very low surface area and the variable catalytically active iron sulfides forms found in pyrites, the precursors present in the mineral matter of most coals.

This paper, presently in the form of a communication to be complemented by the oral presentation and to be expanded for publication in Energy and Fuels, intends to provide evidences that the active forms of iron sulfides have a different function than the other metal sulfides, the function of being reactants and catalysts.

An additional objective of this paper, in conjunction with a series of papers presented by this author in recent years (6), is to stimulate the research community, dedicated to coal liquefaction fundamentals, to undertake a more systematic research approach to discriminate the critical reactions from the numerous ones occurring particularly the lower temperature range, which, in turn, profoundly affect the subsequent reactions occurring at the higher temperatures.

#### INITIAL STAGES OF COAL LIQUEFACTION

This author (7) has stressed the importance of reactions involving heteroatom-containing compounds in coal dissolution and subsequent coal liquid upgrading. of the three major heteroatoms present in coal, the most abundant is the oxygen, and, particularly when it is in the form of carboxylic and phenolic species, it seems to dominate the reactions occurring in the initial stages of liquefaction. Except for the low-rank coals, in which the carboxylics are converted at the temperature range of 250-300°C, with the observed loss of CO<sub>2</sub>, the phenolic chemistry appears to dominate the reactions occurring in the 280-350°C temperature range, for coals of all ranks, except, perhaps, for the low-oxygen german's hard coal. In particular, the phenols are the major contributors for the regressive reactions, causing the high viscosity of coal liquids and increasing the difficulty of upgrading and refining, and, as discover in recent work, the promoters for catalyst deactivation. Lemberston et al.(8) tested a sulfided nickel-molybdenum on alumina catalyst for the hydrogenation/hydrocracking of a mixture of phenanthrene, carbazole and 1-naphtol, and discovered that the catalyst maintain its activity in the presence of the phenanthrene-carbazole mixture, but it is strongly deactivated when 1-naphtol is added to that mixture. This experimental evidence of catalyst deactivation promoted by the phenols confirms the intuitive thoughts emerged some ten years ago

from the experimental data provided by Suntech (9) by which the removal of the phenols from a SRC II distillate solvent caused a seven-fold increase in the kinetics of nitrogen removal by catalytic hydrogenation. At a later date, Garg et al. (10) used a defunctionalized solvent in which most of the phenols and nitrogen compounds were removed from a SRC I process solvent, and obtained high conversion and oil yield with only 0.2-0.5 weight percent addition of pyrite to the coal/solvent slurry. When the untreated solvent was used for comparison, addition of 3-5 percent pyrite was required to obtain the same conversion and oil yield.

The obvious thought, derived from this data, was that a large portion of the active iron sulfide reacted with the oxygen moieties with the loss of catalytic activity, and, only the excess pyrite functioned as the actual catalyst. To prove this point, the work of Montano (11) indicated a strong affinity of an active iron sulfide surface towards oxygen in which the carbon-oxygen bonds are broken even from very stable aromatic ethers to generate aromatic hydrocarbon and catalytically inactive forms of iron sulfate or oxide.

The removal of oxygen moieties from coals, in the initial and subsequent stages of liquefaction, by the reaction with inexpensive iron sulfides, whose precursors happened to have the good fortune of being the most abundant components of the mineral matter in coal, ought to be considered highly desirable from the economic and technological point of view.

#### CONCLUSIVE REMARKS

Derbyshire (3), in his review on catalysis for coal liquefaction, questioned the modest progress obtain in catalytic liquefaction, particularly when research in this field has been conducted for half a century. Absence of a realistic model coal structure, and, of a clear understanding of the reaction chemistry and, the cyclic nature of interest in research of coal liquefaction were the main reasons for the impediment of progress in catalysis, according to Derbyshire.

The data and thoughts presented in this communication seem to complement Derbyshire's assessment, in that the scarce progress in catalytic liquefaction is due to the fact that catalyst activity is more dependent on the feed composition in contact with the catalyst than on the catalyst formulation. Preconversion treatments to remove first the active oxygen species is necessary prior to submit coal-derived extracts to supported catalysts for further conversion to environmentally acceptable fuels.

This suggests that the research approach in coal liquefaction ought to be systematic because there is the likelihood of significant complex relationships between coal structure, reaction mechanisms, thermodynamics, analytical chemistry, kinetics and, finally, catalyst selection.

## REFERENCES

1. D. Gray and M. Neuwirth, Disposable Catalysts in Coal Liquefaction: The Effect of Iron Sulfides. The MITRE Corp./DOE Contract 10280 WP-81W427, September, 1981
2. R. Davidson, Mineral Effects in Coal Conversion, ICTIS/TR 22, London, UK, IEA Coal Research, 1983.
3. F. Derbyshire, Catalysis in Direct Liquefaction: New Direction for Research. IEA Coal Research. In press.
4. D. Garg and E. Givens, Relative Activity of Transition Metal Catalysts in Coal Liquefaction. ACS Fuels Chemistry Preprints. 28, 5, 200-209, 1983.
5. J. Gatsis, Allied Chemicals.- Private Communication.
6. E. Moroni, Origins and Reactions of Alkyls and Alkanes in Direct Coal Liquefaction. ACS Fuels Chemistry Preprints. 33, 1, 384- 86, 1988.
7. E. Moroni, Coal Liquefaction and Upgrading Benefit from Heteroatom Removal. Proceedings of the 1987 International Conference on Coal Science. Maastricht, The Netherland, October 26-39, 1987, 351, and references therein.
8. J. Lemberton, M Touzeyidio and M. Guisnet, Effect of an Acid Catalyst on the Activity of a Sulfided Catalyst for Hydroconversion of Model Compounds. GRECO Hydroconversion and Pyrolysis of Coal. Poitiers, France, Sept. 10-11, 1987.
9. E. Hollstein et al., Coal Conversion to Distillate Fuels. Suntech, Inc./DOE Contract 10592, Final Report, 34, 1982.
10. D. Garg et al., Effect of Solvent Modification on Coal Liquefaction APCI/DOE Contract 50003-38, Final Report, 1985.
11. P. Montano and A. Bommannavar, J. Molecular Catalysis, 20, 393, 1983.

**COPROCESSING OF COAL WITH HIGH METAL CONTENT RESIDS**  
Timothy J. Miller, Sudhir V. Panvelker, Irving Wender, and John W. Tiemey  
University of Pittsburgh, Pittsburgh, PA 15261  
Yatish T. Shah  
University of Tulsa, Tulsa, OK 74114  
Gerald Huffman  
University of Kentucky, Lexington, KY 40506

## INTRODUCTION

The energy industry will have to consider alternative sources for the production of liquid fuels in view of the rapid depletion of conventional light oil reserves. Several processes are being developed for upgrading heavy crudes and bottom-of-the-barrel residual oils.<sup>(1,2)</sup> The heavy oils contain large amounts of metals which interfere with catalytic upgrading to clean distillates by acting as catalyst poisons. In the 1970s, several direct liquefaction processes were developed to produce liquid fuels from coal. One of the drawbacks of these processes is the fact that it is necessary to recycle a significant amount of product oil to slurry feed coal. This leads to increased plant complexity and higher production costs. Coprocessing, where coal is liquefied in a once-through mode in a heavy oil slurrying medium, may form a bridge between the existing petroleum-refining technology and the syntuels industry of the future. Besides producing light products from coal as well as from heavy oil, it can accomplish a high degree of demetallation of oil, by rejecting the metals to the solid residue.

The composition of coal-derived recycle solvents is very different from that of heavy oils. The former are highly aromatic and hydroaromatic while the latter are mostly paraffinic and naphthenic. Thus, it should be expected that coal conversion in a heavy oil, in general, would be less than in a coal-derived solvent in the absence of a catalyst. However, it is possible to achieve a high degree of conversion by proper choice of host oil, operating conditions, or by pretreating the host oil before it is used for liquefaction. Yan and Espenscheid have reported that 90% conversion of Illinois No. 6 coal to pyridine-solubles was achieved by liquefying the coal in bottoms from a fluid catalytic cracking unit without using any catalyst<sup>(3)</sup> as this solvent was highly aromatic. Similar high conversions have been reported by researchers using catalysts.<sup>(4-6)</sup> Curtis et al. have reported that petroleum residua are deficient in labile hydrogen; however, if a catalyst is used under hydrogen atmosphere, coprocessing can proceed with fairly high conversions.<sup>(7)</sup> It is possible to increase the liquefying efficacy of a residuum by its prior hydrocracking, or by adding external hydrogen donors.<sup>(8)</sup>

This paper presents the results of thermal (with no added catalyst) coprocessing of Illinois No. 6 (hvBb) coal with Maya (650°F+) ATB residual oil and with whole Boscan crude. The relationship between reaction conditions and coal conversion and product selectivity has been studied. The removal of vanadium during coprocessing has been investigated. The results on heteroatom removal reactions have also been presented as the amount of heteroatoms in petroleum is often correlated with that of metals.<sup>(9)</sup>

## EXPERIMENTAL

Tables 1 and 2 show analyses of Illinois No. 6 coal and the host oils respectively. A few experiments were made using a coal-like char and an activated carbon (NUCHAR). The char was synthesized in this laboratory from cellulose. All liquefaction experiments were conducted using a horizontal 20 ml microreactor. Typically the reactor was loaded with 8-10 g of reactants along with four 2 mm stainless steel balls as a mixing aid. It was pressurized with hydrogen to 6.9 MPa (1000 psig) at ambient temperature. The reactor was then brought to the desired reaction temperature by immersing it in a heated fluidized sand-bath. The reactor was shaken horizontally (five one-inch displacements per second) to ensure adequate mixing. The desired temperature was attained within 3-4 minutes and this was taken as zero time. At the end of the desired reaction time, the reactor was removed from the sand bath and cooled with water. The products were removed by washing the reactor with tetrahydrofuran (THF). Almost all the runs were made in duplicate.

The reaction products were classified as THF-insolubles (also referred to as coke), asphaltenes, and oils based on their solubility behavior. Asphaltenes were defined as product soluble in THF but insoluble in pentane; oils (often called maltenes) were defined as products soluble in pentane. The vanadium content of samples was determined using inductively coupled plasma (ICP).

## RESULTS AND DISCUSSION

### COAL CONVERSION AND PRODUCT DISTRIBUTION

Illinois No. 6 coal was liquefied in the Maya ATB at temperatures between 410<sup>o</sup>-450<sup>o</sup>C using various coal-to-solvent ratios. Figure 1 shows the effect of coal concentration on coke yields at 425<sup>o</sup>C. The coke (THF-insolubles) yields comprise unreacted organic matter from the coal along with its inorganic matter and the high molecular weight materials produced during the reaction. At short reaction times (<15 minutes), there was a decrease in the coke yields due to partial dissolution of coal. Part of the coal might have liquefied (breakdown of the macromolecular coal structure) under hydrogen pressure at 425<sup>o</sup>C. Perhaps the dissolution was also due to the extraction of a so-called mobile (trapped) phase from the coal. Some covalent bonds such as C-C, C-O, and C-S bonds which form the linkages in the macromolecular coal structure can be cleaved at 425<sup>o</sup>C to form reactive free radicals. A portion of these free radicals can be quenched with molecular hydrogen at high hydrogen pressures or with the hydrogen transferred from the solvent. As mentioned earlier, heavy oils, relative to recycle solvents, are deficient in hydroaromatic hydrogen - the type of hydrogen which can be easily transferred. Table 3 shows the amount of "transferable" hydrogen present in the Maya ATB, the Boscan ATB and, for the purpose of comparison, from two coal liquids.<sup>(10)</sup> (Note that the table shows the transferable hydrogen from the Boscan ATB, whereas the whole crude was used in the experiments in our study. However the data in Table 3 do provide a valid comparison, as the Boscan crude is very heavy and the difference between the whole crude and the ATB is small.) Table 3 shows that the heavy oils contain very little transferable hydrogen as compared to coal liquids. As a result, it should be expected that coal-derived and resid-derived free radicals would tend to form heavier products such as coke once the transferable hydrogen is consumed.

As shown in Figure 1, the coke yields increased with an increase in the coal concentration in the feed. The higher coke yields are due to the increase in the rates of coking in addition to the higher amounts of THF-insolubles originally present in the feed. The rate of coke formation varied with coal concentration as apparent from the difference in the slopes of the coking curves (at longer reaction times) in Figure 1. Coal concentrations below 25 wt.% showed a negligible increase in the rate of coking over the rate of thermal coking of the Maya ATB alone. However, the rate of coking was significantly higher for 40 wt.% coal concentration. The results can be attributed to the limited supply of transferable hydrogen available in the resid and the higher demand for hydrogen imposed by the high coal concentrations.

It is not possible to calculate the actual coal conversion (to THF-solubles) as the THF-insolubles contain the unconverted coal plus the coke formed from the liquefied coal and also from the resid. However, one can use the "net" coal conversion as an approximate measure of liquefaction. The net coal conversion is a measure of the effective contribution of coal to THF-solubles and can be calculated from the yield of THF-insolubles during coprocessing after subtracting from it the amount of coke formed from the processing of resid alone under identical conditions. Figure 2 shows net coal conversion in the Maya ATB as a function of coal concentration in the coprocessing feed. The net coal conversion showed a maxima relative to the reaction time. At higher reaction times, the net coal conversion decreased due to retrogressive reactions. The decrease was more pronounced for higher coal concentrations. Similar trends were obtained when the Boscan crude was used in place of the Maya ATB. As said earlier, the Boscan crude showed a greater tendency to coke. Figure 3 shows net coal conversion obtained with the Boscan crude. The net coal conversion was slightly lower with the Boscan crude. The effect of coal concentration in the feed on the net coal conversion can be seen from Figures 2 and 3. At long reaction times, net coal conversions with the Maya ATB were higher for higher coal concentrations. This is understandable as a high coal concentration leads to increased hydrogen demand and, if the supply is limited, to increased retrogressive reactions. However, at shorter reaction times with the Maya ATB, net coal conversion for 40 wt.% coal concentration was higher than for 25 wt.% coal concentration. The net conversion for 10 wt.% coal with the Maya ATB was intermediate between those for 25 wt.% and 40 wt.% coal concentrations. Obviously, the data are too scattered to draw a statistically valid inference. Most of the converted coal formed asphaltenes on a net basis and very little oils were generated.

The increased occurrence of retrogressive reactions, when the demand for hydrogen outpaces the limited supply of the transferable hydrogen in the resid, was also apparent when the liquefaction temperature was varied. The effect of temperature on the net coal conversion is illustrated in Figure 4. At high

temperatures, the net coal conversion fell sharply (the yield of coke rose) for reaction times greater than 10 minutes due to high demand for hydrogen. The maximum conversion at 450°C was much lower than that at 410°C and at 425°C.

#### DEMETALLATION OF HEAVY OILS

The coprocessing of coal and heavy oils was accompanied by significant demetallation of the heavy oil. The metals present in the asphaltenes and the oils were transferred to the solids formed during coprocessing. The Maya ATB contained 400 ppm of vanadium. A significant amount of this metal content was rejected along with the coke when the resid was processed by itself; however, the demetallation was significantly higher when the resid was processed along with coal. The results are shown in Figure 5. When the resid was processed without any coal, 65% of the vanadium present in the feed was transferred to the coke, whereas 89% of the vanadium was transferred to the coke when the feed contained 40 wt.% coal. The overall demetallation of the oils (maltenes) was relatively easier than that of the asphaltenes fraction.

The Boscan crude contained 1100 ppm of vanadium. The results on demetallation of the Boscan crude are shown in Figure 6. The results are similar to those on the Maya ATB. Although the Boscan crude contained much more vanadium, the amount of vanadium removed with coke was similar to that from the Maya ATB on a percentage basis. With a feed containing 25 wt.% coal and 75 wt.% Boscan crude, 84% of the total vanadium was rejected to coke.

In order to understand the mechanism of demetallation in coprocessing, a few samples of the feedstock, THF-solubles, THF-insolubles, pentane-solubles, and pentane-insolubles were analyzed using X-ray absorption fine structure (EXAFS) spectroscopy using facilities at Stanford University. X-ray absorption near-edge spectra (XANES) of all the samples were very similar and matched that of a vanadyl porphyrin (tetraphenylporphyrin) standard. Although these results are insufficient to identify precisely the type of vanadium compounds present, it can be concluded that the removal of vanadium along with the solids formed is not due to any change in the nature of bonding of vanadium. Vanadium remains chiefly in organometallic complexes very similar to the original porphyrins. This is contrary to that found in catalytic hydrodemetallation where vanadium on adsorption on a catalyst is converted to an inorganic form.<sup>(11)</sup> The samples studied here were obtained on noncatalytic coprocessing at 425°C and at 1000 psi (measured at ambient temperature) hydrogen pressure. It is possible, of course, to have different behavior under more severe conditions or when a hydrogenation catalyst is present.

There are several potential pathways by which the demetallation might have occurred. The metal-containing components might have been adsorbed on the surface of coke. It is also possible that such compounds might have been trapped in the coke matrix during its formation. The third possibility is that the metal components became chemical constituents of the coke. If either of the latter two routes is valid, then the extent of demetallation would depend upon the amount of coke produced during the reaction. If the demetallation occurs through adsorption, the extent of demetallation would not only depend upon the amount of coke produced but could also depend upon the amount of unconverted coal present in the system. Several experiments were made to shed light on the mechanism of demetallation using chars made from cellulose and also using activated carbon in place of coal.

Cellulose when heated to high temperatures (330°C-475°C) in an inert atmosphere yields chars whose elemental analysis and infrared spectra resemble those of coal.<sup>(12)</sup> Chars can be liquefied similar to coal. When a feed containing 90 wt.% Maya ATB and 10 wt.% of a char made from cellulose at 415°C-425°C and under 5.2 MPa nitrogen pressure was coprocessed at 425°C, 80% of the vanadium content was rejected along with coke after one hour reaction time. Under similar conditions, 69% of the vanadium was removed using 10 wt.% coal. It was further observed that the liquefaction and the demetallation behavior of char and its IR spectrum were dependent upon the conditions under which it was synthesized. It can be concluded that the demetallation is dependent upon the chemical nature of the liquefying substance. Since the char did not contain inorganics, the inorganic matter in coal is not responsible for the observed demetallation. Activated carbon in place of coal was equally effective in removing metals. There was no decrease in the yields of THF-insolubles at any reaction time indicating that as expected, the activated carbon, unlike coal, did not liquefy. The net amount of coke produced was higher relative to the processing of the Maya ATB alone. Thus, it is not clear if the demetallation observed with the activated carbon was due to the adsorption of the metal compounds on the activated carbon or it was due to the coke formed during the reaction.

Although the mechanism of demetallation is not clear from this series of experiments, it is possible to make some observations. It is unlikely that demetallation occurs due to the trapping of metal-containing compounds in the coke matrix as it forms, since only a small amount of coke formed can cause large amount of demetallation. In the early stages of coprocessing, when the yield of coke decreases due to the liquefaction of coal, the demetallation is seen to proceed at a rapid rate. This indicates that the demetallation is dependent not on the amount of coke present in the system (which includes the unreacted coal and the coke formed) but rather on the amount of coke formed during the reaction. Thus, physical adsorption of metal-containing compounds on coal is not likely the main mechanism of demetallation. Yan has studied the use of inorganic solids to demetallate heavy oils.<sup>(13)</sup> The extent of demetallation was found to be strongly dependent upon the processing temperature. At 700°F (371°C), metal removal was very small. The demetallation increased rapidly as the temperature was increased to 800°F (427°C). The amount of demetallation was independent of the surface area of the solids at higher temperatures. In a recent paper, Audeh and Yan reported that very low levels of demetallation are observed when an adsorbent such as silica gel is used in place of coal under the conditions of low coking.<sup>(14)</sup> This again indicates that adsorption is not the main mechanism of demetallation although it may be a contributing factor.

Demetallation through chemical reactions is a probable occurrence. It is known that the cokes produced from petroleum resids or coal liquids are anisotropic in nature.<sup>(15)</sup> The transformation of isotropic resid into anisotropic coke occurs via an intermediate anisotropic nematic liquid-crystal phase. The nematic liquid crystals consist of lamellar constituent molecules stacked parallel to each other. The coking process involves continuous polymerization of the constituent molecules of the liquid-crystal phase eventually forming a solid semicoke. The intermediate phase between the starting isotropic liquid and the solid semicoke is called mesophase. Large molecules containing planar regions tend to form mesophase. The asphaltenic molecules present in resids can form mesophase very easily. It has been reported that metals tend to concentrate in mesophase.<sup>(16)</sup> The organometallic structures found in petroleum are planar or have planar regions and hence are probably capable of forming mesophase. It is reasonable to expect that such structures would participate in the polymerization process leading to the formation of coke. It should be pointed out that such condensation need not involve any change in the nature of vanadium bonding. The formation of mesophase is initiated when the concentration of mesophase precursors reaches a threshold level. The enhanced demetallation in the presence of coal is perhaps due to the introduction of components (such as coal-derived asphaltenes) which participate in the process. Recent report that addition of deashed SRC (which is a liquid at the coprocessing temperatures) can demetallate heavy oils<sup>(10)</sup> support this hypothesis. Another cause for the enhanced demetallation may be the interaction between mesophase and solid surfaces. Solid coal particles may increase the amount of mesophase formed.<sup>(17)</sup> It has been observed in this laboratory, using a high-pressure and high-temperature microscope, that the presence of solids aids in the crystallization of mesophase under typical coprocessing conditions. The solid surface may act as a depository for condensed products.

#### HETEROATOM REMOVAL

Illinois No. 6 coal contained 2.98 wt.% sulfur and 0.67 wt.% nitrogen, while the Maya ATB contained 4.6 wt.% sulfur and 0.48 wt.% nitrogen. The amount of heteroatoms in the THF-solubles decreased on coprocessing. Treating 10:90 and 25:75 coal-to-resid feeds for one hour at 425°C removed 40-50% of the sulfur present in the resid to the coke and the product gas. A 35% sulfur removal was observed processing the Maya ATB alone under the same conditions. Similar observations were made on nitrogen removal. 55% of the nitrogen present in the feed was removed when 25:75 coal-to-resid ratio was used compared to 8% removal observed when the Maya ATB was processed alone. The results can be attributed to the association between heteroatoms and metals.

#### CONCLUSIONS

Illinois No. 6 bituminous coal was coprocessed with Maya ATB (650°F+) and with whole Boscan crude under thermal, non-catalytic conditions. Retrogressive reactions hinder production of THF-solubles when the demand for hydrogen increases as when the temperature is high or when the feed contains a high concentration of coal. Coprocessing results in a significant level of demetallation and heteroatom removal as these compounds are removed with the product coke. It is thus possible to achieve over 85% removal of vanadium. Very high levels of demetallation can also be achieved using char or activated carbon in place of coal.

## ACKNOWLEDGEMENTS

This work was supported by a grant from the U.S. Department of Energy (DE-FC-22 85PC80009). We are grateful to Pittsburgh Energy Technology Center for assistance in the experimental work.

## REFERENCES

1. Schultze, B., and Hoffman, B., *Hydrocarbon Proc.*, Vol. 63, 75(1984).
2. Speight, J. G., *Ann. Rev. Energy*, Vol. 11, 253(1986).
3. Yan, T. Y., and Espenscheid, W. F., *Fuel Proc. Tech.*, Vol. 7, 121(1983).
4. Kelly, J., Fouda, S., Rahimi, P., and Ikura, P., "CANMET Coprocessing: A Status Report", *Syn. Fuels Res. Lab. Div. Rep. ERP/ERL 85-52*, 1984.
5. Shinn, J. H., Dahlberg, A. J., Kuehler, C. W., and Rosenthal, J. W., Paper Presented at the 9th Annual EPRI Contractors' Meeting, Palo Alto, CA, 1984.
6. Moschopedis, S., Hawkins, R., and Speight, J., *Fuel Proc. Tech.*, Vol. 5, 213(1982).
7. Curtis, C. W., Tsai, K. J., and Guin, J. A., Paper Presented at the Symposium on New Chemistry of Heavy Ends, Chicago, IL, 1985.
8. Curtis, C. W., Tsai, K. J., and Guin, J. A., *Fuel Proc. Tech.*, Vol. 16, 71(1987).
9. Boduszynski, M. M., *Energy and Fuels*, Vol.1, 2(1987).
10. Cugini, A. V., Lett, R. G., and Wender, I., *ACS Div. Fuel Chem. Prep.*, Vol. 33, No. 1, 71(1988).
11. Wei, J., "Toward the Design of Hydrodemetallation Catalysts", in "Catalyst Design: Progress and Perspective", ed. by L. Hegedus, Wiley, New York, NY, 1987.
12. Friedel, R. A., Queiser, J. A., and Retcofsky, H. L., *J. Phys. Chem.*, Vol. 74, 908(1970)
13. Yan, T., *I&EC Proc. Des. Dev.*, Vol. 23, 415(1984).
14. Audeh, C. A., and Yan, T., *I&EC Research*, Vol. 26, 2419(1987).
15. Marsh, H., and Walker, P. L., Jr., "The Formation of Graphitizable Carbon via Mesophase: Chemical and Kinetic Considerations", in "Chemistry and Physics of Carbon", ed. by P. L. Walker, Jr., and P. A. Thrower, Vol. 15, Marcel Dekker, New York, NY, 1979, pp. 229-286.
16. Imura, T., Yamada, Y., Honda, H., Kitajima, E., and Tsuchitani, M., *Sekiyu Gakkai Shi (J. Jap. Petrol. Inst.)*, Vol. 18, 776(1975), CA 87:120993u.
17. Tillmans, H., Pietzka, G., and Pauls, H., *Fuel*, Vol. 57, 171(1978).

**TABLE 1**  
**ANALYSES OF ILLINOIS NO. 6 COAL**

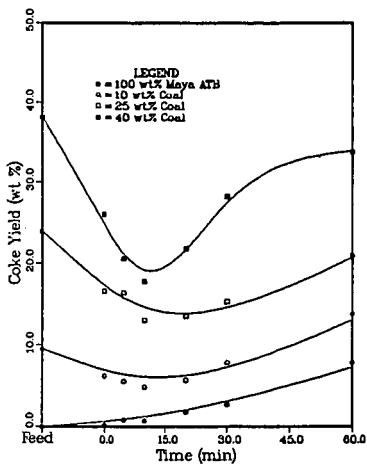
| <u>PROXIMATE ANALYSIS (wt.%)</u> |       | <u>ULTIMATE ANALYSIS (wt.%)</u> |       |
|----------------------------------|-------|---------------------------------|-------|
| Moisture                         | 4.24  | Hydrogen                        | 5.04  |
| Volatile Matter                  | 36.93 | Carbon                          | 67.18 |
| Fixed Carbon                     | 48.18 | Nitrogen                        | 0.89  |
| Ash                              | 10.56 | Sulfur                          | 2.98  |
|                                  |       | Oxygen                          | 13.26 |
|                                  |       | Ash                             | 10.56 |

**TABLE 2**  
**ANALYSIS OF MAYA (650°F+) ATB RESID AND BOSCAN CRUDE**

|                  | <u>MAYA ATB</u> | <u>BOSCAN CRUDE</u> |
|------------------|-----------------|---------------------|
| Gravity (°API)   | 8.8             | 10.0                |
| H/C Atomic Ratio | 1.52            | 1.55                |
| S (wt.%)         | 4.60            | 5.30                |
| N (wt.%)         | 0.48            | 0.60                |
| V (ppm)          | 400             | 1100                |
| Ni (ppm)         | 78              | 100                 |

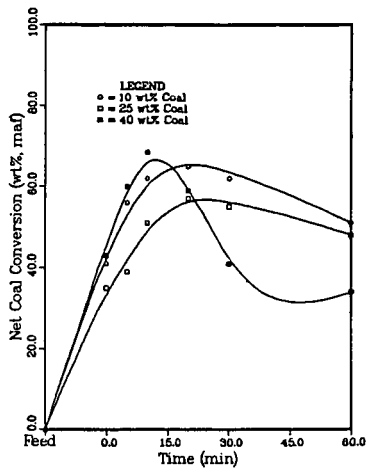
**TABLE 3**  
**TRANSFERABLE HYDROGEN IN RESIDS AND COAL LIQUIDS(10)**

|                          | TRANSFERABLE HYDROGEN |                |
|--------------------------|-----------------------|----------------|
|                          | (mmol/g)              | (% of total H) |
| Maya (650°F+)            | 2.1                   | 4              |
| Boscan (650°F+)          | 1.9                   | 4              |
| Wilsonville VTB          | 3.7                   | 11             |
| Wilsonville ITSL Solvent | 7.5                   | 16             |



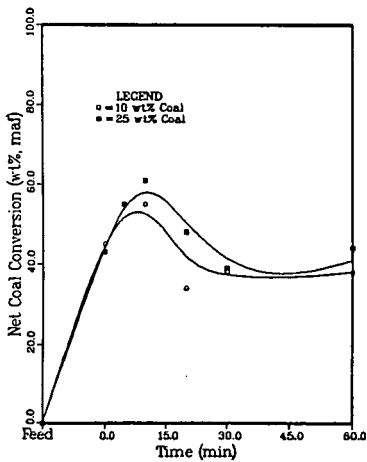
EFFECT OF COAL CONCENTRATION ON COKE YIELDS FROM MAYA ATB AT 425 C

Figure 1



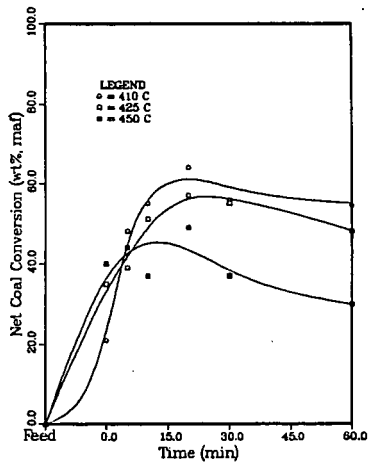
EFFECT OF COAL CONCENTRATION ON COAL CONVERSION IN MAYA ATB AT 425 C

Figure 2



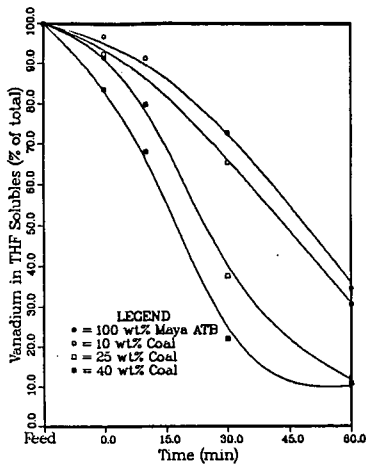
EFFECT OF COAL CONCENTRATION ON COAL CONVERSION IN BOSCAN CRUDE AT 425 C

Figure 3



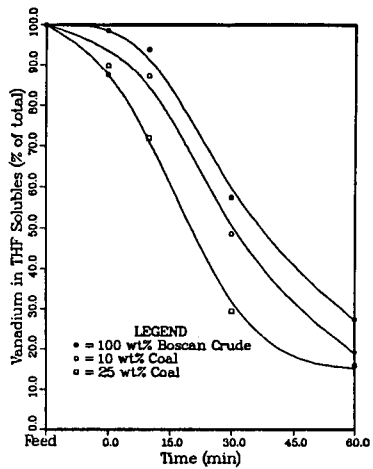
EFFECT OF TEMPERATURE ON NET COAL CONVERSION IN MAYA ATB AND 25 WT% COAL

Figure 4



EFFECT OF COAL CONCENTRATION ON REMOVAL OF VANADIUM FROM MAYA ATB AT 425 C

Figure 5



EFFECT OF COAL CONCENTRATION ON REMOVAL OF VANADIUM FROM BOSCAN CRUDE AT 425 C

Figure 6

STUDIES OF DEACTIVATING SPECIES  
ON COAL LIQUEFACTION CATALYSTS\*

Frances V. Stohl

Sandia National Laboratories, Albuquerque, NM 87185

Ripu Malhotra

SRI International, Menlo Park, CA 94025

INTRODUCTION

Previous studies (1,2) of catalyst samples from laboratory experiments with model compounds and coal-derived hydrotreater feeds from the Wilsonville Advanced Coal Liquefaction R&D Facility have shown that most deactivation is due to hydrotreating strongly basic heterocyclic nitrogen compounds. For example, hydrotreating nitrogen polycyclic aromatic compounds, separated from a hydrotreater feed from Wilsonville run 247, caused a 95% loss of the catalyst's hydrogenation (HYD) activity within a 2 h run. This activity loss was much greater than obtained by hydrotreating the whole hydrotreater feed or the other chemical classes of compounds (aliphatics, neutral polycyclic aromatic compounds, hydroxy polycyclic aromatic hydrocarbons) that made up the feed. Hydrotreating model compounds representative of the different types of nitrogen compounds present in coal liquids, including strongly basic compounds (quinoline, pyridine, acridine), a weakly basic compound (indole), and a neutral compound (carbazole), showed that the strongly basic compounds caused greater deactivation than the other compounds. Losses of about 75% of the HYD activity were observed by hydrotreating the strongly basic compounds in 2 h reactions, compared with a 50% loss for indole and a 24% loss for carbazole.

Quinoline hydrotreating studies (3) were performed to determine the effects of process conditions on deactivation caused by hydrotreating strongly basic nitrogen compounds. The reactions were carried out at two times (5 min, 2 h) and two temperatures (300°C, 400°C). The results showed that the deactivation was the same in all cases. Gas chromatographic (GC) analyses of the liquid products from these runs demonstrated that increasing reaction severity yielded more unidentified compounds (i.e., compounds that were not part of the reported quinoline hydrodenitrogenation (HDN) reaction scheme (4)). At the lowest reaction severity condition (300°C, 5 min), 19% of the liquid product consisted of unidentified compounds, whereas at the highest severity condition (400°C, 120 min) 86% was unidentified. At low severity, only 2% of the nitrogen was removed, as determined by liquid product analyses, whereas at high severity 18% was removed. A comparison of the amount of nitrogen remaining in the liquid product from the high severity reaction with gas chromatographic analyses of the liquid product showed that most of the remaining nitrogen was present in compounds that were formed by side reactions.

The ultimate objectives of the catalyst deactivation work reported here are to determine how the deactivation due to hydrotreating strongly basic nitrogen compounds occurs on the catalyst surface and to identify the compounds that cause the deactivation. The work reported here is aimed at evaluating the usefulness of Field Ionization Mass Spectrometry (FIMS) analyses for our catalyst deactivation studies. Results of the application of FIMS techniques to characterize the compounds volatilized from the aged catalysts and the liquid

\* This work was supported by the U.S. Dept. of Energy at Sandia National Laboratories under contract DE-AC04-76DP00789.

products of our quinoline HDN experiments are described. The results are compared to those obtained for catalysts used at Wilsonville. The field emission method employed in FIMS is a mild, yet efficient, ionization that exclusively produces molecular ions from most chemical compounds. Thus the mass spectra of complex mixtures are not complicated by the presence of large numbers of peaks associated with molecular fragments. FIMS thus provides molecular profiles of samples. It has been used in the characterization of both petroleum and coal derived-materials (5-7). The relative ionization efficiencies of many different classes of organic compounds analyzed by FIMS are very similar, varying by only a factor of two (8).

#### EXPERIMENTAL PROCEDURES

FIMS results are reported for aged catalysts from Wilsonville runs 246 and 247 and for catalysts and products from quinoline hydrotreating experiments (3).

##### Materials

The catalyst used both for processing coal at Wilsonville and for the laboratory hydrotreating experiments was Shell 324M, which contains 12.4 wt% Mo and 2.8 wt% Ni on an alumina support, in the form of extrudates measuring about 0.8 mm in diameter and 4 mm in length. Prior to use in the laboratory experiments, the catalyst was presulfided with a 10 mol% H<sub>2</sub>S/H<sub>2</sub> mixture at 400°C and atmospheric pressure for 2 h. Before analysis, all aged catalyst samples were Soxhlet extracted with tetrahydrofuran, to remove as much soluble material as possible, and then dried overnight at 100°C under vacuum.

##### Wilsonville Catalysts

Two catalyst samples from each of two Wilsonville runs were analyzed by FIMS. The run 246 samples had catalyst ages of 36 and 592 lb resid/lb catalyst and the run 247 catalysts had ages of 28 and 546 lb resid/lb catalyst. Catalyst age was determined from the amount of resid, which is nondistillable material at 600°F and 0.1 mm Hg, in the Wilsonville hydrotreater feed. Activity test results and characterization results of these Wilsonville samples have been reported previously (9).

Run 246 processed subbituminous Wyodak coal using the Double-Integrated Two-Stage Liquefaction (DITSL) mode up to a catalyst age of about 300 lb resid/lb catalyst and the Integrated Two-Stage Liquefaction (ITSL) mode for the remainder of the run. Deashing was performed between the two stages. In the DITSL mode, only the light thermal resid from the deasher went to the hydrotreater, whereas in the ITSL mode all the deashed material went to the hydrotreater. The temperatures in this run ranged from about 320°C to 340°C.

Run 247 processed Illinois #6 coal in the Reconfigured Integrated Two-Stage Liquefaction mode. In this mode, the deashing occurs after the second stage so that all the material from the first stage goes to the hydrotreater. The run temperatures ranged from 350°C to 375°C.

##### Quinoline Hydrotreating Experiments

Each hydrotreating experiment was performed in a 26 cc batch microreactor with 1200 psig H<sub>2</sub> cold charge pressure. Runs were made for either 5 minutes or 2 hours at either 300°C or 400°C. Experiments were performed with 1.5 g of model compound and 0.5 g presulfided catalyst. Activity test results and characterization results for the aged catalysts from these reactions have been reported previously (3).

##### FIMS Analysis

FIMS uses a field emission device to ionize the constituents of the vapor

released from a sample when it is heated in an evacuated chamber. The ions are separated by mass in a magnetic sector mass spectrometer. The field ionization mass spectrometer at SRI International, which was used in this study, consists of an activated tantalum foil field source interfaced with a 60° magnetic sector mass analyzer and a PDP 11/23 computer for data acquisition and analysis. A single catalyst pellet or about 50 mg of liquid product was placed in a sample holder and introduced into the mass spectrometer through a heatable direct-insertion probe. Spectra were collected by scanning the spectrometer repeatedly over the 50 to 800 amu range while the sample was gradually heated. The heating range for the catalyst samples was about 25°C to 450°C, whereas the liquid products were heated from about -60°C to 350°C.

## RESULTS

### Wilsonville Catalysts

Results of the FIMS analyses on the run 246 catalysts (Figure 1 and Table 1) show that the average molecular weights of the volatile species increase with catalyst age; the weight average molecular weight increases from 256 to 278. In addition, the number of peaks increases from 382 to 465 with age. Analyses of the molecular weights show that at least 49% of the peaks are due to nitrogen compounds; compounds with an odd number of nitrogen atoms have odd numbered molecular weights (10). Although there are approximately an equal number of odd and even mass peaks, 60% of the total ion intensity is present in the odd molecular weight peaks. The nine highest intensity peaks from the 36 lb resid/lb catalyst sample and 16 out of the highest 24 peaks are due to nitrogen compounds. In the higher aged catalyst, the highest 14 peaks and 22 out of the highest 24 peaks are due to nitrogen containing compounds.

The FIMS analyses of the two catalyst samples from run 247 (Figure 2 and Table 1) show similar trends to those observed for the run 246 catalysts. The weight average molecular weights increase with catalyst age. The increases are about 24% for these catalysts as compared to about 8% for the run 246 catalysts. About 48% of the peaks in the spectra from the run 247 samples have odd numbered molecular weights. The total number of peaks also increases with catalyst age. About 52% of the total ion intensity in the 28 lb resid/lb catalyst sample and 47% in the 546 lb resid/lb catalyst sample are due to nitrogen compounds. For the 28 lb resid/lb catalyst sample, the highest 6 peaks and 18 out of the highest 24 peaks are due to nitrogen compounds. The higher aged sample from run 247 had 13 nitrogen compounds out of the 24 compounds with the highest peaks.

There is also evidence for the presence of many alkylated compounds in all four of the Wilsonville catalyst spectra. For example, in the 36 lb resid/lb catalyst sample, each peak in the series 216, 230, 244, 258, 272, 286, 300 and 314 differs from the next peak by 14 mass units suggesting that the compounds yielding these spectra differ by one CH<sub>2</sub> group. This series is also present in the other three spectra, although the number of compounds in the series and the intensities of the peaks vary. In addition, there are many other series, with peaks differing by 14 mass units, that suggest the presence of additional alkylated compounds.

### Catalysts from Quinoline Experiments

Results of the FIMS analyses on the catalysts from the quinoline hydrotreating experiments (Figure 3 and Table 1) show that the number of peaks obtained increases with both reaction time and temperature. The volatile material from the catalyst used in the 300°C 5 minute reaction has an average molecular weight comparable to that of quinoline (129), although FIMS spectra of

the volatile material from all the other catalysts have higher average molecular weights than either quinoline or the highest molecular weight compound reported in the quinoline HDN reaction scheme (4) (propylcyclohexylamine, 141). The spectrum for the volatile material from the catalyst from the 300°C 5 minute reaction shows that about 68% of the total ion intensity is due to quinoline. The spectrum of the catalyst from the 300°C 120 minute reaction also shows quinoline as a major peak, but has an additional major peak with a molecular weight of 202. The compound causing this peak and the origin of this compound are unknown. The catalysts from the two 400°C reactions each have the same major peaks, although the intensities are different. The only identifiable peak, based on the quinoline HDN reaction scheme, out of the highest 8 peaks in these patterns is that due to quinoline.

#### Liquid Products from Quinoline Experiments

The spectra obtained from the liquid products (Figure 4) from the quinoline HDN reactions are very different from those obtained from the catalysts. There are many more peaks present in the product spectra than in the spectra of the material volatilized from the catalyst; about half of the peaks in each product spectrum are due to nitrogen compounds. The average molecular weights of the products are also much higher than for the volatile species from the catalyst samples. The spectrum of the product from the 300°C 5 minute reaction has one major peak with a molecular weight of 133 that makes up about 64% of the total ion intensity. This peak is due to tetrahydroquinoline (THQ), 1,2,3,4- THQ, 5,6,7,8-THQ or both. This spectrum is different than that obtained from the catalyst used in this reaction, which had quinoline as the major peak and only a very small amount of THQ. The spectrum from the 300°C 120 minute reaction product also has 133 as the highest peak, but in addition it has a significant peak at 266 and a peak at 399 indicating the presence of THQ dimers and trimers. There is a small peak at 135, which is the molecular weight of o-propylaniline (OPA). The spectrum of the product from the 400°C 5 minute reaction also shows the presence of THQ as the major peak and a peak due to the THQ dimer. There's a larger quinoline peak in this pattern than observed in the 300°C product spectra; this is reasonable since hydrogenation occurs more readily at the lower temperature. The product spectrum from the 400°C 120 minute reaction has 624 peaks with at least 70% of the total ion intensity due to nitrogen compounds. The highest intensity peak in this pattern is at a mass of 135, which is probably due primarily to OPA. There is also evidence in this spectrum of the presence of alkylated species. The series of peaks 129, 143, 157, 171 and 185 indicate the presence of alkylated quinoline compounds. The series 93, 107, 121, 135, 149 and 163 also suggests the presence of alkylated species.

#### DISCUSSION

The results of the FIMS analyses of the Wilsonville catalysts indicate that some nitrogen compounds are preferentially adsorbed on the catalyst. An analysis of a hydrotreater feed from run 247 (11) has shown that the maximum amount of nitrogen compounds in the hydrotreater feed would be approximately 17%, whereas about 50% of the compounds volatilized from the catalysts are nitrogen compounds. This preferential adsorption of nitrogen compounds is not surprising since many nitrogen compounds are basic compounds that would be readily adsorbed on acidic catalyst sites. These results do suggest, in agreement with previous studies (1,2), that nitrogen compounds are the precursors of the compounds responsible for catalyst deactivation. The increase in the average molecular weights of the volatile compounds with catalyst age could be due to several factors: retrogressive reactions occurring on the catalyst surface (due to either time at temperature in the Wilsonville run or

the desorption procedure in the FIMS analyses), or changes in the hydrotreater feed as the run progresses. Hydrotreater feeds, withdrawn from the pilot plant at the same times as the catalyst withdrawals, were not available for FIMS analyses.

Analyses of spectra taken of catalysts from HDN reactions with quinoline are a little easier to interpret than spectra of Wilsonville catalysts because the reactor feed is known and the HDN reaction scheme has been reported (4). Therefore, it is possible to identify some of the peaks in the FIMS spectra and to ascertain which expected peaks are not present.

Results of studies of the Wilsonville catalysts and the quinoline hydrotreating catalysts suggest that FIMS is a very useful technique for helping identify compounds adsorbed on catalysts during reaction. Based on the results of these studies, we have identified several blank and baseline analyses that should be performed in order to elucidate the significance of the analyzed compounds in regard to either studying reaction mechanisms or determining deactivation mechanisms. First, quinoline and several other compounds that are part of the HDN reaction scheme should be adsorbed on the catalyst at room temperature and the samples then analyzed by FIMS to determine if other compounds are formed catalytically in the desorption step of the analysis. Although changes in compounds have not been found to be a problem with liquid samples, this could be a problem on a catalyst surface when high temperatures are present. Second, analyses should be performed on ground -200 mesh catalysts so that diffusional limitations in the catalyst are minimized. Identification of individual compounds in the FIMS spectra is imprecise because of the limited information available for each peak. Attempts to correlate volatilization temperature to compound properties (such as adsorption energy) have not been effective with catalyst samples because of the wide temperature range over which each compound is volatilized. This could be related to the catalyst's effective diffusivity in addition to the compounds properties. If diffusional limitations are minimized, compounds should be volatilized over a smaller temperature range than occurs with extrudates. The volatilization temperature might then be useful in helping identify the compound. Third, FIMS analyses should be repeated on several catalyst pellets from a given hydrotreating reaction. This would not only indicate the reproducibility of the analysis of catalysts, but would also give sufficient catalyst for both elemental analyses (so that the amount of volatile material could be determined) and activity testing (so that the impact of the volatile material on activity could be evaluated). Finally, catalyst samples and hydrotreater feeds removed from the Wilsonville facility at the same time should be analyzed to determine interactions between the feed and catalyst.

The results of the analyses of the liquid products provide information about the effects of reaction conditions on the product. The liquids are completely volatilized in the FIMS analyses so that all compounds are analyzed. In addition, results of the FIMS analyses have been compared to previous quantitative GC analyses of the liquid products from these hydrotreating reactions. For the product from the 300°C 5 minute reaction, GC analysis gave about 5 wt% quinoline, 76 wt% THQ, and 19 wt% unknown compounds (i.e. compounds that are not part of the HDN reaction scheme), and FIMS gave 3 % quinoline, 70 % THQ, and 27 % unknown compounds. The results of these two analyses are in good agreement; the agreement between the GC and FIMS analyses of the liquid products from the other three reactions at the more severe reaction conditions were equally good. These results indicate, in agreement with previous studies, that there are no chemical changes in the samples due to the FIMS analysis. FIMS analysis gives additional information about the compounds that cannot be obtained with GC alone.

## CONCLUSIONS

The results of this study indicate that FIMS analyses are useful for characterizing changes that occur in the feed during hydrotreating. Potential changes that can be quantified include molecular weight distributions, number of compounds and types of compounds. If FIMS analyses are combined with other analytical techniques such as Fourier transform infrared spectroscopy and GC/mass spectrometry, it should be possible to identify many of the compounds in the reaction products. Results of studies of the compounds volatilized from aged catalysts also suggest that FIMS is potentially useful for determining catalytic reaction mechanisms and for studying catalyst deactivation. Additional experiments are being carried out to clarify the interpretation of these results.

## REFERENCES

1. Stohl, F. V. and H. P. Stephens, ACS Division of Fuel Chemistry Preprints 31(4), 251-6, 1986.
2. Stohl, F. V., Proceedings DOE Direct Liquefaction Contractors' Review Meeting, October 20-22, 1986, p.124-131.
3. Stohl, F. V., ACS Division of Fuel Chemistry Preprints 32(3), 325- 31, 1987.
4. Satterfield, C. N. and S. H. Yang, Ind. Eng. Chem. Process Des. Dev. 23, 11-19, 1984.
5. Boduszynski, M. M., Energy and Fuels 1, 2-11, 1987.
6. Boduszynski, M. M., R.J. Hurtubise, T. W. Allen and H. F. Silver, Fuel 65, 223-34, 1986.
7. Boduszynski, M. M., R. J. Hurtubise, T. W. Allen and H. F. Silver, Anal. Chem. 55, 232-41, 1983.
8. St. John, G. A., S. E. Buttrill Jr., and M. Anbar, in Organic Chemistry of Coal, J. Larsen, ed., ACS Symp. Ser. 71, 1978, p.223.
9. Stohl, F. V. and H. P. Stephens, Ind. Eng. Chem. Research 26, 2466-73, 1987.
10. Whitehurst, D. D., S. E. Buttrill Jr., F. J. Derbyshire, M. Farcasiu, G.A. Odoerfer and L. R. Rudnick, Fuel 61(10), 994-1006, 1982.
11. Stohl, F. V. Unpublished results.

Table 1. FIMS data for the catalyst and product samples

Wilsonville Catalysts

|         | <u>Catalyst Age</u> | <u>Wt Av MW*</u> | <u>% Odd MW Intensity</u> | <u>Number of Peaks</u> | <u>% Odd MW Peaks</u> |
|---------|---------------------|------------------|---------------------------|------------------------|-----------------------|
| Run 246 | 36                  | 255.7            | 59.5                      | 382                    | 48.9                  |
|         | 592                 | 277.5            | 60.2                      | 465                    | 49.2                  |
| Run 247 | 28                  | 247.5            | 51.9                      | 401                    | 48.4                  |
|         | 546                 | 304.4            | 46.5                      | 424                    | 46.7                  |

Quinoline HDN Catalysts

| <u>Reaction Conditions</u> | <u>Wt Av MW</u> | <u>% Odd MW Intensity</u> | <u>Number of Peaks</u> | <u>% Odd MW Peaks</u> |
|----------------------------|-----------------|---------------------------|------------------------|-----------------------|
| 300°C, 5 min               | 131.5           | 81.2                      | 41                     | 51.2                  |
| 300°C, 120 min             | 173.6           | 48.7                      | 60                     | 40.0                  |
| 400°C, 5 min               | 174.0           | 52.4                      | 146                    | 34.2                  |
| 400°C, 120 min             | 166.7           | 52.2                      | 343                    | 45.8                  |

Quinoline HDN Product

| <u>Reaction Conditions</u> | <u>Wt Av MW</u> | <u>% Odd MW Intensity</u> | <u>Number of Peaks</u> | <u>% Odd MW Peaks</u> |
|----------------------------|-----------------|---------------------------|------------------------|-----------------------|
| 300°C, 5 min               | 201.9           | 75.8                      | 182                    | 55.5                  |
| 300°C, 120 min             | 275.6           | 55.6                      | 344                    | 52.2                  |
| 400°C, 5 min               | 287.7           | 59.2                      | 560                    | 49.7                  |
| 400°C, 120 min             | 295.2           | 70.3                      | 624                    | 50.0                  |

\* Average molecular weight

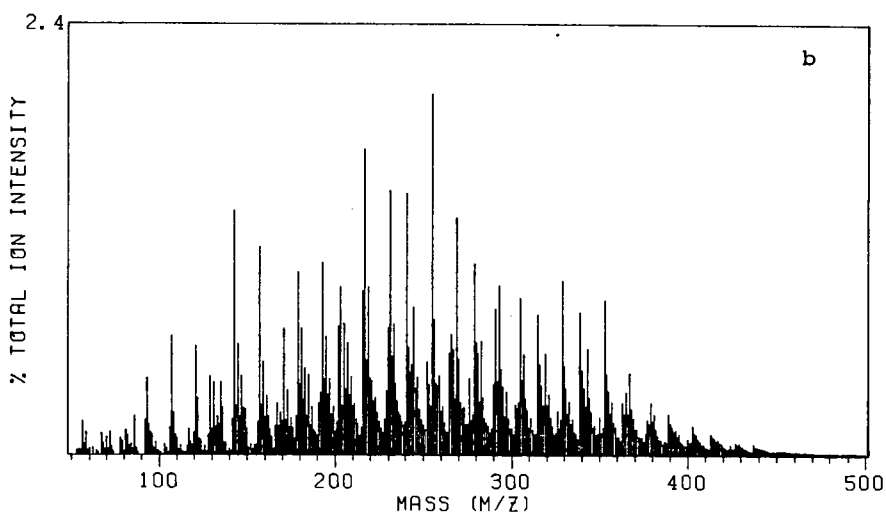
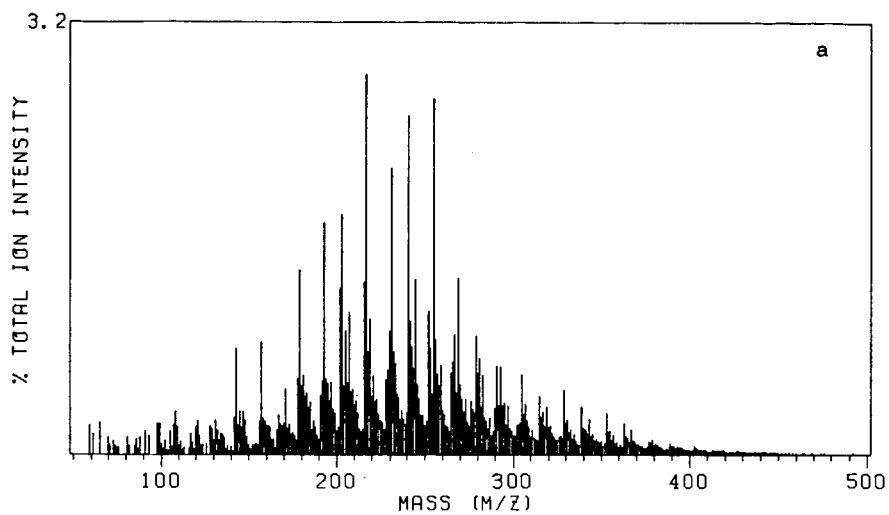


Figure 1. FIMS spectra of Wilsonville run 246 catalysts.  
a - Catalyst age of 36 lb resid/lb catalyst;  
b - Catalyst age of 592 lb resid/lb catalyst.

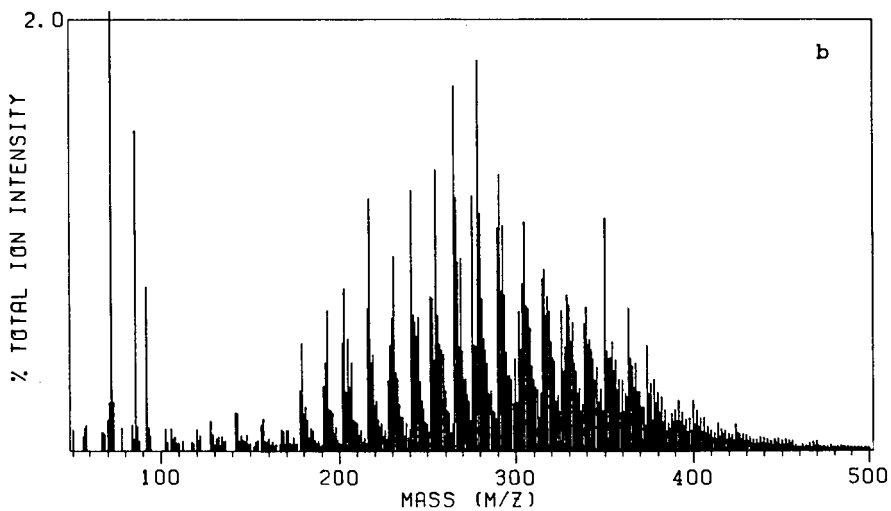
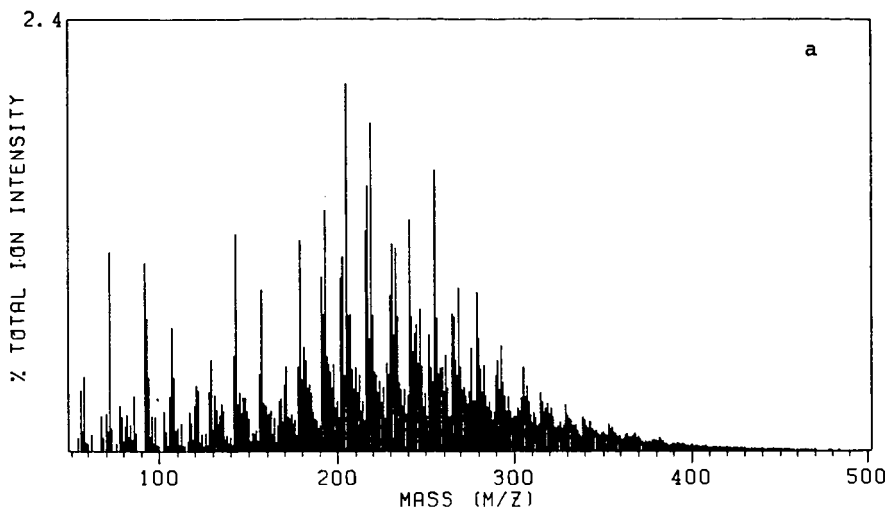


Figure 2. FIMS spectra of Wilsonville run 247 catalysts.  
 a - Catalyst age of 28 lb resid/lb catalyst.  
 b - 546 lb resid/lb catalyst.

Figure 3. FIMS spectra of quinoline HDN catalysts.

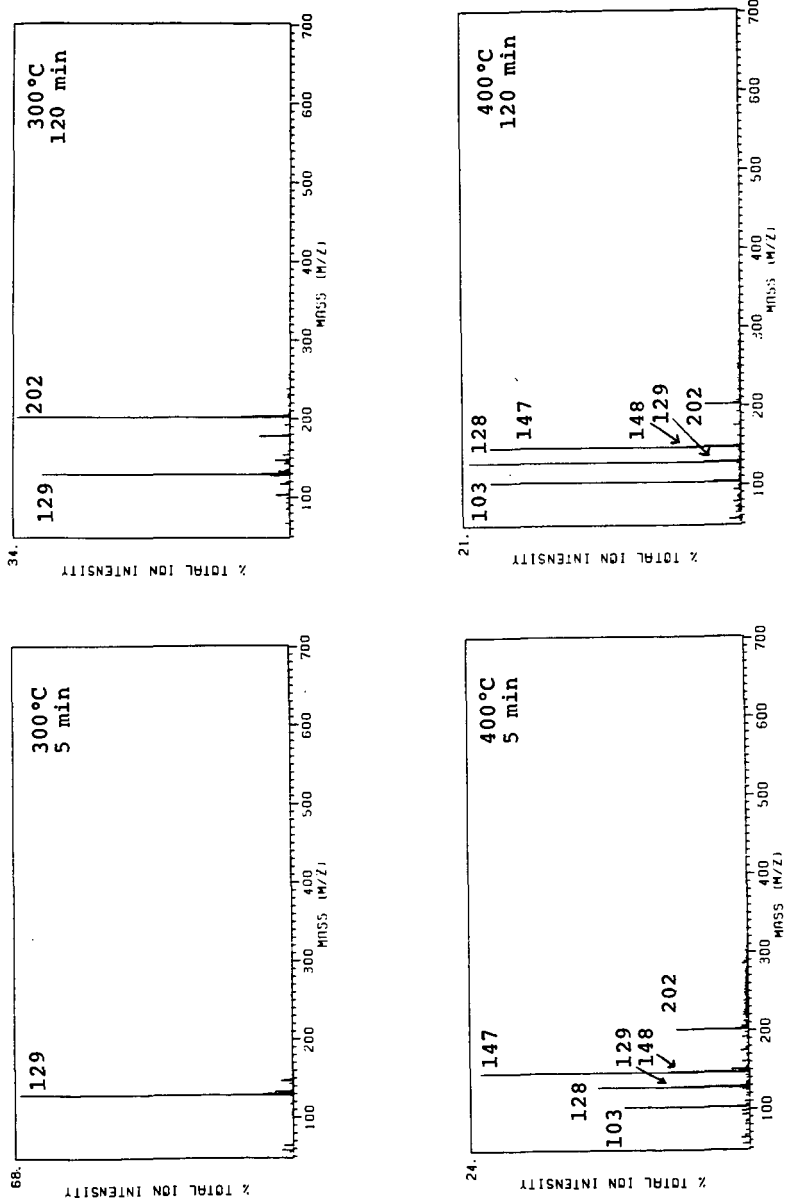
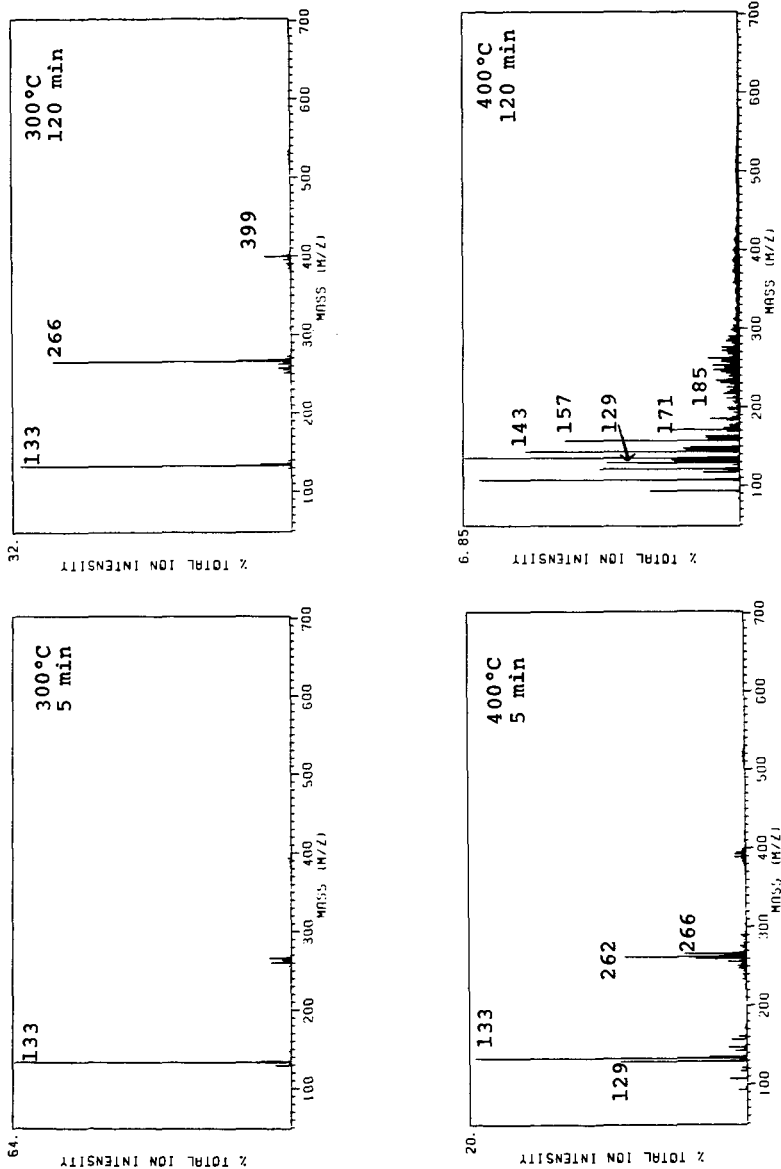


Figure 4. FIMS spectra of liquid products from quinoline HDN reactions.



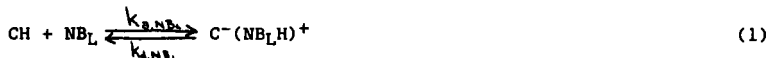
## Nitrogen Base Poisoning of NiMo Liquefaction Catalysts: A Kinetic Study

Bruce D. Adkins, Diane R. Milburn and Burtron H. Davis

Kentucky Energy Cabinet Laboratory  
P. O. Box 13015, Iron Works Pike  
Lexington, Kentucky 40512

### INTRODUCTION

A mechanistic model has been proposed to explain coking on hydrotreating catalysts from four process configurations of the Wilsonville, AL coal liquefaction pilot plant (ref. 1). This model, which utilizes reversible adsorption of nitrogen bases on acid sites, and irreversible poisoning of these sites by sodium, can explain all of the trends seen in the elemental compositions of the catalysts used in six pilot plant runs spanning four process configurations, two coals and two catalysts. The model, presented here for Bronsted acid sites, is:



where CH represents an acid site capable of chemisorbing either one nitrogen base molecule or one sodium atom and BH represents another type of site capable of reacting with sodium but not the nitrogen base.  $\text{NB}_L$  represents a group of nitrogen bases associated with distillate solvent or light thermal resid (LTR) from the Critical Solvent Deashing unit (CSD) and having a lower average molecular weight than  $\text{NB}_H$ , which represents basic nitrogen compounds having a higher average molecular weight, associated with the thermal resid stream (TR) from the CSD.  $\text{C}^-(\text{NB}_L\text{H})^+$  and  $\text{C}^-(\text{NB}_H\text{H})^+$  are the acid-base adducts formed on the catalyst surface. ANa is the sodium present in coal ash, and CNa and BNa are the Na-exchanged acid sites. The essence of this mechanism is that  $\text{NB}_L$ ,  $\text{NB}_H$ , and Na can exchange on the catalyst surface.

In considering the proposed exchanges, the question of overall rate control must be addressed. A simple kinetic analysis is presented in an attempt to determine whether adsorption,  $k_a$ , or desorption,  $k_d$ , is controlling these exchanges.

### Kinetic Analysis

For an exchange between species "1" and "2", illustrated in reactions (1) and (2) or in (2) and (3):

$$\ln \frac{1 - k_1^* \theta_1}{1 - k_1^* \theta_1^0} = k_2^* t \quad (5)$$

where

$$k_1^* = \frac{k_{a1} + k_{d2}k_a^*}{k_a^* k_{d2}}$$

$$k_2^* = \frac{k_{d1} + k_{d2}k_a^*}{1 + k_a^*}$$

and

$$k_a^* = \frac{k_{a1}[1]}{k_{a2}[2]} = \text{"Adsorption selectivity"}$$

where  $k_a$ 's represent first-order adsorption rate constants,  $k_d$ 's represent first-order desorption rate constants,  $\theta_1$  is the fractional surface coverage of species "1" at any time, and  $\theta_1^0$  is the initial surface coverage of "1". Pseudosaturation throughout the exchange is assumed in equation (5), such that  $\theta_1 + \theta_2 = 1$ .

Solving for the three specific reactions proposed in the model, we obtain for the exchange of  $NB_L-NB_H$  shown in reactions (1) and (2):

$$\ln(1 - k_{1,NB_H-NB_L}^* \theta_{NB_H}^0) = -k_{2,NB_H-NB_L}^* t \quad (6)$$

where:

$$\theta_1 = \theta_{NB_H}$$

$$\theta_{NB_H}^0 = 0$$

$$k_{1,NB_H-NB_L}^* = \frac{k_{d,NB_H} + k_{a,NB_H-NB_L}^* k_{d,NB_L}}{k_{a,NB_H-NB_L}^* k_{d,NB_L}}$$

$$k_{2,NB_H-NB_L}^* = \frac{k_{d,NB_H} + k_{a,NB_H-NB_L}^*}{1 + k_{a,NB_H-NB_L}^*}$$

$$k_{a,NB_H-NB_L}^* = \frac{k_{a,NB_H}[NB_H]}{k_{a,NB_L}[NB_L]}$$

The exchange shown in equations (2) and (3), of  $NB_H$  and Na yields:

$$\ln = \frac{1 - k_{1,NB_H-Na}^* \theta_{NB_H}^0}{1 - k_{1,NB_H-Na}^*} \quad (7)$$

where:

$$\theta_1 = \theta_{NB_H}$$

$$\theta_{NB_H}^0 = 1$$

$$k_{1, NB_H-Na}^* = \frac{k_{d, NB_H} + k_{a, NB_H-Na}^* k_{d, Na}}{k_{a, NB_H-Na}^* k_{d, Na}}$$

$$k_{2, NB_H-Na}^* = \frac{k_{d, NB_H} + k_{a, NB_H-Na}^* k_{d, Na}}{1 + k_{a, NB_H-Na}^*}$$

$$k_{a, NB_H-Na}^* = \frac{k_{a, NB_H} [\text{NB}_H]}{k_{a, Na} [\text{ANa}]}$$

The form of equation (7) is troublesome if  $k_{d, Na} \ll k_{d, NB_H}$ . For irreversible sodium chemisorption, a better form is:

$$\ln \theta_{NB_H} = -k_{d, NB_H-Na}^* t \quad (8)$$

where:

$$k_{d, NB_H-Na}^* = \frac{k_{d, NB_H}}{1 + k_{a, NB_H-Na}^*}$$

#### I. Kinetics Calculated from Process Data

Carbon, nitrogen and sodium analyses were used to solve equations (6) through (8) for the various runs examined (ref. 1). Full coverage of  $NB_L$  is determined by the carbon content at saturation in the DITSL runs, which is reached very early in the run, and full coverage of  $NB_H$  is estimated by extrapolating the RITSL carbon data to 0% Na.  $\theta_{NB_H}$  is then:

$$\theta_{NB_H} = \frac{C - C_{NB_L}}{C_{NB_H} - C_{NB_L}} \quad (9)$$

where C represents % carbon,  $C_{NB_L}$  is the % carbon present at saturation of  $NB_L$ , and  $C_{NB_H}$  is the % carbon present at full coverage of  $NB_H$ . An example of the fit for this exchange is shown in Figure 1a.

Nitrogen analyses are used in solving for the  $NB_H$ -Na exchange, making the analyses easier and more certain by eliminating the assumption that all carbon on the catalyst is present in the form of chemisorbed basic nitrogen. A sample of the fit of equation (8) to these data is shown in Figure 1b. Difficulties were encountered attempting to fit eqn. (7), which suggested the irreversible case (eqn. 8) be used instead.

The results obtained by fitting the model to the data allow examination of the two factors controlling the overall rate exchanges on the catalyst: rate(s) of nitrogen base desorption ( $k_d$ 's) and the adsorption selectivity for the two competing species ( $k_a^*$ ). The relationships for limiting cases in the  $NB_L-NB_H$  exchange are shown in Table 1, and for the  $NB_H-Na$  exchange in Table 2.

## II. Kinetics of Laboratory Desorption of Nitrogen Bases

Laboratory experiments were conducted using a CSTR to test the critical assumption that the nitrogen bases desorb from the catalyst. In two separate experiments blends of DITSL catalysts, still in the original process oil, were placed in the reactor extracted in flowing THF at 120°C, the gently stirred in tetralin feed at 250°C and 2000 psi for three weeks. Samples were taken, twice weekly, after cooling and depressurizing the reactor. Analyses of the catalyst showed a decrease in both nitrogen (from 0.45% to a fairly stable 0.15%) and carbon for the first two weeks, after which time a non-nitrogen containing coke formation was seen, probably tetralin derived carbon on the acid sites exposed by base desorption. A value of 0.04 day<sup>-1</sup> was obtained for  $k_{d,NB}$ , which is in good agreement with the values from Tables 1 and 2, considering the effects of the non-nitrogen containing coke have been ignored. However, re-adsorption of nitrogen bases cannot be ruled out as the concentration of desorbed based present in the reactor could have been as high as 200 to 500 ppm at any time.

## III. Comparison with Kinetics of Nitrogen Base Poisoning of Cracking Catalysts

Extensive literature exists on nitrogen base and alkali poisoning of cracking catalysts (e.g., ref. 2). Much less information is available on the poisoning of acidic hydrotreating catalysts, such as Shell 324. We can use cracking catalyst measurements in an attempt to rationalize the kinetic measurements obtained from process and laboratory data. However, the acidity of Shell 324 is likely to be different from that of silica-alumina cracking catalysts.

One of the earliest of these studies was performed by Mills, et al. (ref. 3) in which they studied the adsorption of quinoline on silica/alumina cracking catalysts at 315°C and several pressures. They identified two distinct kinetic regions in the desorption curve, corresponding to what they termed a rapidly desorbing "physisorbed" species, followed by a much slower "chemisorbed" species. Much later Kittrell, et al. (ref. 4) calculated rate constants from these data and suggested that the adsorption and desorption rates for the more rapidly desorbed quinoline should be used to predict reversible nitrogen poisoning of cracking catalysts. The numbers he obtained were approximately  $k_a = 200 \text{ day}^{-1}$ ,  $k_d = 150 \text{ day}^{-1}$ . An attempt to obtain order-of-magnitude consistency between Kittrell et al.'s rate constants and our measurements yields the following relative rates:





Thus, if  $k_a$  and  $k_d$  of the  $\text{NB}_L$  group (which is estimated to have an overall stoichiometry very similar to that of quinoline) are as large as  $200 \text{ day}^{-1}$  and  $150 \text{ day}^{-1}$  respectively, a large kinetic difference in the  $\text{NB}_L$  and  $\text{NB}_H$  species is indicated. It would be highly speculative at this point to assume that these are the two species observed in reference 3. The main inconsistency with this picture is the rapid saturation of  $\text{NB}_L$  and  $\text{NB}_H$  on fresh sulfided catalyst beds that is clearly seen in DITSL and RITSL data.

Next let us assume that the nitrogen bases adsorb rapidly, but is very slow to desorb, analogous to the second species proposed by Mills et al., and using our CSTR measurement of  $k_d = 0.05 \text{ day}^{-1}$ . Fitting the calculations to our model for this case yields:



This ranking accommodates the rapid saturation of RITSL and DITSL with  $\text{NB}_H$  and  $\text{NB}_L$ .

#### IV. Gravimetric Vapor Phase Experiments

The questions raised in this kinetic study can only be answered by kinetic measurements using a differential flow reactor adsorption and desorption. Thus, a high pressure gravimetric reactor system, shown schematically in Figure 2, has been constructed. This will allow us to measure the adsorption and subsequent desorption of several nitrogen compounds at different pressures, and determine their kinetic rate constants. The ability to introduce hydrogen should also shed light on the HDN performance of this catalysts.

#### ACKNOWLEDGMENT

This work was supported by the Commonwealth of Kentucky, Kentucky Energy Cabinet and DOE Contract No. DE-FC-22-85PC80009 as part of the Consortium for Fossil Fuel Liquefaction Science (administered by the University of Kentucky).

#### REFERENCES

1. D. R. Milburn, B. D. Adkins and B. H. Davis, ACS Div. Fuel Preprints, **33** (2), 380 (1988).
2. T. F. Degnan and M. Farcasiu, U.S. Patent No. 4,550,090, October 29, 1985.
3. G. A. Mills, E. R. Boedeker and A. G. Oblad, J. Am. Chem. Soc., **72**, 1554, (1950).
4. J. R. Kittrell, P. S. Tam and J. W. Eldridge, Hyd. Proc., **63** (1985).

Table I.  
Kinetic Analyses of  $NB_L-NB_H$  Exchanges

| Limiting Case—<br>Preferential<br>Chemisorption      |  |  |
|--|--|--|
| $NB_H$ ( $day^{-1}$ )<br>( $k_s^* NB_H NB_L \gg 1$ ) | $k_d, NB_L \approx 0.1$                  | $k_d, NB_L \approx 0.1$                  |
| $NB_L$ ( $day^{-1}$ )<br>( $k_s^* NB_H NB_L \ll 1$ ) | $k_d, NB_L, k_s^* NB_H NB_L \approx 0.1$ | $k_d, NB_L, k_s^* NB_H NB_L \approx 0.1$ |

Table II.  
Kinetic Analyses of  $NB_H-Na$  Exchanges

|  | Wyodak-Shell 324M                         | Illinois #6-Shell 324M                     | Illinois #6-Amocat 1C<br>(No Ash Recycle)  | Illinois #6-Amocat 1C<br>(Ash Recycle)    |
|--|---|--|--|---|
| Limiting Case—<br>Preferential<br>Chemisorption      |   |  |  |   |
| $NB_H$ ( $day^{-1}$ )<br>( $k_s^* NB_H NB_L \ll 1$ ) | $k_d, NB_H, k_s^* NB_H NB_L \approx 0.02$ | $k_d, NB_H, k_s^* NB_H NB_L \approx 0.006$ | $k_d, NB_H, k_s^* NB_H NB_L \approx 0.006$ | $k_d, NB_H, k_s^* NB_H NB_L \approx 0.02$ |
| $Na$ ( $day^{-1}$ )<br>( $k_s^* NB_H NB_L \gg 1$ )   | $k_d, NB_H \approx 0.02$                  | $k_d, NB_H \approx 0.006$                  | $k_d, NB_H \approx 0.006$                  | $k_d, NB_H \approx 0.02$                  |

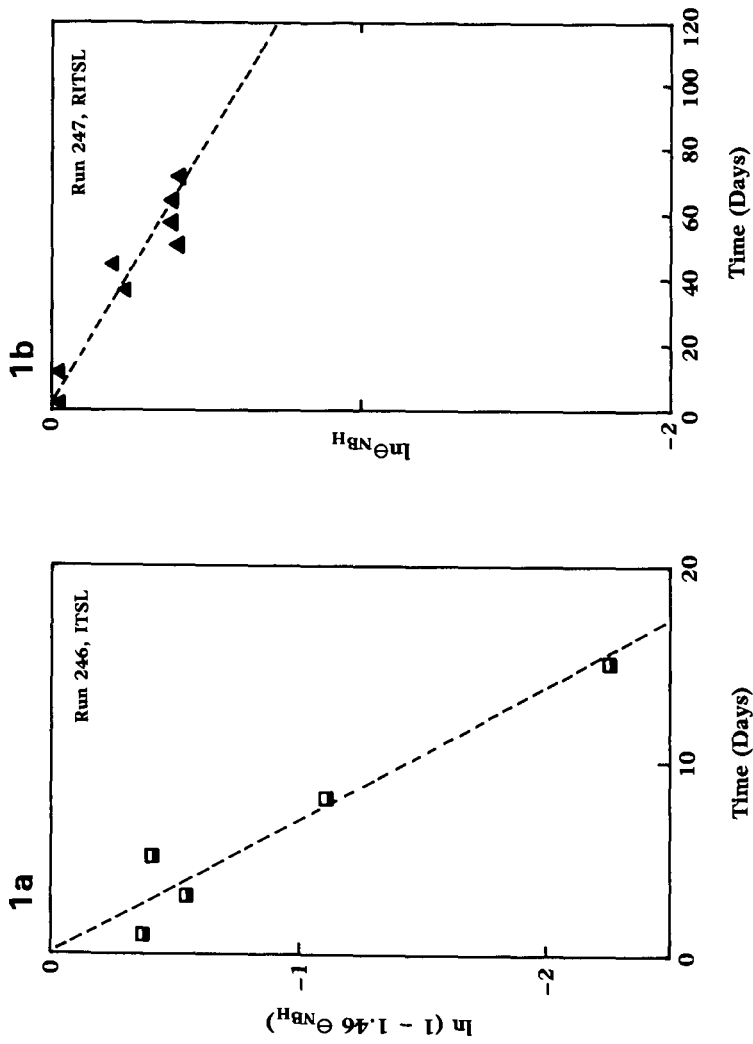


Figure 1a. Process data for the  $NB_L$ - $NB_H$  exchange fitted to equation (6).  
 Figure 1b. Data from the  $NB_H$ -Na exchange fitted to equation (8).

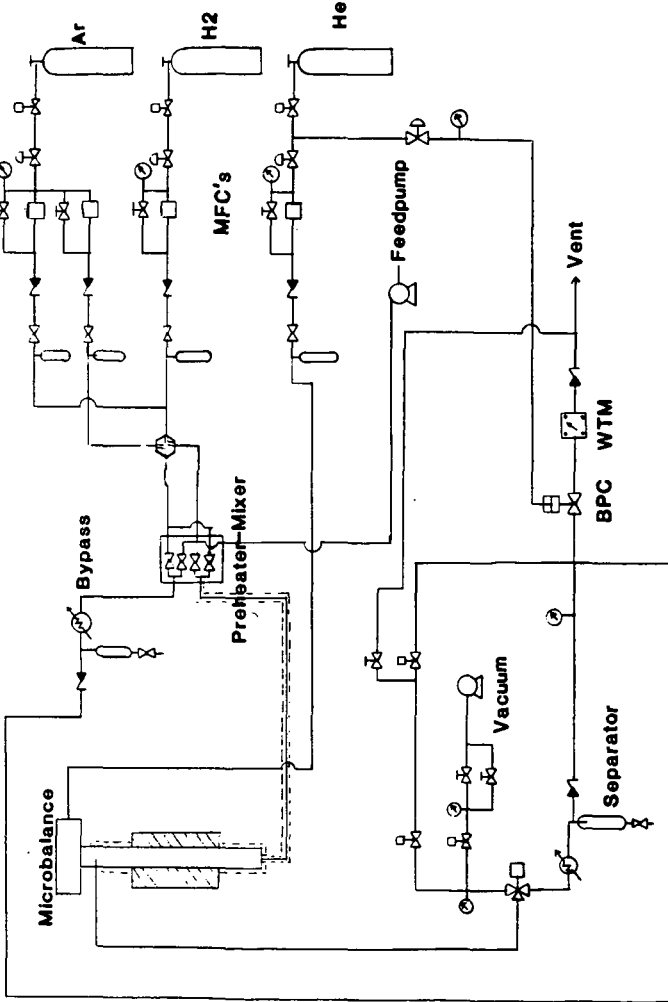


Figure 2. Schematic diagram of the high pressure gravimetric reactor system.

## EFFECT OF PORE STRUCTURE ON CATALYTIC COAL LIQUEFACTION

Young-Woo Rhee, James A. Guin, Christine W. Curtis

Auburn University  
Department of Chemical Engineering  
Auburn University, AL 36849

### Introduction

Considerable evidence for pore diffusional limitations in coal liquefaction has been reported in the literature (1-10). In this research catalysts having different pore structures were prepared using two methods, impregnation and coextrusion. The pore structures were controlled either by a sintering technique or by using combustible fibers (7). The initial activity of prepared catalysts was evaluated in coal liquefaction reactions with tetralin solvent. A model describing the relation between catalyst surface area and catalyst activity was developed by assuming 1) that every pore perfectly communicates and has a cylindrical shape, 2) that the pellet catalyst has a simple bimodal pore size distribution and 3) that a single first-order reaction occurs in the diffusion controlled region. For simplicity, reactant molecular size also was assumed to be uniform.

### Experimental Section

Catalyst Preparation. Catalysts were prepared using Catapal alumina (Vista Chemical Co.) and cellulose fiber (Avicel) using techniques similar to those used by Tischer (7). Ni and Mo were added by two methods: incipient wetness following calcination or prior to the extrusion process itself (coextrusion). Catalysts were presulfided prior to use. Catalysts were evaluated in 3/16 inch pellet form. The powder prepared by grinding the 3/16 inch pellets was also evaluated.

Catalyst Characterization. To measure the pore size distribution and apparent density of the extrudates, a Quantachrome Autoscan-33 porosimeter equipped with the Autoscan data reduction system was used. The maximum intrusion pressure of mercury was 33,000 psig, which corresponds to ca. 64 angstroms in pore diameter. Surface areas were obtained from a Quantasorb system using the multipoint BET method. Apparent density, macropore diameter and macropore volume of each catalyst were calculated from the mercury porosimeter data. True density, micropore diameter and total pore volume were obtained from a combination of pycnometer (water displacement), BET, and Hg porosimetry methods.

Coal Liquefaction. A horizontal welded tubing bomb microreactor of ca. 45 cc volume was used with the following reactants: 3 g Illinois #6 coal, 10 g tetralin, 1 g catalyst, and 1250 psig (cold) H<sub>2</sub>. The reactor was agitated at 425 °C for 60 min in a fluidized bed sand bath. Liquefaction products were classified as gases, oils (pentane soluble), asphaltenes (benzene soluble), preasphaltenes (soluble in a mixture of 10 vol.% methanol and 90 vol.% methylene chloride), and IOM (insoluble organic matter). Solubility fractions were expressed on a solvent-free basis.

## Results and Discussion

Characterization of Catalyst Pore Structure. Physical properties of laboratory prepared catalysts and supports are given in Table 1. A macropore is defined as a pore whose diameter exceeds 500 angstroms. Average pore diameters are calculated from the pore volume and BET surface area data by assuming cylindrical pores. Table 1 shows that the pore size distributions of unimodal 3/16" catalyst supports are dependent on the calcining temperature. As the calcining temperature increases, apparent density and average micropore diameter become larger, and surface area is reduced. This phenomenon results from a destruction of some micropores and reconstruction of macropores by a sintering process. Data for support D in Table 1 indicate that most micropores are destroyed and reoriented at high temperatures. Also, as shown in Table 1, the combustible fiber loading directly increases macropore volume and average macropore diameter.

Coal-Tetralin Reaction System. Catalysts shown in Table 1 were used in tetralin-coal reactions using both 3/16 inch pellets and their powder. The powder form of the catalysts, as shown in Table 2, gave the highest activity, indicating diffusional restrictions in the pellets. As shown in Table 2, calcining temperature had a direct effect on catalyst activity as evidenced by pentane-soluble oil yield. If the activity of the pellet catalysts is plotted versus the surface area, a maximal point in the catalyst activity exists. This interesting phenomenon results from a competition between the effective diffusivity and surface area. In a typical catalytic reaction of small molecules, an increase of surface area generally enhances catalyst activity. However, in a reaction of large molecules this increase can reduce the catalyst activity because of diffusional hindrance in the micropores. Thus, catalyst G, having the highest surface area of the unimodal catalysts, does not yield the most pentane soluble oils, due to the very small pore size and the hindered diffusion through these pores.

One way to increase pore accessibility without significantly reducing specific catalyst surface area is to introduce macropores. Using the technique of combustible fibers, we produced macroporous catalysts J, K, and L having high surface areas of 250-300 m<sup>2</sup>/g. When compared to unimodal catalysts, the bimodal catalysts (J and K in Table 3) give an oils fraction slightly greater than the best unimodal catalyst (I) in Table 2. An increase of fiber loading from 20 to 40 wt% has little additional effect on the activity.

Development of Model. In order to analyze the above results we developed a catalyst model similar to that of Froment and Bischoff (11), i.e. a parallel pore cross linked model with perfectly communicating pores.

For a first order irreversible diffusion controlled catalytic reaction the reaction rate per pellet volume is

$$\begin{aligned} r_v &= k C_s \eta \\ &= k C_s / \phi \\ &= S_x (k D_e)^{1/2} C_s / V_p \\ &= (S_x k_s^2 / V_p) (S_v D_e)^{1/2} C_s \end{aligned} \quad (1)$$

where  $S_v$  is the surface area per pellet volume, and  $D_e$  is the effective diffusivity.

From a material balance in a batch reactor, we obtain

$$-\frac{d(C_s)}{dt} = r_v V_{cat} = r_g W_{cat} = (r_v / \rho_c) W_{cat} \quad (2)$$

Solving eqs (1) and (2) together we obtain

$$\ln(C_s / C_{s0}) = -k' t \quad (3)$$

where  $k'$  is expressed as follows,

$$k' = \frac{S_x k_s^{1/2}}{V_p} \frac{V_{cat}}{(S_v D_e)^{1/2}} \quad (4)$$

or

$$k' = \frac{S_x k_s^{1/2}}{V_p} \frac{W_{cat}}{(S_g D_e / \rho_c)^{1/2}} \quad (5)$$

Equations 4 and 5 are useful for comparing catalyst activity in terms of physical properties such as porosity, density, pore sizes and pellet morphology. Equations (4) and (5) are most convenient when performing reactions using a constant catalyst volume or weight, respectively. In either case the first two terms remain constant if the catalyst shape and the amount of solvent are the same in each reaction.

As a very simple catalyst pore structure model, we adopt a model having only two sizes of cylindrical pores, denoted by radii  $R_1$  and  $R_2$ . Define the total porosity,  $\epsilon = \epsilon_1 + \epsilon_2$ , where  $\epsilon_1$  and  $\epsilon_2$  are void fractions of micro ( $R_1$ )- and macro ( $R_2$ )-pores.

From the definition,

$$\begin{aligned} S_v &= \text{surface area of pores / volume of pellet} \\ S_v &= 2 (\epsilon_1/R_1 + \epsilon_2/R_2) \end{aligned} \quad (6)$$

Introducing dimensionless variables  $\lambda_i = R_m/R_i$  where  $R_m$  is the reactant molecule size (radius),

$$S_v = (2 \epsilon/R_m) [(\epsilon_1/\epsilon) \lambda_1 + (\epsilon_2/\epsilon) \lambda_2] \quad (7)$$

$$S_g = (2 \epsilon/R_m/\rho_s) [(\epsilon_1/\epsilon) \lambda_1 + (\epsilon_2/\epsilon) \lambda_2]/(1 - \epsilon) \quad (8)$$

In a dimensionless form,

$$\langle S_v \rangle = \epsilon [(\epsilon_1/\epsilon) \lambda_1 + (\epsilon_2/\epsilon) \lambda_2] \quad (9)$$

$$\langle S_g \rangle = \epsilon/(1 - \epsilon) [(\epsilon_1/\epsilon) \lambda_1 + (\epsilon_2/\epsilon) \lambda_2] \quad (10)$$

In the hindered diffusion regime, the effective diffusivity  $D_e$  is

$$D_e = (\epsilon D_m / \tau) [(\epsilon_1 / \epsilon) K_{R1} K_{P1} + (\epsilon_2 / \epsilon) K_{R2} K_{P2}] \quad (11)$$

where the frictional resistance,  $K_{Ri}$  and partition factor,  $K_{Pi}$  are expressed as follows (12).

$$K_{Ri} = 1 - 2.104 \lambda_i + 2.09 \lambda_i^3 - 0.95 \lambda_i^5 \quad (12)$$

$$K_{Pi} = (1 - \lambda_i)^2 \quad (13)$$

Equation 11 assumes the tortuosity  $\tau$  is not a function of pore size.

In a dimensionless form,

$$\langle D_e \rangle = \epsilon [(\epsilon_1 / \epsilon) K_{R1} K_{P1} + (\epsilon_2 / \epsilon) K_{R2} K_{P2}] \quad (14)$$

Define  $k_v$  and  $k_g$  from equations 4 and 5 as follows:

$$k_v = (S_v D_e)^{1/2} \quad (15)$$

$$k_g = (S_g D_e / \rho_c)^{1/2} \quad (16)$$

In a dimensionless form,

$$\langle k_v \rangle = \langle S_v \rangle^{1/2} \langle D_e \rangle^{1/2} \quad (17)$$

$$\langle k_g \rangle = \langle k_v \rangle / (1 - \epsilon) \quad (18)$$

Substituting equations 9 and 15 into equations 17 and 18 gives

$$\langle k_v \rangle = \epsilon [(\lambda_1 \epsilon_1 / \epsilon + \lambda_2 \epsilon_2 / \epsilon) \times (\epsilon_1 / \epsilon K_{R1} K_{P1} + \epsilon_2 / \epsilon K_{R2} K_{P2})]^{1/2} \quad (19)$$

$$\langle k_g \rangle = \epsilon / (1 - \epsilon) [(\lambda_1 \epsilon_1 / \epsilon + \lambda_2 \epsilon_2 / \epsilon) \times (\epsilon_1 / \epsilon K_{R1} K_{P1} + \epsilon_2 / \epsilon K_{R2} K_{P2})]^{1/2} \quad (20)$$

where  $0 \leq \lambda_1 \leq 1$ .

**Model Application.** The batch reactions conducted in this work were performed with constant catalyst weight and thus eq (20) is most useful for activity comparison. The major difficulty with direct application of eq (20) is that the reactant molecule radius  $R_m$  is unknown and, of course, has a wide distribution in coal reactions. To circumvent this problem, we utilize the fact that for a unimodal catalyst ( $\epsilon_2=0$ ), eq (20) has a maximum at  $\lambda_1=0.18$  (12). This fact, together with the data of Table 2 showing an optimal micropore size of ca. 85 angstroms (catalyst I), can be used to define an approximate  $R_m$  of 15 angstroms. With this assumed value of  $R_m$ ,  $\langle k_g \rangle$  can be computed from eq (20) using the catalyst properties in Table 1. The results of these calculations are given in Table 4.

Comparison of  $\langle k_g \rangle$  values with pentane soluble oils yield as given in Table 4 shows reasonable qualitative agreement, in view of the many approximations

made, e.g. first order reaction, single molecule size, etc. The bimodal catalysts have a slightly higher activity in terms of oils yield, however, the effect is not great. Model calculations indicate that a major advantage of the bimodal catalysts may appear later during catalyst deactivation when pore sizes are reduced due to coke and metal deposits, and reactant diffusion becomes more hindered compared to the fresh catalysts.

### Nomenclature

|           |  |
|-----------|--|
| $C_s$     | Reactant concentration, mole/cm <sup>3</sup>   |
| $D_e$     | Effective diffusivity, cm <sup>2</sup> /s  |
| $D_m$     | Molecular bulk diffusivity, cm <sup>2</sup> /s   |
| $k$       | Reaction rate constant in equation 1, 1/s  |
| $k'$      | Reaction rate constant defined in equations 4 and 5, 1/s                               |
| $k_g$     | Reaction rate constant defined in equation 16, cm <sup>7/2</sup> /g/s <sup>1/2</sup> . |
| $K_p$     | Steric coefficient defined in equation 13  |
| $K_r$     | Frictional drag coefficient defined in equation 12                                     |
| $k_s$     | Surface reaction rate constant, cm/s   |
| $k_v$     | Reaction rate constant defined in equation 15, cm <sup>2</sup> /(g-s) <sup>1/2</sup>   |
| $R$       | Pore radius, cm  |
| $r_g$     | Reaction rate based on catalyst weight, mole/g-cc                                      |
| $R_m$     | molecule radius, cm  |
| $r_v$     | Reaction rate based on catalyst volume, mole/cc-s                                      |
| $S_g$     | Surface area per unit catalyst weight, cm <sup>2</sup> /g                              |
| $S_v$     | Surface area per unit catalyst volume, 1/cm  |
| $S_x$     | External surface area of pellet, cm <sup>2</sup> /g                                    |
| $V$       | Pore volume  |
| $V_p$     | Pellet volume, cc/g  |
| $V_{cat}$ | Catalyst volume per unit volume of liquid in reactor                                   |
| $W_{cat}$ | Catalyst weight per unit volume of liquid in reactor                                   |

### Greek Letters

|            |   |
|------------|---|
| $\epsilon$ | Porosity                                |
| $\lambda$  | Ratio of molecule radius to pore radius |
| $\rho_c$   | Pellet density, g/cc                    |
| $\rho_s$   | Catalyst solid density, g/cc            |
| $r$        | Tortuosity                              |
| $\phi$     | Thiele modulus                          |
| $\eta$     | Effectiveness factor                    |

### Subscripts

|   |           |
|---|-----------|
| 1 | micropore |
| 2 | macropore |
| o | initial   |
| t | total     |

### Symbol

|     |                     |
|-----|---------------------|
| < > | dimensionless group |
|-----|---------------------|

Acknowledgement: This work was supported by the U.S. Department of Energy as research conducted by the Consortium for Fossil Fuel Liquefaction Science under Contract No. UK-RF-42181687.

#### References

1. Ho, P. N., and Weller, S. W., Fuel Processing Technol., 4, 21 (1981).
2. Curtis, C. W., Guin, J. A., Kamajian, B. L., and Moody, T. E., Fuel Processing Technol., 12, 111 (1986).
3. Curtis, C. W., Tsai, K. J., and Guin, J. A., Ind. Eng. Chem. Research, 26, 12 (1987).
4. Alpert, S. B., Wolk, R. H., Maruhnic, P. and Chervenak, M. C., U.S. Patent 3,630,888 (Dec. 1971).
5. Shimada, H., Kurita, M., Sato, T., Yoshimura, Y., Kawakami, T., Yoshitomi, S., and Nishijima, A., Bull. Chem. Soc. Jpn., 57, 2000 (1984).
6. Tischer, R. E., Narain, N. K., Stiegel, G. J., and Cillo, D. L., J. Cat., 95, 406 (1985).
7. Tischer, R. E., J. Cat., 72, 255 (1981).
8. Nalitham, R. V., Lee, J. M., Lamb, C. W., and Johnson, T. W., Fuel Processing Technol., 17, 13 (1987).
9. Shimura, M. Shiroto, Y., and Takeuchi, C., Ind. Eng. Chem. Fundam., 25, 330 (1986).
10. Guin, J. A., Tsai, K. J., and Curtis, C. W., Ind. Eng. Chem. Process Des. Dev., 25, 515 (1986).
11. Froment, G. F. and Bischoff, K. B., "Chemical Reactor Analysis and Design," Wiley, New York, 1979.
12. Ruckenstein, E. and Tsai, M.C. AIChE.J. 27 697 (1981).

Table 1. Physical Properties of Catalysts

| Catalyst Name                                  | Calcining Condition<br>(°C-hrs) | V <sub>t</sub> (cc/g) |                  | V <sub>1</sub> (cc/g) | V <sub>2</sub> (cc/g) | S <sub>g</sub> (m <sup>2</sup> /g) |     | ρ <sub>c</sub> (g/cc) | ρ <sub>s</sub> (g/cc) | d <sub>1</sub> (angstroms) | d <sub>2</sub> |
|--|---------------------------------|-----------------------|------------------|-----------------------|-----------------------|------------------------------------|-----|-----------------------|-----------------------|----------------------------|----------------|
|  |                                 | Hg                    | H <sub>2</sub> O |                       |                       | Hg                                 | BET |                       |                       |                            |                |
| <u>3/16" Supports used for Impregnation</u>    |                                 |                       |                  |                       |                       |                                    |     |                       |                       |                            |                |
| A  | 500 - 16                        | .43                   | .45              | .45                   | a                     | 240                                | 220 | 1.30                  | 3.09                  | 81                         | a              |
| B  | 750 - 16                        | .44                   | .43              | .43                   | a                     | 203                                | 161 | 1.29                  | 2.86                  | 106                        | a              |
| C  | 1000 - 16                       | .37                   | .34              | .34                   | a                     | 113                                | 97  | 1.50                  | 3.09                  | 142                        | a              |
| D  | 1200 - 16                       | .19                   | .20              | .01                   | .19                   | 5                                  | 3   | 1.98                  | 3.32                  | 500                        | 1832           |
| <u>Coextruded 3/16" Catalyst: no fiber</u>     |                                 |                       |                  |                       |                       |                                    |     |                       |                       |                            |                |
| G  | 500 - 16                        | .03                   | .40              | .39                   | a                     | 11                                 | 287 | 1.47                  | 3.50                  | 55                         | a              |
| I  | 580 - 16                        | .31                   | .42              | .42                   | a                     | 172                                | 197 | 1.49                  | 3.95                  | 85                         | a              |
| <u>Coextruded 3/16" Catalyst: 20 wt% fiber</u> |                                 |                       |                  |                       |                       |                                    |     |                       |                       |                            |                |
| J  | 500 - 16                        | .30                   | .47              | .41                   | .06                   | 98                                 | 301 | 1.29                  | 3.27                  | 56                         | 1560           |
| <u>Coextruded 3/16" Catalyst: 40 wt% fiber</u> |                                 |                       |                  |                       |                       |                                    |     |                       |                       |                            |                |
| K  | 500 - 16                        | .62                   | .80              | .40                   | .40                   | 110                                | 272 | .90                   | 3.19                  | 61                         | 2348           |
| L  | 580 - 16                        | .73                   | .81              | .42                   | .39                   | 156                                | 258 | .90                   | 3.33                  | 66                         | 2253           |

Note: V<sub>t</sub>: total pore volume measured by Hg or H<sub>2</sub>O intrusion  
V<sub>1</sub>: micropore volume from V<sub>t</sub>(H<sub>2</sub>O) - V<sub>2</sub>  
V<sub>2</sub>: macropore volume obtained from Hg porosimeter  
S<sub>g</sub>: specific surface area by Hg porosimeter or BET analysis  
ρ<sub>c</sub>: apparent density by Hg displacement  
ρ<sub>s</sub>: true density obtained from H<sub>2</sub>O pycnometry  
d<sub>1</sub>: average micropore diameter 4V<sub>1</sub>/BET micropore area  
d<sub>2</sub>: average macropore diameter 4V<sub>2</sub>/Hg macropore area  
a: no macropores

Table 2. Effect of Calcining Temperature on Product Distribution

| Catalyst Name                   | Catalyst Shape | Sintering Temperature (°C) | Product Distribution (wt.%) |      |             |                 | Coal Conversion (wt%) |    |
|---------------------------------|----------------|----------------------------|-----------------------------|------|-------------|-----------------|-----------------------|----|
|                                 |                |                            | Gases                       | Oils | Asphaltenes | Pre/Asphaltenes | IOM                   |    |
| None                            | ----           | ----                       | 7                           | 33   | 36          | 17              | 7                     | 94 |
| G                               | Pellets        | 500                        | 6                           | 41   | 23          | 14              | 16                    | 84 |
|                                 | Powder         | 500                        | 5                           | 72   | 8           | 5               | 10                    | 89 |
| I                               | Pellets        | 580                        | 6                           | 53   | 20          | 9               | 12                    | 88 |
|                                 | Powder         | 580                        | 6                           | 78   | 6           | 4               | 6                     | 94 |
| <u>Impregnated on support C</u> |                |                            |                             |      |             |                 |                       |    |
|                                 | pellets        | 1000                       | 7                           | 47   | 24          | 11              | 11                    | 88 |
|                                 | powder         | 1000                       | 6                           | 73   | 13          | 4               | 4                     | 95 |
| <u>Impregnated on support D</u> |                |                            |                             |      |             |                 |                       |    |
|                                 | pellets        | 1200                       | 6                           | 34   | 36          | 15              | 9                     | 90 |

Table 3. Effect of Fiber Loading on Product Distribution

| Catalyst Name | Fiber Loading (wt%) | Catalyst Shape | Product Distribution (wt.%) |      |             |                 | IOM | Coal Conversion (wt%) |
|---------------|---------------------|----------------|-----------------------------|------|-------------|-----------------|-----|-----------------------|
|               |                     |                | Gases                       | Oils | Asphaltenes | Pre/Asphaltenes |     |                       |
| G             | 0                   | Pellets        | 6                           | 41   | 23          | 14              | 16  | 84                    |
|               |                     | Powder         | 4                           | 72   | 9           | 5               | 10  | 89                    |
| J             | 20                  | Pellets        | 5                           | 55   | 19          | 9               | 12  | 87                    |
|               |                     | Powder         | 4                           | 77   | 6           | 5               | 8   | 91                    |
| K             | 40                  | Pellets        | 6                           | 57   | 16          | 8               | 13  | 87                    |
|               |                     | Powder         | 4                           | 76   | 6           | 5               | 9   | 91                    |

Table 4. Comparison of Model Catalyst Activity and Experimental Oil Yields

| Catalyst | $\lambda_1$ | $\lambda_2$ | $\epsilon_1$ | $\epsilon_2$ | $\langle S_g \rangle$ | $\langle k_g \rangle$ | Oils Yield (wt%) |
|----------|-------------|-------------|--------------|--------------|-----------------------|-----------------------|------------------|
| C        | .11         | a           | .52          | a            | .119                  | .281                  | 47               |
| D        | .03         | .0082       | .03          | .37          | .007                  | .065                  | 34               |
| G        | .27         | a           | .58          | a            | .373                  | .360                  | 41               |
| I        | .18         | a           | .62          | a            | .294                  | .452                  | 53               |
| J        | .27         | .0096       | .54          | .07          | .376                  | .442                  | 55               |
| K        | .25         | .0064       | .36          | .36          | .330                  | .730                  | 57               |

Note: a) Catalyst contains no macropores.

# HONDO ASPHALTENE DIFFUSION IN MICROPOROUS TRACK-ETCHED MEMBRANES

By

R.C. Sane and T.T. Tsotsis, Department of  
Chemical Engineering, University of Southern California  
Los Angeles, CA 90089

and

I.A. Webster, UNOCAL Science and Technology Division  
Unocal Corporation  
P.O. Box 76, Brea, California 92621

## 1. ABSTRACT

The configurational diffusion of asphaltenes isolated from Hondo crude has been examined. Diffusion studies were performed with track-etched membranes with pore diameters in the range 100A to 4000A. The asphaltene is perceived as a lumped compound, containing a molecular weight range of heteroatomic species. The asphaltene does not diffuse as a single species, but may delaminate before diffusion. We report on the interesting phenomenon of the Hondo asphaltenes' vanadium fragments diffusing in 100A pores more rapidly, than the same asphaltenes' nickel fragments. This phenomenon is shown to be consistent with some previously reported conjectures on the relative distribution of nickel and vanadium within the asphaltene micelle.

## 2. INTRODUCTION

During the refining of heavy oils, contaminants such as nickel, vanadium and nitrogen must be catalytically removed from the oil. In hydroprocessing the nitrogen is reduced to ammonia, while the nickel and vanadium deposit as sulfides within the pores of the catalyst. Better HDM catalyst design mandates a greater understanding of the diffusion of an oil's metallorganics in the catalyst. Most HDM reactions are strongly diffusion limited at commercial process conditions as evidenced by the rinded nickel and vanadium intra-catalyst pellet metal profiles measured by electron microprobe.

A large fraction of a resid's heteroatoms are complexed in the solubility class called asphaltenes. Asphaltenes are polyaromatic sheet-like structures of large size and molecular weight.

In an attempt to mimic the diffusive transport of whole oil asphaltenes within a catalyst's pores, we have investigated the diffusion of an asphaltene, dissolved in pure xylene, through porous membranes with a range of pore sizes. Our results clearly indicate:

- The lumped compound nature of asphaltenes i.e. they are a solubility class, and as such are comprised of a spectrum of molecular types, each exhibiting a different diffusion coefficient.
- Hindered diffusion of asphaltenes is an important transport mechanism in resid upgrading catalysts.
- The asphaltene exclusion principle operates at low pore diameters.

### 3. EXPERIMENTAL

Asphaltenes were isolated by n-pentane extraction from Hondo California crude oil. The crystalline like asphaltene powder was redissolved in xylenes to form a 5 weight percent asphaltene model feedstock. Diffusion experiments were conducted in a custom built stainless steel, agitated Wicke-Kallenbach type diffusion cell (1,2). The temperature was controlled at 45°C. The cell's two compartments were separated by polycarbonate membranes (PCM), whose pore size ranged from 100A to 4000A over the entire experimental sequence. The PCMs were purchased from from Nuclepore Corporation, Pleasanton, CA. PCMs are thought to simulate the porous structure of a catalyst, but in a highly idealized sense, since all tortuosity effects have been removed.

The experimental plan is outlined in Figure 1. The strategy was to use a single charge of the asphaltene solution in an experiment where the membrane pore diameter was initially held low i.e. at 100A. The batch-batch diffusion experiment was then monitored by removing samples for analysis from the low concentration (LC), initially pure xylene, side of the membrane.

After a predetermined time the experiment was temporarily suspended and the membrane changed to a larger pore diameter (in the sequence 150A, 300A and 4000A). Simultaneous with each membrane change the LC side has recharged with fresh xylene. The key point, however, is that the original asphaltene solution charge was carried through the entire experiment (Fig. 1), and permitted to lose asphaltene solute by successively recontacting it with pure xylene across increasing membrane pore diameters.

This experimental protocol permits us to examine the relative diffusion rates of the variously sized species which constitute an asphaltene.

Analysis of the LC side samples was performed by X-ray fluorescence for sulfur, nickel and vanadium, and by size exclusion chromatography (SEC) for molecular weight distributions. SEC data will be reported elsewhere.

#### 4. RESULTS and DISCUSSION

The data from the diffusion of Hondo asphaltenes across the range of pore diameters (100-4000A) tested, is depicted in Figs 2 to 4. Sulfur, vanadium and nickel concentrations on the LC side of the membranes are shown as a function of time.

This raw data has been manipulated to generate Fig 5 where the relative initial slope for each species (S,V,Ni) at each pore diameter has been plotted. In addition, Fig 6 is an expanded view of the low time results for nickel and vanadium through the 100A membrane.

This data permits us to form the following evaluation:

- HINDERED TRANSPORT. By following the n-pentane asphaltene isolation procedure, we isolated an oil solubility class, comprised of a spectrum of molecular types and sizes. In this communication we infer little about asphaltene structure but note that it is an ongoing endeavor of our work to reconstruct asphaltene macrostructure from asphaltene diffusion studies. Figures 2 to 4 demonstrate the hindered nature of the transport of asphaltenes in a typical upgrading catalysts' sized pores. The data in these Figures also strongly suggests that small pores could exclude larger asphaltenic fragments.
- DISTRIBUTION OF HETEROATOMS IN ASPHALTENE FRAGMENTS. A semi-quantitative assessment of the data can be made from Fig. 5 which depicts initial slopes of the concentration versus time data as a function of membrane pore diameter.

With respect to each of the three diffusing asphaltene heteroatoms, sulfur, nickel, and vanadium we note:

-Sulfur appears evenly distributed among the various asphaltene sub-fragments, as evidenced by the almost proportional increase in initial transport rate with pore diameter.

-Nickel seems to be concentrated in species with sizes between 150A and 300A since the increase in relative transport rates between these pore diameters is a factor of 8, whereas the increase

between 300A and 4000A is only by a factor of 1.4.

-Vanadium seems to be concentrated with smaller fragments as indicated by the steady increase in vanadium transport rates only up to the 300A pore diameter.

• LOCATION OF METAL COMPOUNDS WITHIN HONDO ASPHALTENE MICELLE.

Figure 6 depicts our initial LC side data for nickel and vanadium diffusing in 100A pores. The interesting observation is that at low times vanadium species cross the membranes while nickel species are excluded. This finding has important implications in residuum hydroprocessing catalyst design. Perhaps vanadium could be selectively removed from the oil by judiciously engineering the catalyst pore size to exclude nickel fragments. The results of Fig. 6 suggest two things:

-The vanadium atoms are complexed in organometallic fragments which are physically smaller than the asphaltene's nickel fragments, or,

-Within the asphaltene micelle the vanadium species are more concentrated on the periphery of the asphaltene micelle, than the nickel species. As the asphaltene may "onion-skin delaminate" prior to diffusion, more rapid transport of the vanadium species would be expected.

The latter explanation is consistent with the work of Larson and Beuther (3) who, from reactivity studies, suggested that the vanadium to nickel ratio is higher on the edge of an asphaltene, than in the asphaltene core.

This demonstrates how it may be possible to infer some information on asphaltene structure from basic diffusivity data.

5. CONCLUSIONS

In summary, we have examined the diffusion of n-pentane isolated asphaltenes from Hondo crude across porous membranes containing molecularly sized pores (Fig. 1) and conclude:

- asphaltanes can be viewed as a lumped compound containing a range of molecular weights.
- diffusion is hindered, and depends strongly on the relative size of asphaltene fragment size and pore diameter. (Figs. 2 to 4)

- Sulfur, nickel, and vanadium heteroatoms may concentrate in different molecular size ranges. (Fig. 5)
- With 100A sized pores, initial diffusion data showed permeation of vanadium, but not nickel (Fig. 6). From this observation, we made some inferences on catalyst design and asphaltene structure.

6. REFERENCES

1. Sane, R. C., Webster, I.A., and Tsotsis, T. T. "A study of asphaltene diffusion through unimodal porous membranes", Paper No. 14f presented at AIChE Annual Meeting, New York, New York, November 1987. Paper available through the Engineering Societies Library, United Engineering Center, 345 East 47th Street, New York, NY 10017.
2. Sane, R. C., Webster, I. A. and Tsotsis, T. T. in "Catalysis, 1987", Proc. 10th North American Meeting of the Catalysis Society, J. W. Ward (Editor), May 1987, San Diego, California, Pub. Elsevier, 1988.
3. Larson, O. A. and Beuther, H., "Processing aspects of vanadium and nickel in crude oils", PREPRINTS Div. Pet. Chem., ACS, 11 (2), 595 (1966).

FIGURE 1  
**EXPERIMENTAL SEQUENCE**

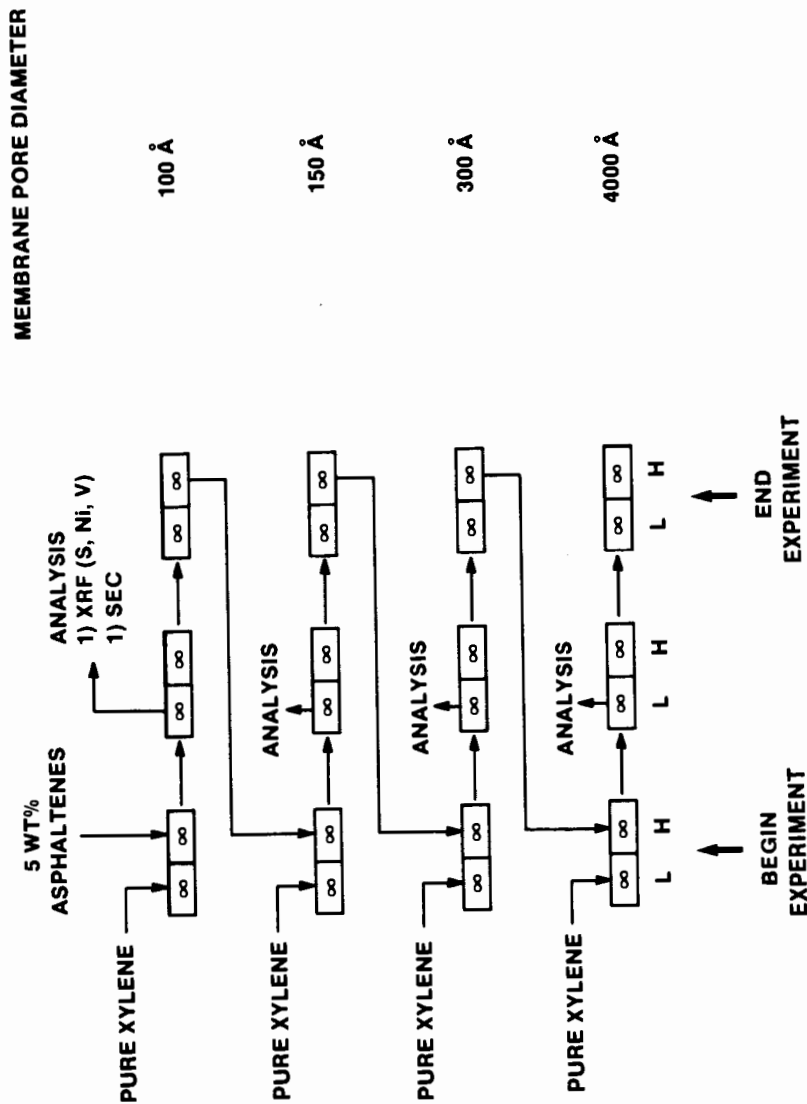


FIGURE 2: Low concentration side sulfur concentrations

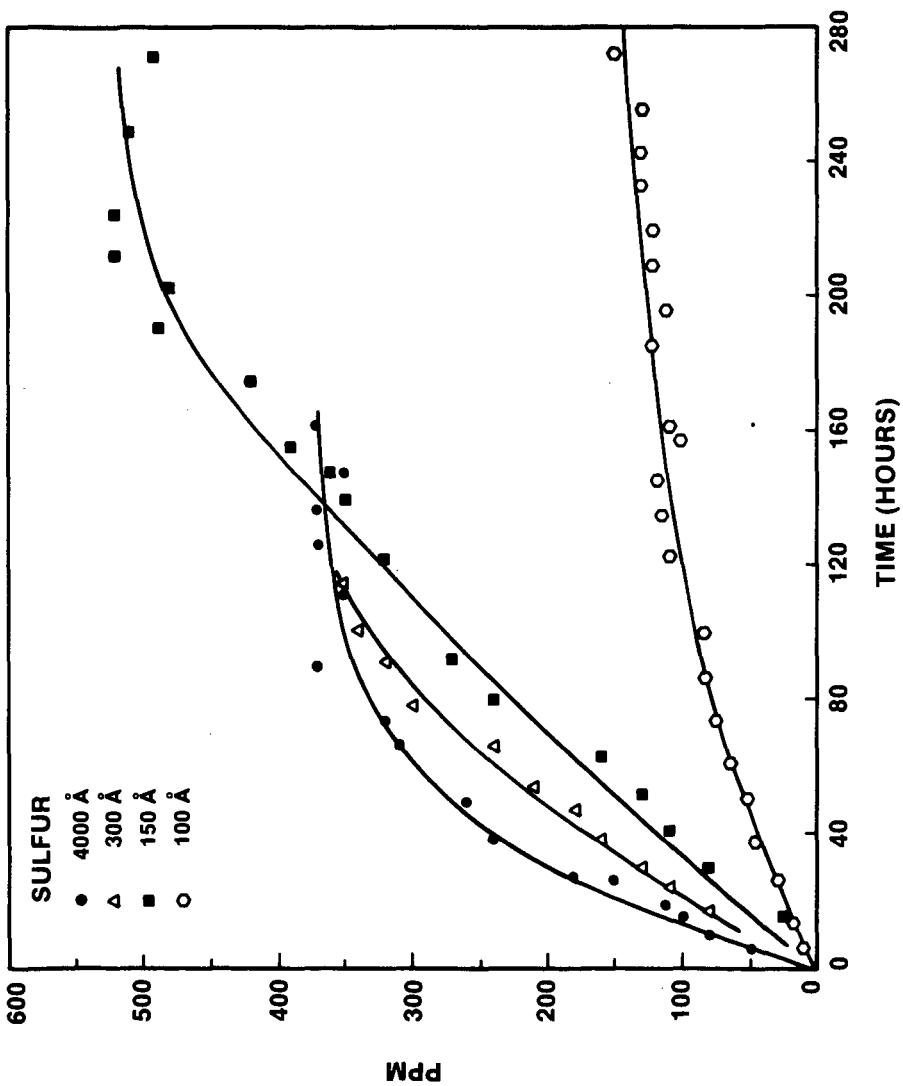


FIGURE 3: Low concentration side vanadium concentrations

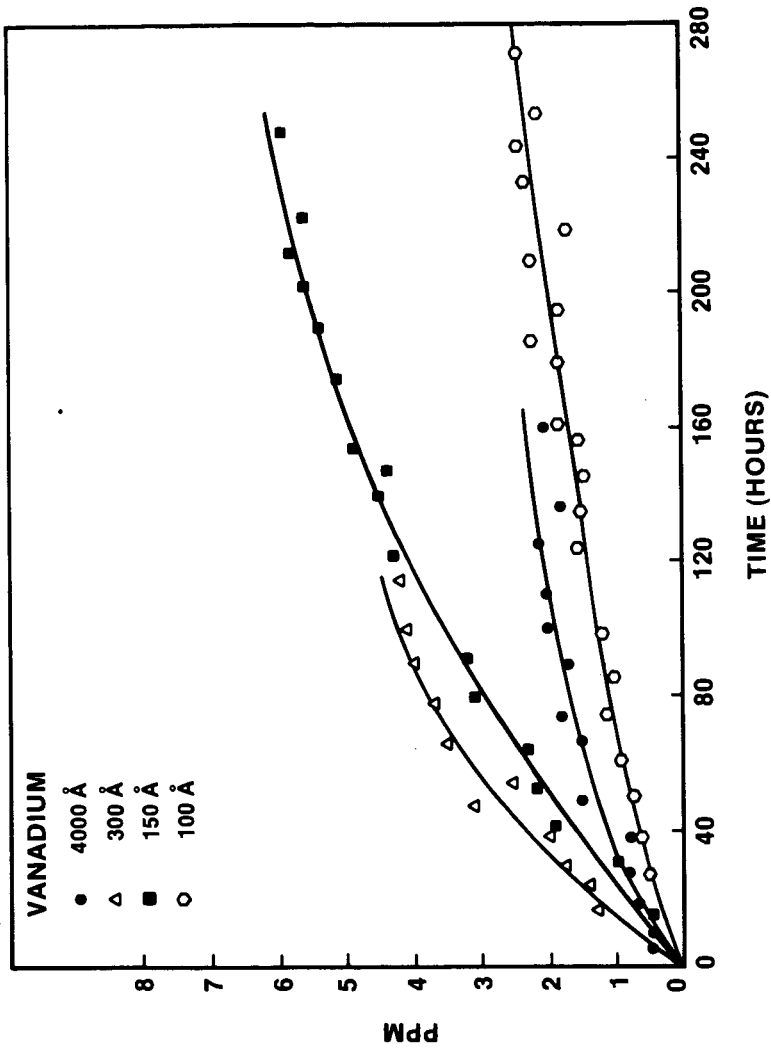


FIGURE 4: Low concentration side nickel concentrations

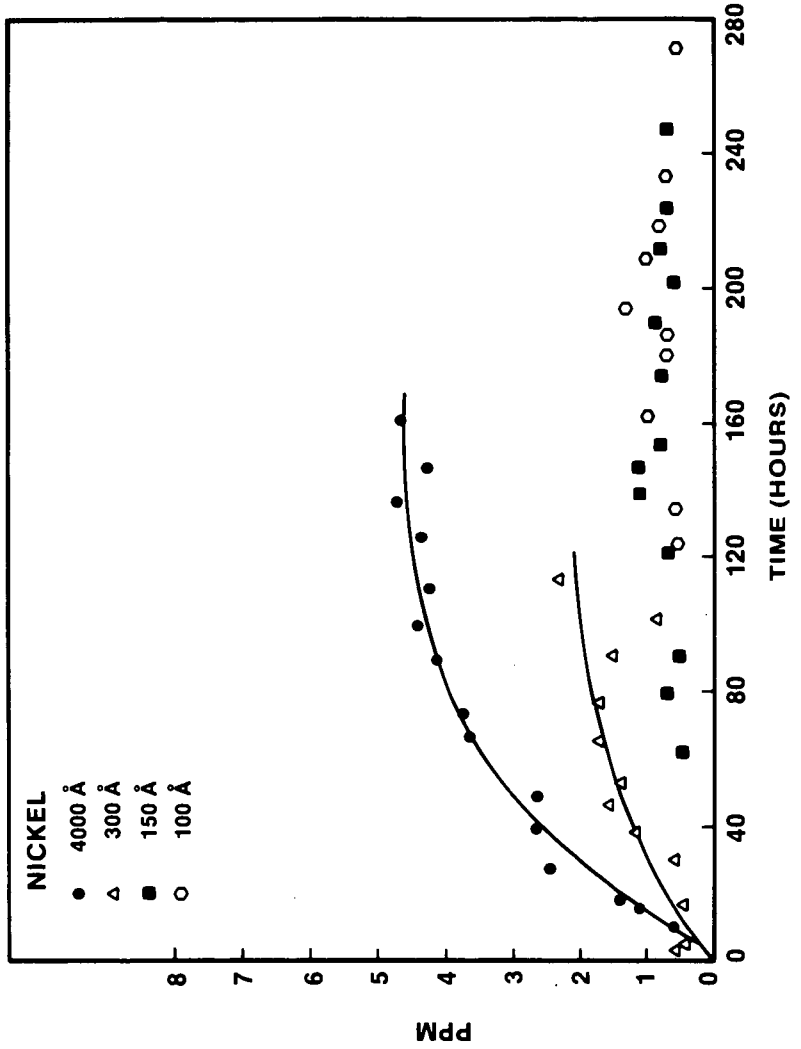


FIGURE 5  
RELATIVE INITIAL TRANSPORT RATES (PPM/HOUR)

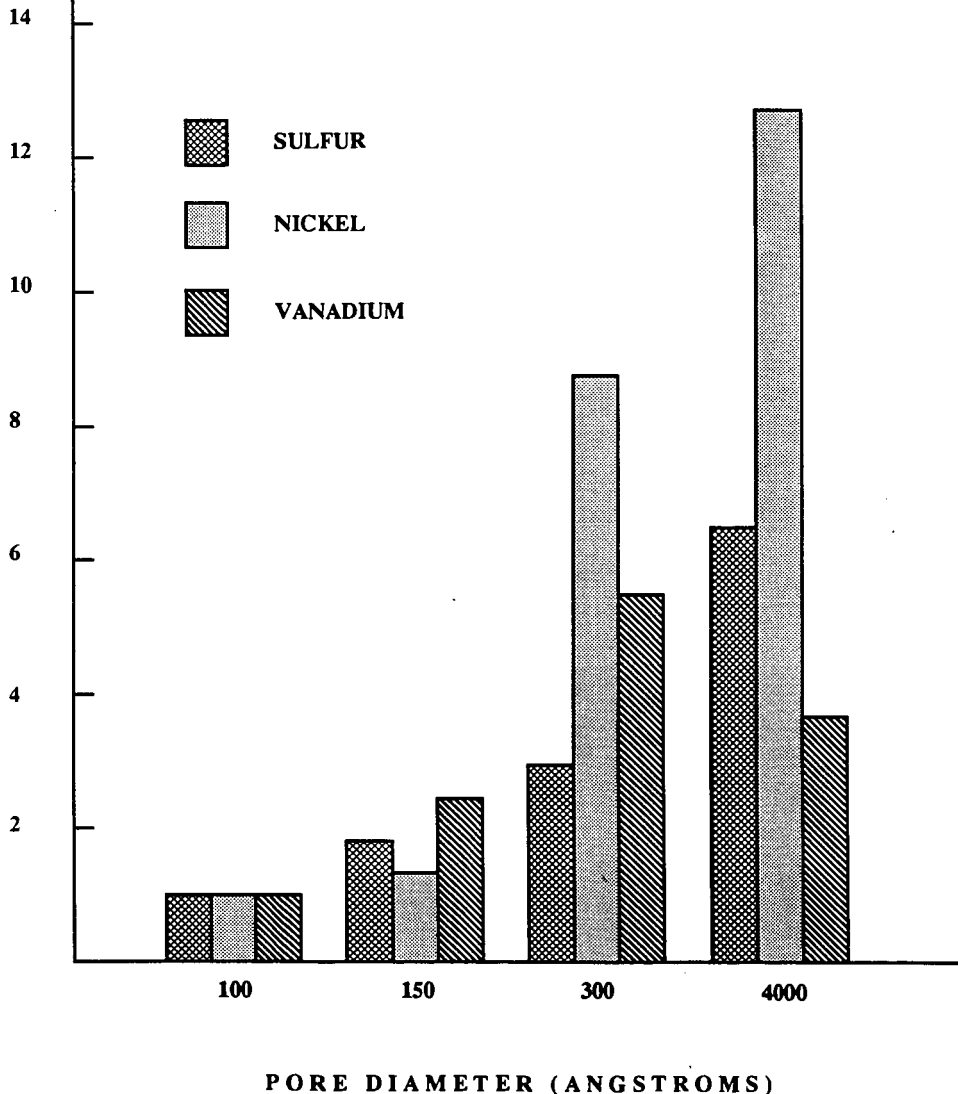
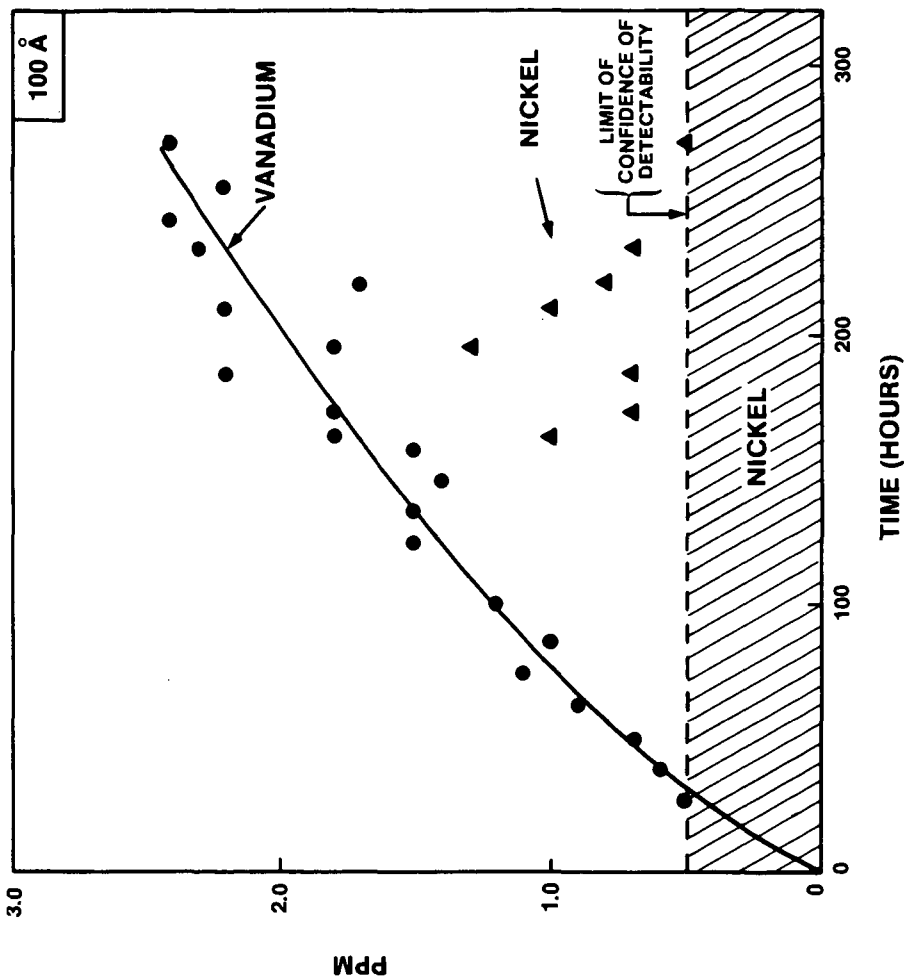


FIGURE 6: Low concentration side nickel and vanadium concentrations for 100A pore diameter membrane



## Deactivation of a Hydrogenation Catalyst: Importance of Mass Transfer

Arthur R. Tarrer, Hyon H. Yoon, Vinay P. Wagh  
Chemical Engineering Department, Auburn University, AL 36849

### Introduction

Over the past few years, a study for a private company has been ongoing at Auburn in parallel with its coal liquefaction program, that involves the development of a hydrogenation process using feedstocks that can be derived from coal. For economic reasons this hydrogenation process had to be done at low severity conditions, i.e., at low temperatures ( $\sim 100^{\circ}\text{C}$ ) and at low hydrogen partial pressures ( $\sim 100$  to  $200$  psi.). It was found that the hydrogenation could be done in the required low pressure and temperature ranges only after a variety of design and operational changes had been made to increase hydrogen gas/liquid mass transfer rates. A new hydrogenation reactor design was developed for the purpose of facilitating hydrogen gas/liquid mass transfer, such that gas compression requirements and gas (VOC) emissions could be kept a minimum.

In this research project, as in coal liquefaction processes, the need exists to reduce process severity by minimizing hydrogen partial pressure requirements. Reducing hydrogen partial pressures can change the relative rates of different reactions (condensation versus hydrogenation) and can result in catalyst deactivation and low conversions. The relative roles that gas/liquid mass transfer and transport mechanisms play in this is important. Design and operational changes can be made, as were done in the above work, to increase mass transfer rates and overcome limitations caused by the mass transfer. Whereas, limitations caused by kinetics, can be overcome by using a more active and selective catalyst. In reducing process severity, mass transfer related parameters and kinetic activity related parameters (e.g., catalyst activity/selectivity) must be changed simultaneously.

In the following discussion, first it will be shown that both a reduction in hydrogen partial pressure and an increase in temperature for the hydrogenation of a heavy coal-derived fraction (SRC) lead to catalyst deactivation. This reaction data for model compound hydrogenation at high severity conditions and at low severity conditions will be presented. In so doing, the responses in catalyst activity/deactivation to changes in kinetic and mass transfer parameters will be examined. A comparison will then be made between the observed responses and governing mechanisms at high severity conditions, and some conclusions will be drawn regarding the importance of mass-transfer parameters--particularly gas/liquid mass transfer--in maintenance of catalyst activity at low severity conditions.

### Effect of Hydrogen Partial Pressure and Temperature on Catalyst Activity/Deactivation

Coking is generally accepted to be the chief cause of catalyst deactivation during the hydrogenation of coal liquids. Like any other reaction, coking reactions proceed at a faster rate and to a greater extent at elevated temperatures. The effect of reaction temperature on deactivation rate has been studied here by measuring the activity of a hydrogenation catalyst (Shell 324 Ni-Mo-Al<sub>2</sub>O<sub>3</sub>) deactivated at different temperatures while hydrogenating a coal liquid (SRC fraction). Naphthalene hydrogenation activity is used here as an indicator of catalyst activity (1) and is given in terms of percent hydrogenation of the naphthalene. Percent hydrogenation (or catalyst activity) is plotted versus the coal liquid (SRC) hydrogenation temperature in Figure 1. As to be expected, present hydrogenation decreases rapidly with increasing temperature.

The effect of hydrogen partial pressure on the extent of deactivation is studied similarly by charging a microreactor with hydrogen at different pressures at room temperature. Naphthalene hydrogenation activity is plotted against reactor charge pressure in Figure 2. The plot shows that percent hydrogenation decreased as the hydrogen pressure in the reactor was decreased.

The above observation--that catalyst was deactivated to a greater extent at reduced hydrogen pressures--agrees with the findings reported for hydrotreating petroleum residue. Sie (2) found that the steady-state carbon level on a catalyst depends on the hydrogen partial pressure in the reactor; an approximate inverse linear relationship between these two parameters was observed. Similarly, in aromatizing cyclohexane, Ruderhausen and Watson (3) observed a linear relationship between the amount of carbon deposition and hydrogen partial pressure. Donath (4) observed that decalin splitting activity for a WS<sub>2</sub> catalyst was decreased considerably at lower pressures. A decrease in hydrogen partial pressure may cause a decrease in the amount of adsorbed hydrogen on the catalyst surface, due to lower mass transfer rates or because the dissolved hydrogen concentration in the reactant is lower, as will be discussed later. As a result, there would probably be an increase in the rate of condensation over that of hydrogenation. This would cause more coke formation at the lower hydrogen pressures.

### High Severity Hydrogenation Studies

In this section, naphthalene hydrogenation is used as a model reaction to demonstrate the relative importance of kinetic and mass-transfer parameters on catalyst activity/deactivation. It is to be shown that under high severity conditions, for certain catalysts, naphthalene hydrogenation follows an apparent first-order kinetics, depending on both naphthalene concentration and dissolved hydrogen concentration (i.e., hydrogen partial pressure). Also, gas-liquid mass transfer does not appear to have any significant influence on hydrogenation rates, and no significant deactivation appears to occur for this model reaction as long as the sulfide state of the catalyst is maintained.

A series of naphthalene hydrogenations were done in a microreactor at different hydrogen partial pressures. During hydrogenation, it was assumed that the hydrogen pressure was maintained constant at the mean value of the initial hydrogen pressure and the hydrogen pressure recorded at the end of the

reaction. Figure 3 gives a first-order plot relating hydrogen partial pressure to naphthalene conversion,  $x$ . Apparently, naphthalene rates vary with hydrogen partial pressure (thus, dissolved hydrogen concentration) in a first-order manner, under these conditions. The intrinsic rate constant,  $k$ , obtained from the slope of the figure for naphthalene hydrogenation on a presulfided CoMo/Al<sub>2</sub>O<sub>3</sub> catalyst at 380°C has a value of  $4.5242 \times 10^{-3}$  g liquid/(g catalyst min. psia of H<sub>2</sub>).

The reaction parameter used most often to evaluate the relative importance of gas-liquid mass transfer is agitation rate. Varying the agitation rate changes the observed reaction rate only when gas/liquid mass transfer is at least partially rate controlling (5). A plot of naphthalene conversion versus agitation rate is shown in Figure 4. A microreactor was used here. In the absence of steel balls, given by curve 1, the effect of agitation on conversion was marginal up to 500 cpm; however, there was a sudden increase in the conversion in the agitation range 500-550 cpm, and further increase in agitation had no significant effect on conversion which remained constant at about 40 percent. It should be noted that the drop in conversion in the low agitation range (<500 cpm) may be due to poor catalyst dispersion (6). Obviously, in the higher agitation range (>500 cpm), as was used in collecting the deactivation data with coal liquids shown earlier, Figure 1, gas/liquid mass transfer does not appear to be controlling (7).

Catalyst deactivation rate during naphthalene hydrogenation was evaluated by performing successive hydrogenations with a presulfided catalyst in the absence of CS<sub>2</sub> and in its presence. The catalyst activity in terms of percent hydrogenation is given in Figure 5. Since hydrogen was consumed in the hydrogenolysis of CS<sub>2</sub>, the amount of hydrogen in the reaction vessel had to be increased in order to maintain the amount of hydrogen available to the reaction at a level equivalent to those reactions without CS<sub>2</sub>. In the CS<sub>2</sub> reactions, the percent of excess hydrogen was 1340%, as compared to 1400% without CS<sub>2</sub>. The amount of CS<sub>2</sub> added was equivalent to five times the amount used ordinarily to sulfide shell 324 NiMo catalyst.

Apparently, the activity of the catalyst remained essentially constant in all the reaction cycles, with and without CS<sub>2</sub> added. The sulfur content of aged catalysts was measured after the final naphthalene hydrogenation in the successive reaction series. The fresh presulfided catalyst, presulfided/no CS<sub>2</sub> catalyst, and presulfided/CS<sub>2</sub> catalyst had sulfur contents of 8%, 7%, and 7.6% respectively. The presulfided/no CS<sub>2</sub> catalyst as well as the presulfided/CS<sub>2</sub> catalyst had a slightly lower sulfur content compared to that of the fresh presulfided catalyst. Also, the presulfided/no CS<sub>2</sub> catalyst had a slightly less wt.% sulfur than the presulfided/CS<sub>2</sub> catalyst. However, the activity of the presulfided catalyst was nearly the same in the presence as well as in the absence of CS<sub>2</sub>. It should be noted that the amount of bulk sulfur may not be a true indication of the extent of sulfiding. In summary, the data show that no significant catalyst deactivation occurred under the reaction conditions used here.

#### Low Severity Hydrogenation Studies

In all of the above hydrogenations, the reaction severity was relatively high (temp. >300°C, pres. > 800 psi H<sub>2</sub>). The hydrogenations to be considered in the following section were those done for a private company and were at

relatively low severity conditions. Here, again using model reactants (naphthalene and *o*-methyl styrene), it will be shown that gas/liquid mass transfer must be considered, because of the high catalyst activity. High catalyst activities are required here in order to attain high conversions under the low severity hydrogenation conditions. A comparison will be made between activities observed with a reactor having poor mass transfer characteristics and one having good mass transfer characteristics. By altering the reactor having poor mass transfer characteristics and making appropriate changes, activities are shown to improve and under these conditions--at which mass transfer becomes no longer controlling--no appreciable catalyst deactivation will be shown to occur.

Hydrogenation of naphthalene was performed at 90°C and 100 psi of H<sub>2</sub> at 25°C in a microreactor (Table 1). Six weight percent catalyst loading of Raney nickel 2800 was used. After 15 min of reaction naphthalene conversion was 100% to tetralin; no significant decalin formation was observed. Assuming first-order kinetics with respect to naphthalene concentration, the kinetic rate constant was about 0.8 min<sup>-1</sup> based on 15 min. of hydrogenation required to attain 100% conversion.

To study the influence of gas/liquid mass transfer on low severity naphthalene hydrogenation, a different type of reactor--a 300 cc. autoclave--was used. The gas/liquid mass transfer rates in this autoclave were known to be poorer than that in the microreactor used in the above studies. Figure 6 gives a plot of the mass transfer parameters  $k_L a$  versus the mixing parameter,  $M$ . These values were obtained using sulfite oxidation. The maximum  $k_L a$  values in the bubble column, the stirred tank, and the microreactor (TMBR) were 0.1, 0.25, and 3.8 s<sup>-1</sup>, respectively. Coefficients as high as 0.15 and 0.5 s<sup>-1</sup> have been reported in literature in bubble columns, and stirred vessels (Van't Riet, 1979), respectively, but none approached the value obtained here for the microreactor (TMBR). From Figure 6 it is observed that the gas-liquid mass transfer rate in the TMBR was roughly an order of magnitude greater than in the autoclave and the bubble column reactors (7).

A comparison is made in Table 2 between the naphthalene conversion observed in the microreactor (TMBR) and that in the 300 cc autoclave. In general, while performing the hydrogenation in the autoclave, a steady state catalyst activity could not be obtained. The reproducibility of the reaction rates was consequently poor. This was observed to be true also for low severity *o*-methyl styrene (AMS) hydrogenation at low severity conditions using a relatively high activity catalyst. With AMS, in the microreactor as well as the autoclave, the reaction rate was observed to increase with increased agitation, indicating that mass transfer resistances were the controlling factors (Table 3).

The following changes were made to improve the gas/liquid mass transfer rates in the autoclave: 1) baffles were installed 2) the hydrogen partial pressure was increased (100 to 600 psi) 3) toluene was used instead of hexadecane to reduce the reaction mixture viscosity 4) the maximum stirring rate (2800 rpm) was used. Once these changes were made, the naphthalene conversion was the same in the autoclave as it was in the microreactor. A series of hydrogenations were also made in the autoclave to evaluate catalyst deactivation (Figure 7). Under these conditions of high mass transfer rates, no significant catalyst deactivation was observed.

### Summary

Catalyst deactivation was observed to occur while hydrogenating coal liquids under high severity conditions. The rate of catalyst deactivation increased as the hydrogen partial pressure was reduced and as the reaction temperature was increased. For the model reactant naphthalene, however, under high severity conditions, no catalyst deactivation was observed to occur; gas/liquid mass transfer was not controlling; and the hydrogenation appeared to be kinetically controlled having a first-order dependency on dissolved hydrogen concentration (i.e. hydrogen partial pressure) and on naphthalene concentration. Under low severity conditions when a higher activity catalyst was required, on the other hand, mass transfer was observed to be controlling factor both for naphthalene and AMS hydrogenation. Also, with high mass transfer rates no significant catalyst deactivation was observed, but with low mass transfer rates significant catalyst deactivation was observed.

The implications of these observations are that mass transfer as well as kinetic related parameters must be addressed in searching for lower severity coal liquefaction processes. The observed catalyst deactivation with coal liquid hydrogenation cannot be attributed solely to kinetics--catalyst selectivity etc. Poor hydrogen mass transfer could have been a major factor in causing the observed deactivation, even though, for the model reactant naphthalene, mass transfer was not observed to be limiting. Many of the coal liquefaction reactions have higher hydrogenation rates than does naphthalene, and when the hydrogen transport mechanism is not able to meet these higher rate demands, deactivation can occur. To achieve lower severity conditions, higher activity catalysts are needed as was true here with naphthalene, and for higher activity catalysts, higher gas/liquid mass transfer rates are required to minimize deactivation. Higher mass transfer rates can be achieved as was shown here for naphthalene hydrogenation through reactor design changes and appropriate operational changes. In the study done for the private company referred to here, a novel reactor design was developed for their specific purpose.

### References

1. Nalitham, R. V., "Parameters and Kinetic Studies on Deactivation and Regeneration of Hydrotreating Catalysts in Solvent Refined Coal Upgrading Process and an Evaluation of the Liquid Vaporization Effects on Hydrotreater Performance." Dissertation, Auburn University, 1983.
2. Sie, S. T., "Catalyst Deactivation," Proceedings of the International Symposium, Elsevier Scientific Publishing Company, New York, NY, 557 (1980).
3. Rudershausen, C. G., and Watson, C. C., Chem. Eng. Sci., 3, 110 (1954).
4. Donath, E. E., Advances in Catalysis, Vol. VIII, Academic Press, New York, NY, 239 (1956).
5. Roberts, G. W., "The Influence of Mass and Heat Transfer on the Performance of Heterogeneous Catalysis in Gas/Liquid/Solid System." In Catalysis in Organic Synthesis, Academic Press, N.Y. (1976).
6. Shah, D. M., "Solvent Effects in Naphthalene Hydrogenation and Benzo thiophene HDS and Studies of Delayed Catalyst Contacting in Single Stage Coal Liquefaction." Thesis, Auburn University, (1982).
7. Gollakota, S. V., "An Investigation of Mass Transfer Phenomena in Coal Liquefaction: Assessment of Resistances and Reactor Types." Dissertation, Auburn University, (1984).

Table 1. Conversion of Naphthalene to Tetralin Using Raney Nickel 2800 and Different Reaction Times (Microreactor)

| Reaction time, min | Conversion of Naphthalene to Tetralin, area % |
|--------------------|---|
| 5                  | 31  |
| 15                 | 100   |
| 30                 | 100   |
| 60                 | 100   |
| 90                 | 100   |

Reaction Mixture:

Naphthalene - 0.3 g  
 Tetralin - 2.7 g  
 Raney Nickel - 0.1 g

Reaction Conditions:

Temperature - 90°C  
 H<sub>2</sub> Pressure - 100 psi at 25°C  
 Reactor Volume - 45 cc  
 Agitation - 860 cpm

1st Order Reaction Rate,  $k = 0.8 \text{ min}^{-1}$ , based on 15 minute reaction time.

Table 2. Comparison Between Naphthalene Conversion in Microreactor with High Mass Transfer Rates and in 300 cc Autoclave with Low Mass Transfer Rates.

| Reaction Time, min | Reactor Type | Conversion of Naphthalene, area % |
|--------------------|--------------|-----------------------------------|
| 15                 | Microreactor | 100                               |
| 60                 | Autoclave    | 65                                |

Reaction conditions were the same as those shown in Table 1.

Table 3. Molar Reaction Rates in Alpha-Methyl Styrene Hydrogenation

| RPM  | Autoclave<br>r, g-moles/hr.lit. | CPM  | TBMR<br>r, g-moles/hr.lit. |
|------|---------------------------------|------|----------------------------|
| 650  | 0.025                           | 400  | 0.75                       |
| 1050 | 0.3                             | 600  | 0.9                        |
| 1650 | 0.74                            | 800  | 1.15                       |
| 2150 | 0.84                            | 1000 | 1.5                        |
|      |                                 | 1200 | 1.75                       |

Experimental Conditions:

Temperature - 20°C  
 Catalyst loading - 13.1 g/l (TBMR)  
 - 6.6 g/l (Autoclave)

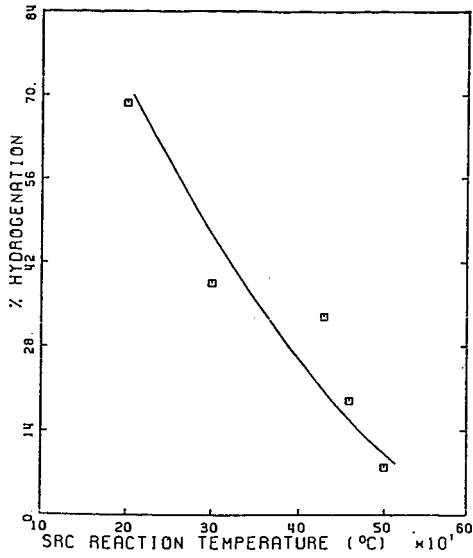


Figure 1. Effect of SRC Reaction Temperature on Catalyst Deactivation (NiMo/Al<sub>2</sub>O<sub>3</sub>). (1)

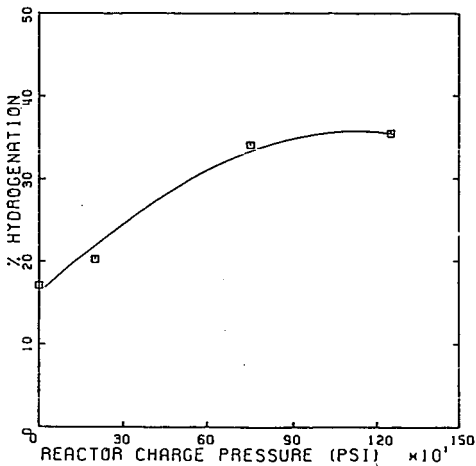


Figure 2. Effect of Hydrogen Pressure on Catalyst Deactivation (NiMo/Al<sub>2</sub>O<sub>3</sub>). (1)

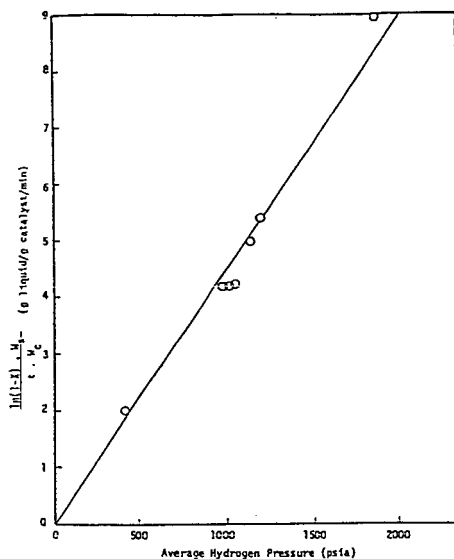


Figure 3. Effect of Hydrogen Pressure on Naphthalene Reaction Rate (CoMo/ $\text{Al}_2\text{O}_3$ ). (6)

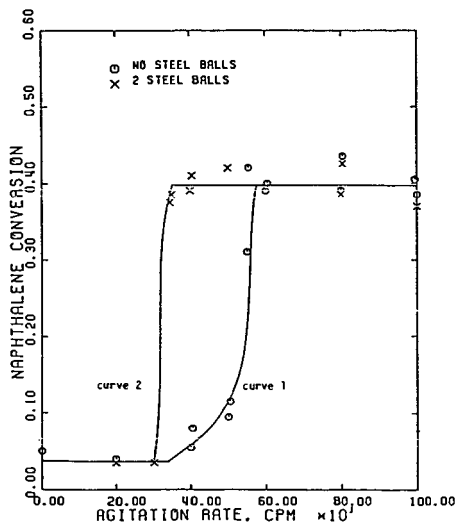


Figure 4. Naphthalene Conversion to Tetralin as a Function of Agitation Rate (CoMo/ $\text{Al}_2\text{O}_3$ ). (7)

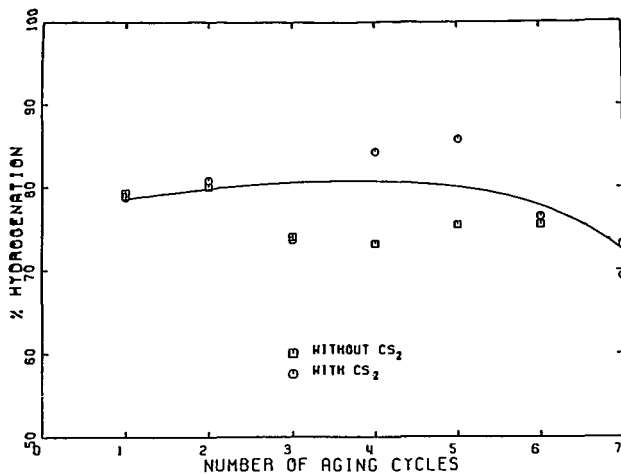


Figure 5. Comparison of the Activity of the Presulfided Catalyst in Successive Naphthalene Hydrogenation Reactions with/without the Addition of CS<sub>2</sub> (NiMo/Al<sub>2</sub>O<sub>3</sub>). (1)

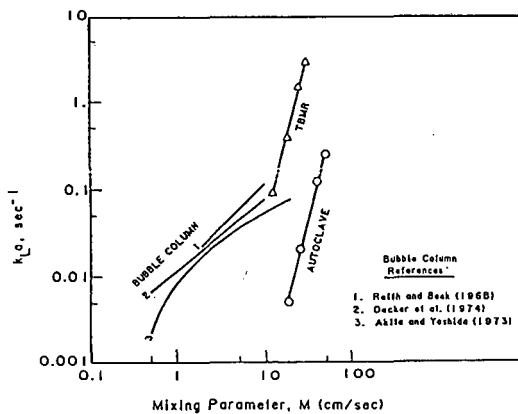


Figure 6. Comparison of  $k_{L,a}$  in different Reactor Types. (7)

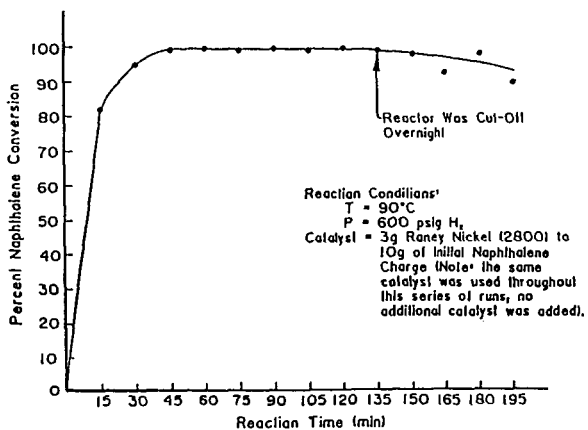


Figure 7. First Series, Batch Hydrogenation of Naphthalene to Tetralin in a 300 cc Autoclave.

## SPECTROSCOPIC STUDY OF CATALYSIS BY ZINC CHLORIDE OF COAL DEPOLYMERIZATION

H. Paul Wang, J.-P. Wann, and Edward M. Eyring

Department of Chemistry, University of Utah  
Salt Lake City, Utah 84112

### ABSTRACT

Diffuse reflectance infrared spectroscopy was used to monitor in situ reactions which ether groups undergo during the depolymerization of  $\text{ZnCl}_2$ -impregnated Wyodak coal at elevated temperatures. Subtraction procedures were used to obtain difference spectra that revealed small changes in IR band intensity between 2000 and 1000  $\text{cm}^{-1}$ . Evidence was obtained indicating that the  $\text{ZnCl}_2$ -impregnated coal samples could be depolymerized in an inert argon atmosphere. However, the degree of the cleavage of ether linkages catalyzed by  $\text{ZnCl}_2$  in an inert atmosphere is about 30 % of that in a high pressure hydrogen atmosphere (68 atm). The effect of solvent on impregnation of  $\text{ZnCl}_2$  in coal samples was also studied. A higher degree of cleavage of what appears to be a phenyl ether linkage was found for  $\text{ZnCl}_2$ -impregnated coal prepared in methanol compared to similar preparations in water and in acetone.

### INTRODUCTION

It is believed that ether oxygen plays an important role in linking the macromolecular units in coal. Wachowska and Pawlak [1] have indicated that ether groups represent the main linkages between aromatic clusters. Early works have shown that a catalyst such as  $\text{ZnCl}_2$  will promote the liquefaction of coal at temperatures below those at which pyrolysis can occur [2]. Mobley and Bell [3] noted that  $\text{ZnCl}_2$  may catalyze the cleavage of ether linkages and thereby promote a reduction in molecular weight.

The average chemical properties of coal have been widely studied using infrared spectroscopy. Recent improvements in the infrared techniques make it possible to measure the infrared spectra of coal powders in situ with the diffuse reflectance method. The present work was undertaken to determine the extent to which the cleavage of ether linkages is catalyzed by  $\text{ZnCl}_2$ . We have also applied this method to the study of the effect of solvent on impregnation of  $\text{ZnCl}_2$  in coal samples.

## EXPERIMENTAL

Reagent grade  $ZnCl_2$  (used as received) was impregnated on the THF preextracted Wyodak Coal from different solvent media such as methanol, water, and acetone. The  $ZnCl_2$ -impregnated coal samples (25% by weight of extracted Wyodak Coal) was then dried at 353 K overnight. Hydrotreatment of the coal samples were done in a tubing bomb reactor in high pressure hydrogen (68 atm) at 635 K.

Infrared spectra were recorded on a Digilab FT-IR spectrometer (FTS-40). For all spectra reported, a 64-scan data accumulation was obtained at a resolution of  $4\text{ cm}^{-1}$ . In order to observe small changes in band intensity, subtraction procedures were used to obtain difference spectra that more effectively compare spectra measured under various conditions. Almost identical base lines for infrared spectra measurements were also obtainable which facilitated calculation of the small spectroscopic changes between different samples using the subtraction method.

About 50 mg of each coal sample was dried at 373 K for one hour in the flowing argon (30 ml/min.) in a controlled environmental chamber (Spectra Tech Inc., Model No.0030-025) which was designed for diffuse reflectance infrared spectroscopy (DRIFTS) at elevated temperatures. In situ infrared spectra of coal samples were measured at temperatures ranging up to 723 K.

## RESULTS AND DISCUSSION

It is expected that the presence of the  $ZnCl_2$  catalyst during coal liquefaction may accelerate the cleavage of ether linkages (depolymerization) in the coal matrix. The C-O stretching vibrations between  $1265$  and  $1000\text{ cm}^{-1}$  [4] were investigated using in situ infrared spectroscopy. Figure 1 shows the difference infrared spectra obtained at three different temperatures in an inert argon atmosphere. Each spectrum is the difference between the infrared spectra obtained from the original and the  $ZnCl_2$ -impregnated (from acetone media) coal samples. The negative features between  $1265$  and  $1000\text{ cm}^{-1}$  in Figure 1 indicate that the cleavage of ether linkages (depolymerization) was catalyzed by  $ZnCl_2$ . The fact that the depolymerization occurred at a temperature as low as 493 K suggests the possibility of a low-temperature coal liquefaction process catalyzed by  $ZnCl_2$ . It should be noted that pyrolysis may occur at temperatures higher than 630 K. Furthermore, the negative features between  $1350$  and  $1500\text{ cm}^{-1}$  are in part due to  $CH_2$  and  $CH_3$  bending [4]. The negative feature occurring near  $1740\text{ cm}^{-1}$  is present because of the C=O stretching groups [4]. The present work focuses on the study of C-O stretchings in the infrared spectra measured since the formation of C-O bonding is not expected at our reaction conditions.

Generally, the objective of the pyrolysis of coal is to improve the tar/oil yield at the expense of char and gas formation. Thus it is important to study the redistribution of

the hydrogen available within the coal mass and the effect of the hydrotreatment on the depolymerization of coal. The depolymerization of coal samples was investigated in the presence of externally added hydrogen (68 atm). The comparison for the spectra of the depolymerization at 590 K between hydrotreated (573 K and 68 atm hydrogen) and non-hydrotreated coal samples (ZnCl<sub>2</sub> impregnated from acetone) is shown in Figure 2. Difference infrared spectra are used to reveal the net changes in the C-O stretching region. These spectra indicate that the degree of cleavage of ether linkages catalyzed by ZnCl<sub>2</sub> in an inert atmosphere is about 30% of that in a high pressure hydrogen atmosphere (68 atm).

The effect of solvent media used in the ZnCl<sub>2</sub> impregnation on depolymerization of coal samples is shown in Figure 3. The difference spectra were calculated by subtraction of the infrared spectrum of original coal measured at 590 K in the flowing argon from those of ZnCl<sub>2</sub>-impregnated coal samples prepared in media such as water, acetone, and methanol. A high degree of cleavage of what appears to be a phenyl ether linkage Ph-O-CH<sub>2</sub>-R (~1030 cm<sup>-1</sup>) was found for ZnCl<sub>2</sub>-impregnated coal prepared in methanol compared to similar preparations in water and in acetone. It seems that the dispersion of ZnCl<sub>2</sub> in the coal matrix depends on the media used in impregnation of the catalyst. Thus one should not underestimate the effect of the interactions between solvent media and functional groups of coal on the catalytic depolymerization process.

#### SUMMARY

The following conclusions have been reached on the basis of this work.

1. The subtraction routines used to obtain difference spectra can reveal small changes in the highly complex infrared spectra of coal.
2. ZnCl<sub>2</sub>-impregnated coal samples could be partially depolymerized in an inert argon gas atmosphere.
3. The degree of cleavage of ether linkages catalyzed by ZnCl<sub>2</sub> in an inert atmosphere is about 30% of that in a high pressure hydrogen atmosphere.
4. A higher selectivity in cleavage of a phenyl ether linkage was found for ZnCl<sub>2</sub>-impregnated coal prepared in methanol compared to similar preparations in water and acetone.

#### ACKNOWLEDGEMENTS

Financial support by the U. S. Department of Energy, Fossil Energy Division, through the Consortium for Fossil Fuel Liquefaction Science, Contract No. UKRF-4-21033-86-24, is gratefully acknowledged.

#### REFERENCES

1. H. Wachowska and W. Pawlak, Fuel, 1977, 56, 422.
2. R. E. Wood and W. H. Wiser, Ind. Eng. Chem., Proc. Design Dev., 1976, 15, 144.
3. D. P. Mobley and A. T. Bell, Fuel, 1979, 58, 661.
4. N. E. Cooke, O. M. Fuller, and R. P. Gaikwad, Fuel, 1986, 65, 1254.

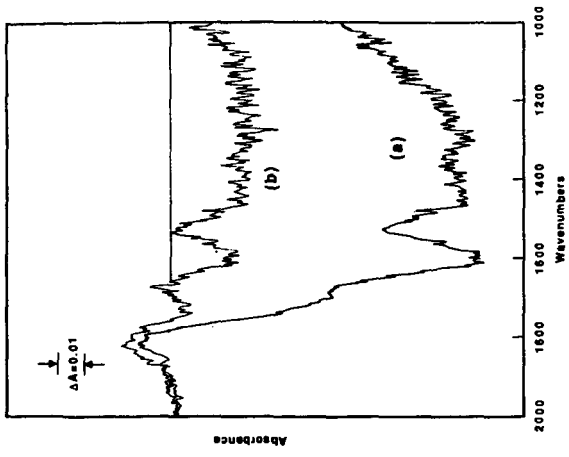


Figure 2  
Effect of Hydrotreatment on coal depolymerization.  
Difference spectra between original and hydrotreated (a)  
and non-hydrotreated (b) ZnCl<sub>2</sub>-impregnated coal samples.

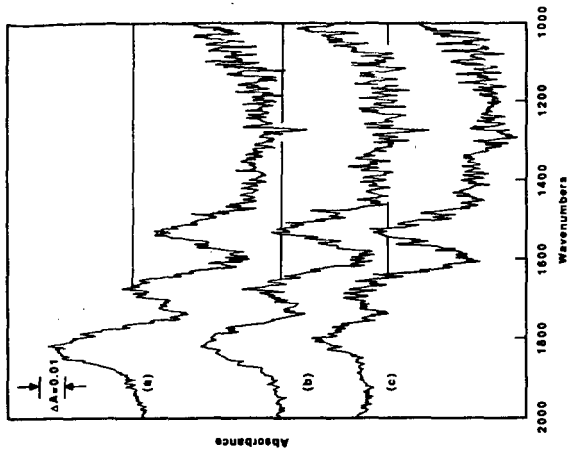


Figure 1  
Infrared difference spectra for coal depolymerization  
catalyzed by ZnCl<sub>2</sub>. Difference spectra measured  
between original and ZnCl<sub>2</sub>-impregnated wyodak coal at  
(a) 675 K, (b) 590 K, and (c) 493 K.

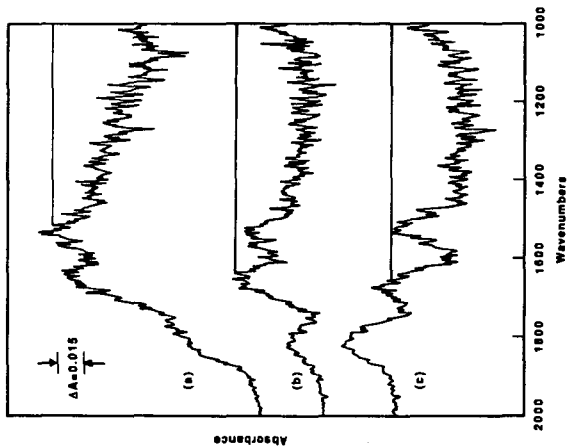


Figure 3  
Effect of solvent media used in impregnation of ZnCl<sub>2</sub> in coal samples on the coal depolymerization. Difference spectra between original and ZnCl<sub>2</sub>-impregnated coal (a) in methanol, (b) in water, and (c) in acetone.

CORRELATION OF BITUMINOUS COAL HYDROLIQUEFACTION ACTIVATION  
ENERGY WITH FUNDAMENTAL COAL CHEMICAL PROPERTIES

S.-C Shin, R.M. Baldwin\*, and R.L. Miller  
Chemical Engineering and Petroleum Refining Dept.  
Colorado School of Mines

ABSTRACT

The rate and extent of direct coal hydroliquefaction for 5 bituminous coals from the Argonne Premium Sample Bank have been measured. Data were obtained in batch microautoclave tubing bomb reactors at three temperatures (375, 400, 425 °C) and 5 residence times (3, 5, 10, 15, 40 minutes) in 1-methylnaphthalene vehicle under a hydrogen blanket. Data on rate of conversion of coal to THF and toluene solubles were modeled with a simple reversible rate expression, and activation energies for conversion to each solvent solubility class determined.

Data on carbon and proton distribution in the coals were obtained by  $^1\text{H}$ -NMR (Combined Rotational and Multiple Pulse Spectroscopy) and  $^{13}\text{C}$ -NMR (CPMAS/Dipolar Dephasing). A strong correlation of activation energy with the aliphatic hydrogen content of the coal was found for conversion to THF solubles. Toluene solubles activation energies were found to be highly correlated ( $R^2 > 90\%$ ) with total oxygen, and protonated aliphatic carbon.  $^{13}\text{C}$ -NMR data indicated a high degree of correlation between protonated aliphatic carbon and total oxygen for only the bituminous coals from the Argonne suite, suggesting the importance of etheric oxygen in crosslinking structures for determination of bituminous coal reactivity.

Introduction

The relationship between coal chemical and structural features and coal reactivity has been the subject of considerable research for well over 70 years, dating from the original observations of Bergius (1) regarding the influence of carbon content on hydroliquefaction yield. Early studies of the influence of coal properties on coal reactivity were focused on an attempt to find a single parameter or group of parameters capable of correlating physical, chemical, and geochemical properties with the degree of conversion to some solvent soluble products under a fixed set of reaction conditions (2-8). Given et al. (9-12) developed multiparameter statistical correlations for coal reactivity for an extensive suite of U.S. coals. These correlations were partitioned according to the geographical location of the coal in order to increase the significance of the relationships. Other researchers have attempted to correlate coal hydroliquefaction reactivity with the mineral matter in coal, most notably pyrite, and other physical and chemical properties (13-18). Neavel (19) and Furlong et al. (20) introduced the concept of using reaction rate as a reactivity parameter while Shin et al (21) attempted to combine reaction rate and reaction extent into a single reactivity parameter which could then be correlated to coal properties. Gutmann (22) correlated reaction rate constants with the sulfur content of lignite coals. Other reactivity

relationships based on information from instrumental techniques such as pyrolysis/mass spectrometry have been developed by Baldwin et al. (23).

All of the above attempts to relate coal liquefaction reactivity to coal properties have suffered from two severe limitations. First, the parameters employed as reactivity definitions have generally fallen into two categories: 1) reactivity as defined by a point-yield definition at fixed time and temperature (e.g. toluene solubles at 60 minutes, 450 °C) or; 2) reactivity as defined by a reaction profile with time at fixed temperature. While both of these "traditionally" used reactivity definitions can be correlated with liquefaction reactivity, the correlations developed are not truly universal in that they may not hold at different time and/or temperature levels. This point is demonstrated conclusively below. The second major limitation of prior studies is that the correlations have not been developed in terms of fundamental structural and chemical properties of coal. In many cases, derived coal properties such as volatile matter, fixed carbon, rank, heating value, etc. have been used as the independent variables in multi-parameter statistical models. As pointed out by Neavel (24), such correlations are of limited significance.

The above discussion highlights the need for a reactivity parameter that is independent of both time and temperature, yet which can be correlated with basic coal chemical properties. Further, detailed knowledge of the chemical structure of coal is needed so that the reactivity correlations developed have some significance in terms of the chemistry of the liquefaction process. We have attempted to address both of these problem areas by using activation energy as a reactivity definition, and by exploring the use of structural information from two new NMR techniques (<sup>1</sup>H-NMR/CRAMPS and <sup>13</sup>C-NMR/CPMAS with dipolar dephasing) which do permit determination of fundamental chemical structural features important in coal liquefaction reactivity.

#### Experimental

Five bituminous coals from the Argonne Premium coal collection were liquefied in 1-methylnaphthalene vehicle. Characterization data for the Argonne coals are shown in Tables 1 and 2. Experimental runs were carried out in batch tubing bomb microautoclave reactors at 375, 400, and 425 °C, and at 3, 5, 10, 15, and 40 minute residence times. All runs were performed in a hydrogen atmosphere under a cold pressure of 6.2 MPa. Data on the rate and extent of coal conversion to THF and toluene solubles were collected using a standard solvent fractionation procedure. Further details concerning experimental methods have been reported elsewhere (25).

The experimental program consisted of two phases. During the first phase, an examination of the effect of vehicle on the measured liquefaction reactivities was carried out using 3 aromatic compounds (1-methylnaphthalene, naphthalene, and phenanthrene). The second phase of the project concerned

measurement of the data, kinetic modeling, and correlation with coal properties.

Proton NMR data for the Argonne coals was obtained from the National Science Foundation Regional Center for NMR at Colorado State University, utilizing the technique of Combined Rotational and Multiple Pulse Spectroscopy (CRAMPS). Basic data on the proton distribution in these coals are shown in Table 3. Information on the carbon distribution via dipolar dephasing of  $^{13}\text{C}$ -NMR data was obtained from Dr. R.L. Pugmire at the University of Utah, and these data are presented in Table 4.

### Discussion of Results

Effect of Vehicle on Liquefaction Reactivity In order to properly evaluate and compare the inherent reactivities of different coals, a non-hydrogen donor liquefaction vehicle was required so that reactivity differences between similar coals within a given rank or sub-rank could be magnified. The first phase of this experimental program was thus concerned with an evaluation of the effect of three aromatic vehicles on relative reactivities. Liquefaction experiments were performed on the 5 Argonne bituminous coals in 1-methylnaphthalene (1-MN), naphthalene, and phenanthrene, and the relative reactivities of these coals assessed by toluene conversion at 5 and 40 minutes. Figure 1 presents the results of the 40 minute runs. These data clearly indicate that the relative reactivities are independent of choice of vehicle, and that conversions in 1-methylnaphthalene are equivalent to the other two aromatic vehicles. Data from the 5 minute runs led to similar conclusions. Because of the added ease of operation afforded by 1-MN, this material was utilized as the liquefaction vehicle in all subsequent experiments.

Rate Data and Modeling Rate data for conversion of the Argonne coals to THF and toluene solubles were measured. Reproducibility of the data was checked by performing duplicate experiments on the Illinois #6 coal. Various kinetic models were investigated for purposes of data fitting, including the following:

- first-order irreversible
- first-order reversible
- second-order irreversible
- second-order reversible
- first order (forward)/second order (reverse)
- Anthony-Howard model (26)

Rate data from the liquefaction experiments were fit to each of these models for all 5 coals, and model discrimination performed using a goodness-of-fit ( $R^2$ ) criterion. Statistical results from data fitting indicated that the best model overall from among these candidates was the first/second reversible model. The analysis of variance from regression modeling of the Illinois #6 coal (the replicated data set) gave very low values for the pure error mean square, indicating that the data were highly reproducible. A parity plot for toluene solubles conversion for Illinois #6 coal and the first/second-order reversible kinetic model is shown in Figure 2. As can be seen, the model provides a satisfactory descriptive expression for the data being observed.

Traditional Correlations As mentioned above, the traditional parameters that have been used for coal liquefaction reactivity correlations are point-yield conversion and a kinetic rate constant. We thus began our correlational efforts by exploring similar types of relationships. Figure 3 presents three correlations using the point-yield reactivity definition. Here, conversion to toluene solubles at 5 minutes is used as the yield parameter. As shown, a very strong correlation ( $R^2=98\%$ ) exists between toluene conversion at 5 minutes and  $425^\circ\text{C}$  and total oxygen plus total carbon in the coal. However if this same correlation is extended to a different time (40 minutes) at the same temperature, a much weaker correlation ( $R^2=61\%$ ) results. If the temperature is changed to  $375^\circ\text{C}$  while time is held constant (5 minutes), essentially no correlation ( $R^2=0$ ) exists. Figure 4 shows the same sort of effect, but using a kinetic constant (from the first/second model) as the reactivity parameter. A very strong correlation is found at  $425^\circ\text{C}$  between the rate constant for conversion to THF solubles and the total carbon content of the coal ( $R^2=94$ ). Since the rate constant is time independent, this is a valid reactivity parameter as long as the temperature is not altered. However, if the temperature is reduced to  $400$  and then to  $375^\circ\text{C}$ , the same correlation weakens significantly and then disappears, with  $R^2$  falling to 54% and 12% respectively at the lower temperatures. This graphically illustrates the inadequacy of both of these "traditional" reactivity parameters, which are either time and/or temperature dependent.

The above discussion demonstrates the need for a reactivity parameter that is time and temperature independent. This leads logically to consideration of activation energy as a fundamental reactivity parameter, since:

- activation energy includes temperature effects;
- activation energy should reflect more closely the chemical nature of the parent coals;
- activation energy is obtained by measuring time and temperature effects, but the result is time and temperature independent.

Activation Energy Correlation Intuitively, the behavior noted above might be interpreted as a shift in the controlling mechanism for the liquefaction reaction, with one type of chemical functionality dominating the reaction at one set of conditions. This would be accompanied by a gradual shift to different reaction pathways and hence different chemical functionalities at other temperatures and times. This concept of a distribution of reaction pathways was the basis for the development of the Anthony-Howard model (26). However, when this expression was applied to our rate data little variation in the derived activation energies between the different coals was found. A strong dependency of the derived activation energies with coal type was found, however, for the first/second rate model. These data are presented in Table 5. Exceedingly good fits to the expected Arrhenius temperature dependency were found for the toluene and THF rate constants, as indicated by the

coefficients of determination ( $R^2$ ) in Table 5. It is important to recognize that these activation energies are not fundamental parameters, but the large differences in activation energies found for these 5 coals suggest that this parameter should be useful as a relative reactivity indicator.

Before initiating correlation of reactivity with coal properties, it is important to determine which of the coal characteristics available are independent parameters, and which are highly correlated with other characteristics and thus are simply derived properties. Eight coal characteristics, including basic data from proximate and ultimate analysis along with the proton NMR (CRAMPS) information, were first investigated in this manner. Volatile matter and total carbon were found to be strongly correlated with aliphatic carbon content, while total carbon was found to be highly correlated with carbon aromaticity. Total sulfur, ash, and aromatic (and hence aliphatic) hydrogen content of the coal were found not to be related with any of the other properties of the coal.

Table 6 presents the results of correlation of the liquefaction activation energies for the 5 bituminous coals with the independent coal properties. The activation energy for coal conversion to toluene solubles was found to be strongly ( $R^2=93\%$ ) correlated with the total oxygen content of the coal, while the activation energy for conversion to THF solubles was found to be highly correlated ( $R^2=95\%$ ) with aliphatic hydrogen content. These correlations are shown graphically in Figures 5 and 6. Correlation of activation energies for conversion to toluene and THF solubles were not found to be highly correlated with any of the other coal properties in Table 6, suggesting that the relationships found between reactivity and these two coal properties are unique.

Data from the  $^{13}\text{C}$ -NMR were next investigated, and simple single-parameter correlations of these properties with THF and toluene activation energies attempted. Intercorrelations between the various  $^{13}\text{C}$ -NMR properties and other coal characteristics were first investigated in a manner similar to the above. The only intercorrelation found from this data set was for total oxygen and protonated aliphatic carbon ( $\text{sp}^3$ -hybridized and  $\text{CH}$  or  $\text{CH}_2$ ). The correlation between these two parameters for the 6 Argonne bituminous coals (including Blind Canyon) was almost 99%, however when the data for the subbituminous and lignite coals was added, the correlation no longer held. These data are shown graphically in Figure 7. This finding may have strong implications with respect to coal structure, and the differences in reactivity found between low rank and high rank coals in general. The activation energy for conversion to toluene solubles was found to be very highly correlated ( $R^2=93\%$ ) with protonated aliphatic carbon. No other correlations of coal properties from the  $^{13}\text{C}$ -NMR data and toluene or THF activation energies were found.

The strong intercorrelation found between protonated aliphatic

carbon and total oxygen for the 6 bituminous Argonne coals can be interpreted structurally in terms of etheric groups in the cross-linking structures between aromatic clusters. While based on a rather limited data set, this relationship and the correlation found between total oxygen and toluene activation energy would seem to suggest that the carbon-oxygen bonds in crosslinking structures are of extreme importance in determining coal reactivity. Data from the  $^{13}\text{C}$ -NMR also provides an estimate of the relative abundance of etheric carbon-oxygen structures (All-O in Table 4). However, when this parameter is correlated with the toluene activation energy a less than adequate ( $R^2=77\%$ ) relationship is found as shown in Figure 8. One coal (Stockton) in this data set represents a significant outlier, and if this coal is removed from the regression, the adequacy of the relationship improves to 97%. Due to the limited number of coals in this study, these observations and conclusions must be treated as tentative at this time. Further research on a wider suite of bituminous coals is needed.

#### Acknowledgements

This research was supported by the U.S. Department of Energy under grant no. DE-FG22-85PC80907. The authors would also like to acknowledge the contributions of Dr. Ronald J. Pugmire and his group at the University of Utah ( $^{13}\text{C}$ -NMR data) and Dr. Charles Bronnmann at the NSF Regional Center for NMR ( $^1\text{H}$ -NMR data) at Colorado State University. Dr. Shin would like to express his gratitude to the Ministry of Energy and Resources, Seoul, Korea.

#### References Cited

1. Berguis, F., Jour. Gasbeleucht. (1912), 54
2. Francis, W., FUEL (1932), 11, 171
3. Petrick, A.J., Gaigher, B., and Groenewoud, P., Jour. Chem. Met. Min. Soc. South Africa (1937), 38
4. Wright, C.C., and Sprunk, G.C., Penn State College Min. Ind. Exp. Sta. Bull. (1939), 28
5. Fisher, C.H., Sprunk, G.C., Eisner, A., Clarke, L., Fein, M.L., and Storch, H.H., FUEL (1940), 19, 132
6. Shatwell, H.G., and Graham, J.L., FUEL (1925), 4, 25
7. Horton, L., Williams, F.A., and King, J.G., Dept. Sci. and Ind. Res. (1936), Fuel Research Tech. Paper 42
8. Fisher, C.H., Sprunk, G.C., Eisner, A., O'Donnell, H.J., Clarke, L., and Storch, H.H., U.S. Bureau of Mines (1942), Tech. Paper 642
9. Given, P.H., Cronauer, D.C., Spackman, W., Lovell, H.L., Davis, A., and Biswas, B., FUEL (1975), 54, 34
10. \_\_\_\_\_, FUEL (1975), 54, 40
11. Abdel-Baset, M.B., Yarzab, R.F., and Given, P.H., FUEL (1978), 57, 89
12. Yarzab, R.F., Given, P.H., Spackman, W., and Davis, A., FUEL (1980), 59, 81
13. Mori, K., Tanfuchi, M., Kawashima, A., Okuma, O., and Takahashi, T., ACS Div. Fuel Chem. Preprints (1979), 24, no. 2
14. Durie, R.A., ACS Div. Fuel Chem. Preprints (1979), 24, no. 2

15. Gray, D., Barrass, G., Jezko, J., and Kershaw, J.R., FUEL (1980), 59, 146
16. Mukherjee, D.K., and Chowdhury, P.B., FUEL (1976), 55
17. Guin, J.A., Tarrer, A.R., Prather, J.W., and Johnson, D.R., Ind. Eng. Chem. Proc. Des. and Devel. (1978), 17, 118
18. Gray, D., FUEL (1978), 57
19. Neavel, R.C., FUEL (1976), 55, 237
20. Furlong, M.W., Baldwin, R.M., and Bain, R.L., FUEL (1982), 61
21. Shin, S-C., Baldwin, R.M., and Miller, R.L., Energy and Fuels (1987), 1, 377
22. Gutmann, M., Radeck, D., Konig, M., and Kell, G., Proc. Int. Conf. Coal Science (1987), 187
23. Baldwin, R.M., Durfee, S.L., and Voorhees, K.W., Fuel Proc. Tech. (1987), 15, 281
24. Neavel, R.C., FUEL (1986), 65, 312
25. Shin, S-C., M.S. Thesis no. T-3267 (1988), Arthur Lakes Library, Colorado School of Mines
26. Anthony, D.B., and Howard, J.B., AIChE Jour. (1976), 22, 625

Table 1. Characterization Data of Argonne Premium Coals  
(Elemental & Proximate Analysis)

| Coal Seam         | State | Rank | Elemental Analysis* |     |    |      | Proximate Analysis** |      |      |
|-------------------|-------|------|---------------------|-----|----|------|----------------------|------|------|
|                   |       |      | C                   | H   | O  | Stot | Ash                  | V.M  | F.C  |
| Illinois #6       | IL    | HVB  | 77                  | 5.7 | 10 | 5.4  | 14.8                 | 35.4 | 44.7 |
| Pittsburgh #8     | PA    | HVB  | 83                  | 5.8 | 9  | 1.6  | 9.7                  | 34.9 | 53.6 |
| Lewiston-Stockton | WV    | HVB  | 81                  | 5.5 | 11 | 0.6  | 20.1                 | 28.6 | 49.4 |
| Upper Freeport    | PA    | MVB  | 87                  | 5.5 | 4  | 2.8  | 13.1                 | 25.1 | 60.7 |
| Pocahontas #3     | VA    | LVB  | 91                  | 4.7 | 3  | 0.9  | 5.3                  | 17.1 | 77.1 |

\* All the values are given based on wt % (d.a.f basis), except for sulphur which is in dry wt %. These data furnished by Argonne National Laboratory, Argonne, Illinois.

\*\* All the values are given based on as received basis (wt %). These data measured by Huffman Laboratories, Inc., Golden, Colorado

Table 2. Characterization Data of Argonne Premium Coals  
(Carbon-13 N.M.R and Proton N.M.R)

| Coal Seam         | State | Rank | Carbon-13 N.M.R.* |        | Proton N.M.R. ** |       |        |        |
|-------------------|-------|------|-------------------|--------|------------------|-------|--------|--------|
|                   |       |      | C-tot             | C-arom | C-alip           | H-tot | H-arom | C-alip |
| Illinois #6       | IL    | HVB  | 6.42              | 4.42   | 2.00             | 5.7   | 2.74   | 2.96   |
| Pittsburgh #8     | PA    | HVB  | 6.92              | 5.17   | 1.75             | 5.8   | 2.21   | 3.59   |
| Lewiston-Stockton | WV    | HVB  | 6.75              | 5.00   | 1.75             | 5.5   | 1.68   | 3.82   |
| Upper Freeport    | PA    | MVB  | 7.25              | 5.92   | 1.33             | 5.5   | 2.10   | 3.40   |
| Pocahontas #3     | VA    | LVB  | 7.58              | 6.75   | 0.83             | 4.7   | 2.57   | 2.13   |

\* All the values based on moisture and ash-free atomic basis (wt % divided by m.w of carbon). Aromaticity data measured by Utah University using C-NMR (CPMAS). These data were furnished by Dr. Ronald Pugmire.

\*\* All the values based on moisture and ash-free atomic basis (wt % divided by m.w of hydrogen). Proton NMR data measured by NSF Regional NMR Center (Colorado State University, Fort Collins, Colorado) using H-NMR (CRAMPS).

Table 3. Aliphatic and Aromatic Hydrogen Contents of Argonne Coals: Proton-NMR (CRAMPS)

| coal           | aromatic H<br>(%) | aliphatic H<br>(%) |
|----------------|-------------------|--------------------|
| Illinois #6    | 48.0              | 52.0               |
| Pittsburgh #8  | 38.1              | 61.9               |
| Stockton       | 30.6              | 69.4               |
| Upper Freeport | 38.2              | 61.8               |
| Pocahontas     | 54.6              | 45.4               |

Proton spectra obtained at a proton Larmor frequency of 187 MHz using a BR-24 pulse sequence. The 90 pulse width was 1.1 us and the cycle time of 36 tau was 108 us. Samples were spun at the magic angle at a nominal rate of 2 KHz.

Spectra measured by the National Science Foundation Regional NMR Center, Colorado State University, Fort Collins, Co.

Table 4. Carbon Structural Distribution of the Argonne Coals

|                      | Illi #6 | Pitt #8 | Stockton | Upper F. Pocahontas |
|----------------------|---------|---------|----------|---------------------|
| Aliphatic-total(SP3) | 28%     | 28%     | 25%      | 19%                 |
| Ali-H                | 18      | 13      | 18       | 8                   |
| Ali-N                | 10      | 15      | 7        | 11                  |
| (Ali-O)              | (5)     | (3)     | (4)      | (2)                 |
| Aromatic-total(SP2)  | 72%     | 72%     | 75%      | 81%                 |
| Aro-Ring             | 72      | 72      | 75       | 81                  |
| Aro-R-H              | 26      | 27      | 27       | 28                  |
| Aro-R-N              | 46      | 45      | 48       | 53                  |
| Aro-R-N-P            | 6       | 6       | 5        | 4                   |
| (Aro-R-N-A           | 18      | 17      | 21       | 20                  |
| Aro-R-N-B            | 22      | 22      | 22       | 29                  |
| Aro-Carbonyl         | 0       | 0       | 0        | 0                   |

Ali-H=fraction of total carbon that is sp<sup>3</sup>-hybridized and CH or CH<sub>2</sub>.  
 Ali-N=sp<sup>3</sup>-hybridized and CH<sub>3</sub> or nonprotonated, Ali-O=sp<sup>3</sup>-hybridized and bonded to oxygen. Aro-R-H=sp<sup>2</sup>-hybridized and protonated.  
 Aro-R-N=sp<sup>2</sup>-hybridized and nonprotonated, Aro-R-N-P=sp<sup>2</sup>-hybridized and phenolic or phenolic ether, Aro-R-N-A=sp<sup>2</sup>-hybridized and alkylated, Aro-R-N-B=sp<sup>2</sup>-hybridized and at a bridgehead position.

Data on carbon distribution obtained from Dr. R.J. Pugmire, University of Utah.

Table 5. Activation Energies of 5 Bituminous Argonne Coal

| Coal Seam         | Toluene solubles |              | THF solubles |              |
|-------------------|------------------|--------------|--------------|--------------|
|                   | E (Kcal/m)       | R-Square (%) | E (Kcal/m)   | R-Square (%) |
| Illinois #6       | 20.9             | 99.8         | 17.5         | 99.5         |
| Pittsburgh #8     | 15.5             | 95.2         | 24.5         | 96.3         |
| Lewiston-Stockton | 26.8             | 94.3         | 29.5         | 98.3         |
| Upper Freeport    | 9.9              | 97.0         | 20.1         | 99.3         |
| Pocahontas #3     | 4.3              | 100          | 7.5          | 98.3         |

Table 6. Correlation of Activation Energy with Coal Properties

o Adjusted Coefficient of Determination (%)

| Coal Property | Activation Energy<br>(toluene solubles) | Activation Energy<br>(THF solubles) |
|---------------|---|-------------------------------------|
| C-aliphatic   | 64.8                                    | 32.0                                |
| C-aromatic    | 67.9                                    | 21.9                                |
| H-total       | 23.8                                    | 42.4                                |
| H-aliphatic   | 32.5                                    | 95.1<br>-----                       |
| O-total       | 93.2<br>-----                           | 36.2                                |
| S-total       | 0.0                                     | 0.0                                 |
| Ash           | 72.8                                    | 37.1                                |
| H-tot/C-tot   | 50.7                                    | 29.2                                |
| O-tot/C-tot   | 91.6                                    | 29.9                                |
| O-tot + C-tot | 27.4                                    | 0.0                                 |
|               |   |                                     |

Figure 1. Solvent Effect on Reactivity Ranking  
(Reaction Time: 40 min)

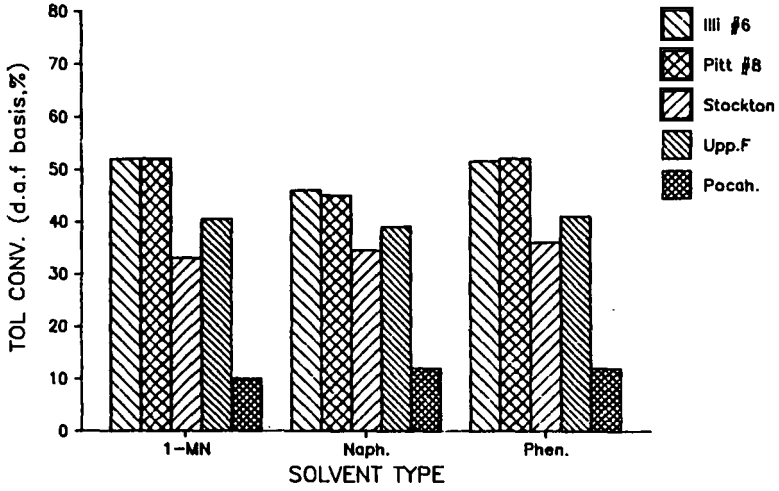


Figure 2. Parity Plot (toluene solubles)

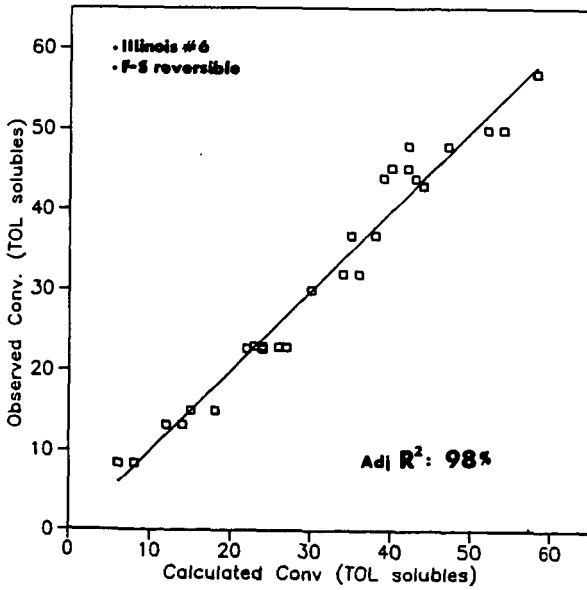


Figure 3. Example I

Point-Yield Reactivity vs. Total C+O

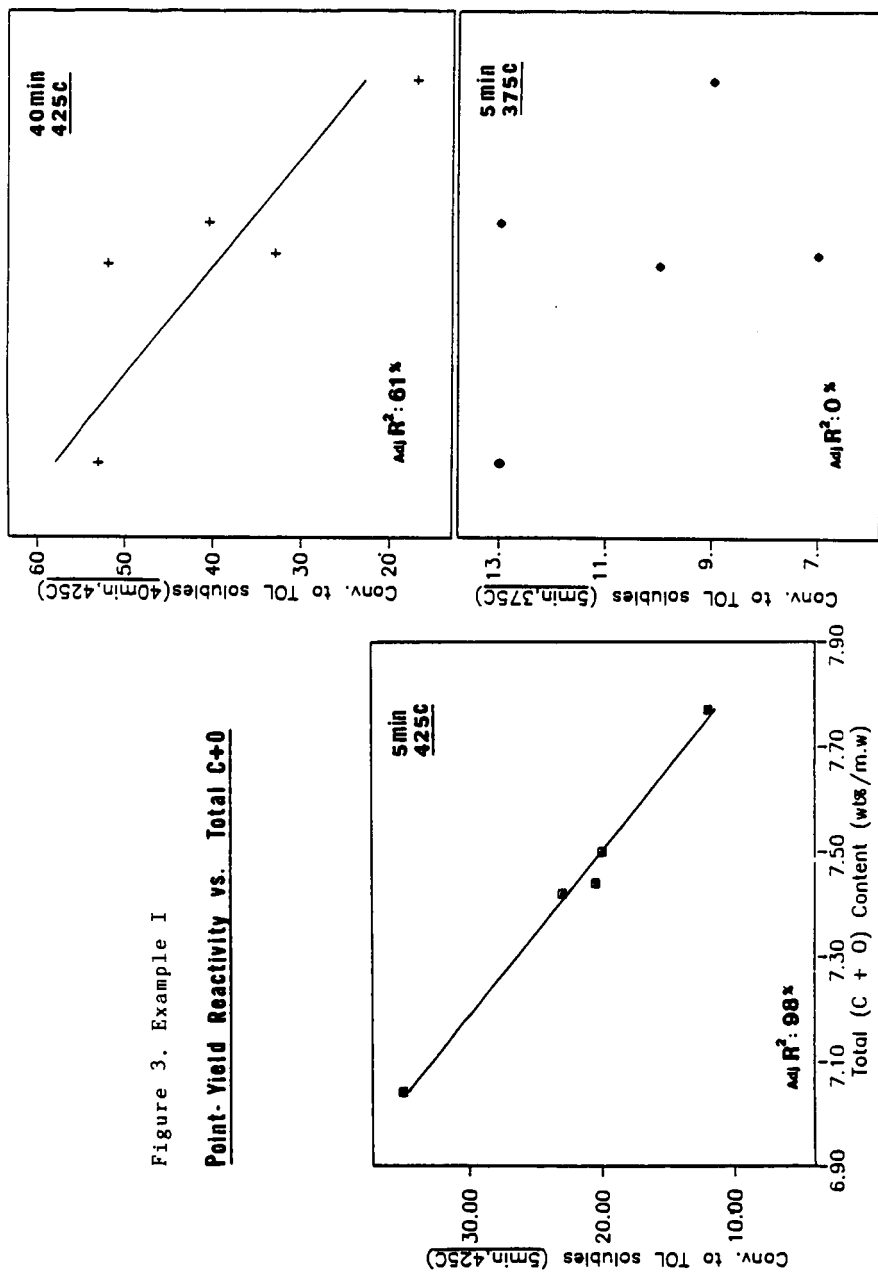


Figure 4. Example II  
Kinetic Constant vs. Total Carbon

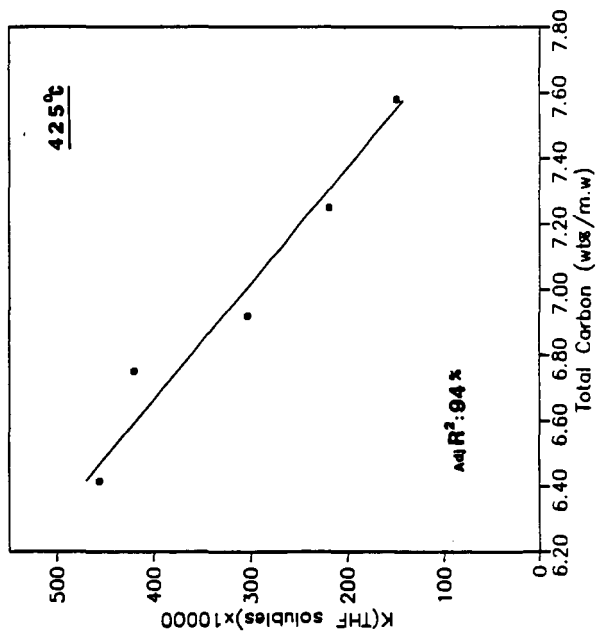
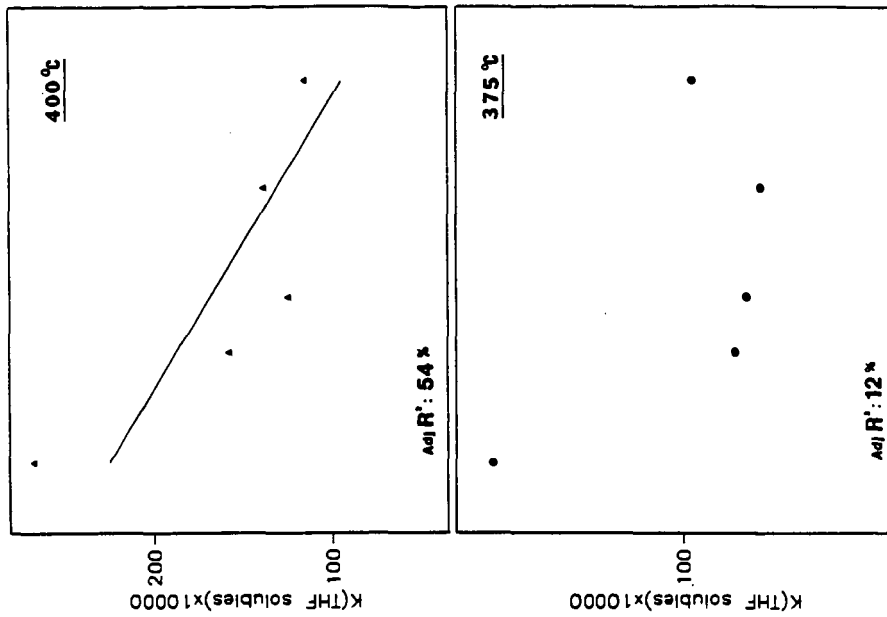


Figure 5. Correlation of Activation Energy (toluene solubles) vs. Oxygen Content

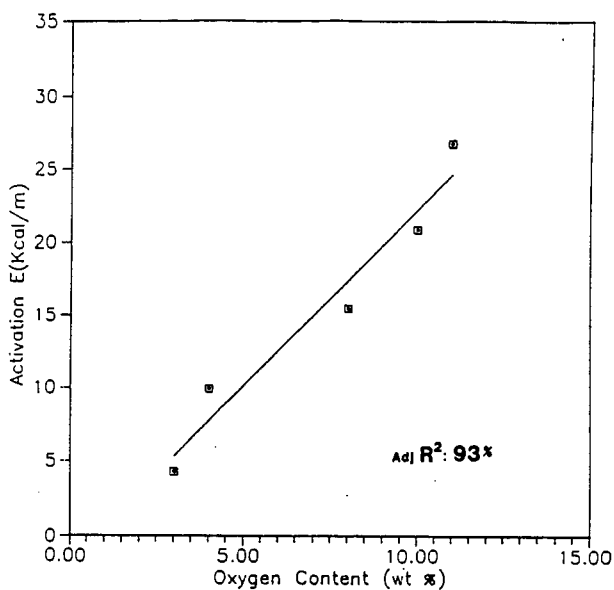


Figure 6. Correlation of Activation Energy (THF solubles) vs. Aliphatic Hydrogen

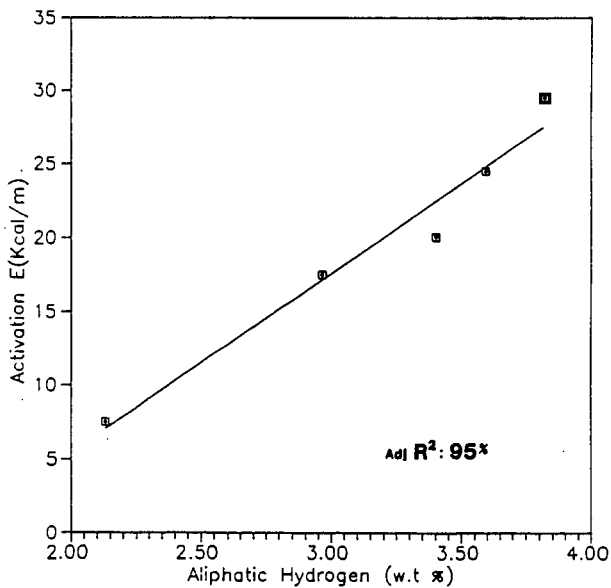


Figure 7. Interrelationship between Total Oxygen and Linking Aliphatic Carbon Content

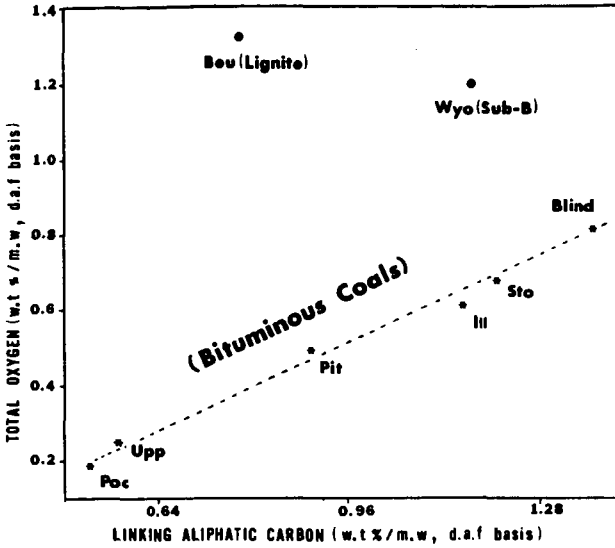
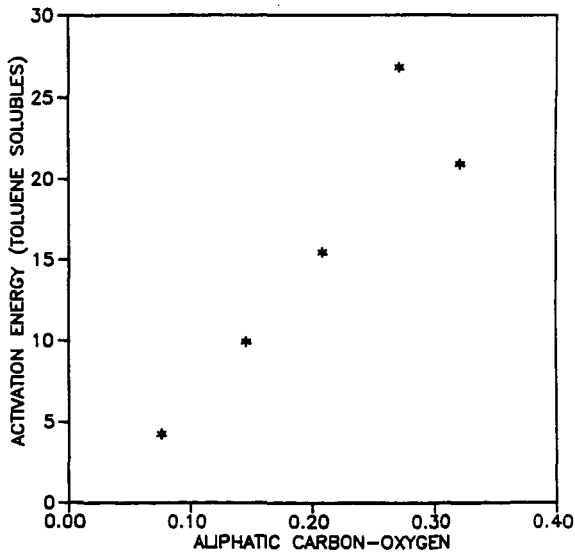


Figure 8. Correlation of Activation Energy (toluene solubles) vs. Aliphatic Carbon-Oxygen



## COAL STRUCTURE AND BEHAVIOR--INTERFACIAL CHEMISTRY IN COAL

David S. Ross, Albert S. Hirschon, and Thomas K. Green  
SRI International, Menlo Park, California 94025

### Introduction and Background

A model for the organic phase of coal recently suggested by Shinn is shown in Figure 1 (1). This model is based on a reconstruction of the parent structure of an Illinois No. 6 coal following a thorough evaluation of reported product data from various liquefaction processes. The model structure contains 11% oxygen, with about 35% of the total O present as ether oxygen. This ether fraction is the same as the value we established in recent work on the fate of oxygen in an Illinois No. 6 coal during thermolysis and conversion (2).

Insofar as it presents an organic network of linked aromatic units, the model is similar to others presented earlier, as summarized by Davidson (3a) and Gray and Shah (3b). However, the Shinn model is closely tied to more recent evidence from liquefaction and analytical studies and as such is the most realistic picture of the organic phase available. Like earlier models, this model is limited to the organic components in coal and ignores the mineral phase. Shinn acknowledges that avoiding the heterogeneous aspect of coal structure precludes a full understanding of its structure and therefore its behavior.

This point is key to the discussion here, as is emphasized by the fact that the structure in Figure 1 is not consistent with some facts on coal behavior recently uncovered by us and others. We submit as a working hypothesis that the reactive centers in coal include and may be dominated by substantial interfacial regions common to both the organic and mineral phases. The focus of our attention is not the catalytic effects of mineral matter in coal conversion to liquids or gases, which have been investigated during the past three decades (4) or longer, but rather the chemistry at the organic/mineral boundary specifically.

While most inorganic material in coal is present in a discrete mineral phase over a range of sizes, from large crystallites to micron-size grains (5), Mraw, et al. demonstrated the presence of very small clay inclusions down to 10 nm in size (6). They speculated that the fine grain size corresponds to a very high surface area, which in turn could play a role in the chemistry of coal. More recently, Allen and VanderSande reported even smaller, ultrafine mineral material, estimating abundance of up to 15% of the full mineral assay (7). Their technique required comparison of pairs of x-ray spectra of respectively a particle and the organic matrix 1-2 particle diameters away for comparison. As is seen in Figure 2, while the particle in question clearly is rich in titanium, both spectra, in particular that from the organic matrix, show aluminum and silicon. It would thus appear that the organic phase includes clay inclusions with characteristic sizes extending below their 2 nm resolution limit, perhaps extending to collections of hundreds of atoms. The result would be an organic/mineral interface of enormous extent.

This picture of an integrated structure could be tied with the recent findings that are otherwise unreconcilable with conventional structures. Towne, et al. found that the addition of water to conventional H-donor media substantially increased the

extent of liquefaction (10). Brandes and Graff found that hydrothermal treatment activated coal for subsequent mild gasification (11a,b). Perhaps the most striking aspect of this work was the finding that their brief pretreatment changed the swelling characteristics of the coal so that water itself became a swelling agent. Bienkowski et al. have reported a beneficial effect on liquefaction (12) in line with some of our work, where aqueous pretreatment activates the coal toward subsequent liquefaction (13).

## Results

In an attempt to evaluate the importance of interfacial chemistry to coal behavior, we have conducted studies at 400°C with both H<sub>2</sub>O and D<sub>2</sub>O, using both Illinois No. 6 coal (PSOC 1098) and pure organic compounds. We were directed to this approach through accounts in the geochemical literature, in which considerable attention is paid to kerogen/mineral interactions tied to petroleum production (14,15).

Figure 3 summarizes our effort, and virtually none of the material presented here is consistent with the organic structures depicted in Figure 1. We found that while coal recovered from simple hydrothermal treatment in D<sub>2</sub>O/N<sub>2</sub> for 20 minutes under nitrogen contained more than 90% of the starting carbon, 30% of the starting hydrogen and about half the starting oxygen were lost. Our account of the anomalous O-loss has recently appeared (2). These losses could not be accounted for by CO<sub>2</sub> and light hydrocarbon evolution. Of the remaining protium in the product, 53% had been exchanged for deuterium. The product had been subjected to back-exchange in H<sub>2</sub>O at mild conditions to convert the phenolic hydrogen to protium, so the large levels of exchange were strictly for hydrogen bonded to carbon.

In other runs the coal was converted to products that were 50-60% toluene soluble (TS) by replacing the N<sub>2</sub> with CO. The D-fractions for both TS and toluene insoluble (TI) fractions (back-exchanged) were 53% and 59% respectively, or a composite value essentially the same as that for the produce from the N<sub>2</sub> run. Thus, the conversion chemistry operated on the material that had undergone isotope exchange rapidly and prior to conversion to the TS fraction, a very useful finding since structural factors subsequently developed from NMR work for the TS fraction could then be tied to the original structure with some confidence.

<sup>1</sup>H NMR studies on the TS fractions from parallel H<sub>2</sub>O and D<sub>2</sub>O runs revealed little exchange for the β- and γ-alkyl hydrogens in the coal. About 57% of the aromatic protium was exchanged, a result in accord with the known phenolic exchange chemistry under these conditions (16) and consistent with the known phenolic content of the coal and the structure in Figure 1. For the benzyl hydrogen, however, the result was striking. We found that fully 76% of the benzyl hydrogens in the TS fraction were replaced by deuterium in the 20-minute treatment.

These findings can be compared with those from work with work under the same conditions with pure organic materials. At 20 minutes in D<sub>2</sub>O we found no trace of exchange for benzene, toluene, or bibenzyl. Indeed, we had to extend the period to 1200 minutes to observe the introduction of deuterium into the benzylic positions in bibenzyl and the toluene derived from it, while benzene and toluene themselves were still virtually unexchanged after this extended period.

Thus, the benzyl-protium exchange rate in coal is roughly 100 times faster than that for bibenzyl and considerably faster than that for toluene. This result can be translated to suggest that the thermal generation of free radical sites in the coal

operates at a rate two to three orders of magnitude greater than that for bibenzyl. However no feature in the organic structures proposed for coal can generate such a flux of reactive free radicals by a wide margin. Indeed, we are aware of no chemistry for structures such as that in Figure 1 which can accommodate our findings for both the H and O components of the organic phase.

## Discussion

Accordingly, we are led to consider a scenario in which the chemistry involves significant reactions at the organic/mineral interface. Two accounts from areas outside coal chemistry lend support to our view. The first is geochemical work on the origins of petroleum by Hoering (17). The results and rationale are rather detailed, and they are discussed fully in Appendix A. In summary, Hoering reports anomalous incorporation of deuterium into hydrocarbons released from shale-bound kerogen upon hydrothermal pyrolysis in  $D_2O$  that we view as reconciled only through action directly at the kerogen/shale interface. The parallel to our results with coal is compelling and suggests similarity in both chemical structure and chemistry.

The second occurs in research tied to work in highway degradation, as reported by Ensley and coworkers (18a,b). Prepared bitumen/clay interface samples were studied and showed a distinct interphase volumes with a striated structure, were disrupted by water, and were most likely regions rich in H-bonding between the polar fractions of the bitumen and the mineral surface. At present, little is known about about the specific chemical speciation within the region (19). The disruptive action of water seen here is that we suggest plays a role in the beneficial effects of water pretreatment observed for coal, and can act as a probe into coal structure.

Our findings could have considerable impact on both fundamental coal chemistry and the practical aspects of coal use. The potential effects on the understanding of coal behavior derive from the fact that clays are known to inhibit free radical reactions. For example, the free radical polymerization of methyl methacrylate is fully suppressed in the presence of montmorillonite, even at temperatures as high as  $100^\circ C$  (20). Given the presence of a variety of clays in the mineral phase in coals, this striking factor raises the question of the significance of free radical chemistry generally in coal and supports the view put forward in this proposal that the overall structure of coal, including the nature of its reactive centers, can be viewed from a new perspective.

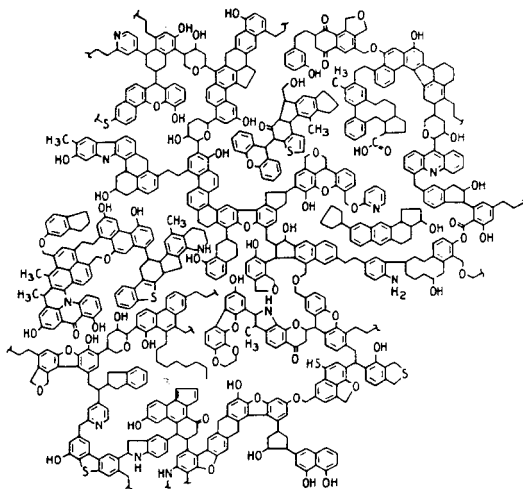
The implications for practical ends can also be noted. We can presume that the polar, heteroatom-containing portions of the organic phase migrate over geologic time to the mineral surfaces, resulting in heterogeneous distribution of the N- and S-containing components within the organic phase, concentrated around the mineral microinclusions. Just such a slanted distribution has been noted for the organic material removal from Green River shale (21). Thus, properly conducted hydrothermal pretreatment or microbial/enzymatic delamination at the mineral/organic interface could lead to separation of heteroatom components and mineral material.

Finally, geochemical studies on the role of the mineral matrix in the pyrolysis of petroleum yielding kerogen show that hydrocarbon retention and char formation correlates with the clay content of the matrix (22). Increased clay levels lead to greater carbonization. By extension, we suggest that the presence of ultrafine clay inclusions in coal contribute to the retrogressive chemistry operative during liquefaction and mild gasification and indeed may be the major factor in such action.

#### REFERENCES

1. J. H. Shinn, *Fuel*, 63 (9), 1187-1196 (1984).
2. D. S. Ross, T. K. Green, R. Mansani, and G. P. Hum, *Energy and Fuels*, 1, 292-294 (1987).
3. a. R. M. Davidson, "Molecular Structure of Coal, Report No. ICTIS/TR 08, IEA Coal Research, London, 1980.  
b. J. A. Gray and Y. T. Shah, in Reaction Engineering in Direct Coal Liquefaction, Y. T. Shah, Ed., Addison-Wesley Publishing Co., Reading, Mass., 1981, pp. 24-101.
4. R. M. Davidson, "Mineral Effect in Coal Conversion," Report No. ICTS/TR22, IEA Coal Research, London, 1983.
5. R. C. Neavel in Chemistry of Coal Utilization, Second Supplementary Volume, M. A. Elliott, ed., Wiley-Interscience/John Wiley and Sons, New York, 1981, pp. 121-122.
6. S. C. Mraw, J. P. DeNeufville, H. Freund, Z. Baset, M. L. Gorbaty, and F. J. Wright, in Coal Science, Vol. 2, J. Larsen, M. Gorbaty, and I. Wender, Eds., Academic Press, New York, 1983, pp. 1-26.
7. R. M. Allen and J. B. VanderSande, *Fuel*, 63, 24-29 (1984).
8. A. Meyer, D. Farin, and D. Avnir, *J. Am. Chem. Soc.*, 108, 7897-7905 (1986).
9. a. B. K. G. Theng, The Chemistry of Clay-Organic Reactions, John Wiley and Sons, New York, NY, 1974.  
b. C. Breen, J. Adams, and C. Riebel, *Clays and Clay Minerals*, 33 275-284 (1985).
10. S. Towne, Y. Shah, G. Holder, G. Deshpande, and D. Cronauer, *Fuel*, 64, 883-889 (1985).
11. a. S. D. Brandes and R. A. Graff, *Am. Chem. Soc. Div. of Fuel Chemistry Preprints*, 32 (3), 385-393, (1987).  
b. R. A. Graff and S. D. Brandes, *Energy and Fuels*, 1, 84-88 (1987).
12. P. R. Bienkowski, R. Narayan, R. A. Greenkorn, and K-C Chao, *Ind. Eng. Chem. Res.*, 26, 202-205 (1987).
13. D. S. Ross, T-C. Miin, and A. S. Hirschon, unpublished results.
14. M. Tarafa, J. Hunt, and I. Ericsson, *J. Geochem. Expl.*, 18, 75-85 (1983).
15. J. Espitalie, K. Makadi, and J. Trichet, *Org. Geochem.*, 6, 365-382, (1984).
16. I. F. Tupitsyn and V. I. Komarov, *Reakts. Sposobn. Org. Soedin.*, 6, 616-626 (1969).

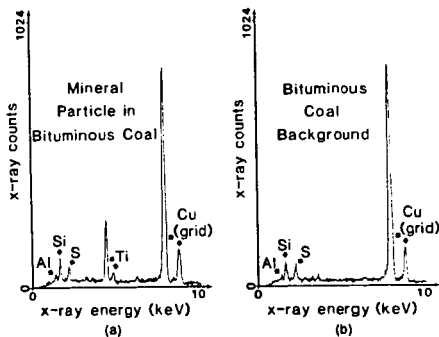
17. T. Hoering, *Org. Geochem.*, 5 (4), 267-278 (1984).
18. a. E. Ensley, H. Plancher, R. Robertson, and J. Petersen, *J. Chem. Ed.*, 55 (10), 655-658, (1978).  
b. E. Ensley, *J. Appl. Chem. Biotechnol.*, 25, 671-682 (1975).
19. J. Peterson, personal communication.
20. Reference 9, p. 271.
21. J. McKay and M. Blanche, *Liq. Fuels Techn.* 3 (4), 489-521.
22. J. Espitalie, M. Medac, and B. Tissot, *AAPG Bulletin*, 64, 59-66 (1980).



SOURCE: J. H. Shinn, *Reactive Model of Coal Structure*, *Fuel* 63, 1190 (1984).

RA-320583-331

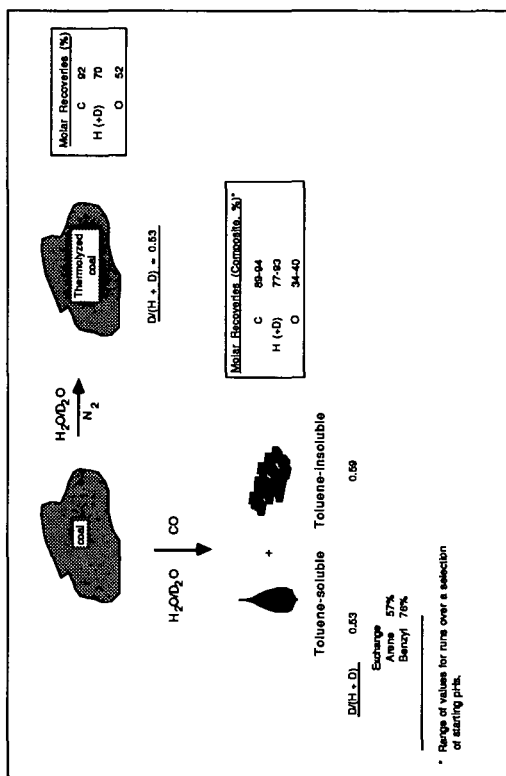
Figure 1. Model of bituminous coal structure.



SOURCE: R. M. Allen and J. B. VanderSande, *Analysis of Sub-Micron Coal Mineral Matter*, *Fuel* 63, 27 (1984)

RA-320583-332

Figure 2. Examples of x-ray spectra from bituminous sample.



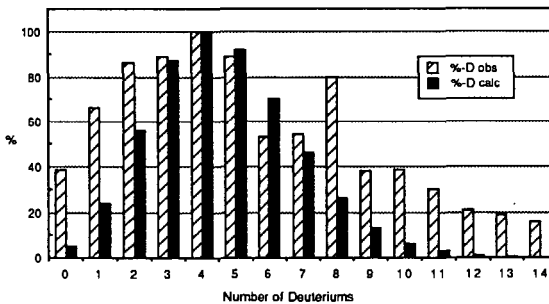
RA-20868-33

Figure 3. Coal studies at 400°C/20 min.

APPENDIX A

GEOCHEMICAL SUPPORT FOR THE PROPOSED COAL MODEL

Our proposition of a significant and reactive mineral/organic interface in coal is supported by a somewhat parallel set of results developed in research into petroleum formation by Hoering, who reported on pyrolyses of samples of previously extracted Messel shale (1). The pyrolyses were conducted in  $D_2O$  at  $330^\circ C/3$  days, and they generated a series of saturated hydrocarbons resembling natural petroleum. The hydrocarbons were extensively deuterated. A portion of the product was a series of n-alkanes in the range of 14-30 carbon atoms, with each alkane containing distributions of isomers with 0 to more than 14 deuterium atoms. The maximum deuterium substitution was in the 4-6 range as shown in Figure A-1 for the  $C_{18}$  product, a profile representative of the entire suite of isolated alkanes.



Source: T. C. Hoering, *Org. Geochem.*, 5, 267-278 (1984).

Figure A-1. Deuterium distribution.

The distribution is broad, with the  $D_0$  case nearly 40% of the  $D_4$  material, and significant deuteration continues out to beyond  $D_{14}$ . The author ruled out the presence of preexisting, trapped alkanes, since in that case undeuterated product would have dominated the samples. Moreover, in control experiments in which the shale was purposefully spiked with an n-alkane, it was recovered virtually entirely untagged. The purposeful addition of a terminal n-alkene resulted in the recovery of about half the corresponding alkane, a curious result suggesting the presence of reducing chemistry, but with the product containing only small quantities of deuterium.

Thus, both preexisting alkanes or olefin precursors can be eliminated as origins of the multilabeled n-alkanes. Also ruled out on the basis of the deuterium isotope

distribution is their formation from thermal production of the corresponding n-alkyl radicals through kerogen pyrolysis, followed by a successive deuterium attachment chain. The distribution expected from such a process can be estimated by numerical simulation of sequential exchange, ignoring isotope effects which would be insignificant at these temperatures. The result, adjusted so that the maximum substitution is at C<sub>4</sub>, is presented in Figure A-1, and it is considerably more narrow than the one observed, with the bulk of the substitution falling between C<sub>2</sub> and C<sub>7</sub>. The calculated D<sub>0</sub> level is only about 10% of that observed, and virtually no substitution is expected beyond C<sub>11</sub>.

The calculated profile is firm and applies to any sequential exchange mechanism which the rate is the same for all steps. Thus the considerably broader distribution observed in Hoering's data dictates either several different mechanisms operating in parallel, an unlikely proposition, or different precursors for each isotope isomer. We adopt the latter view here.

We suggest that alkane precursors exist at the mineral surface, attached to the surface over several points. Theng has discussed a similar situation for the adsorption of linear polymers on clay (2). D<sub>2</sub>O then engages in some chemistry yet to be uncovered, releasing the alkane and creating a C-D bond at the point of attachment. The reducing chemistry noted for the case of the consumed alkene could play a significant role.

We propose, by extension, a similar scheme for coal. We envision mineral/organic attachment at the portions of the coal structure leading to benzylic positions following hydrothermal treatment.

#### REFERENCES

1. T. C. Hoering, *Org. Geochem.*, 5 (4), 267-278 (1984).
2. B. Theng, *Clays and Clay Minerals*, 30, 1-10 (1982).

## AMPHOTERIC REACTIONS OF SUPERCRITICAL WATER WITH COAL MODELS

Akiko K. Horiuchi<sup>1</sup>, Howard T. Fish<sup>1</sup> and Michael A. Mikita<sup>2\*</sup>

<sup>1</sup>Department of Chemistry, University of Colorado at Denver  
Denver, Colorado 80204

<sup>2</sup>Department of Chemistry, California State University Bakersfield  
Bakersfield, California 93311

### INTRODUCTION

For the past several years this laboratory has been studying water assisted coal liquefaction. Initial experiments were designed to determine whether water could replace all or part of the donor solvent in coal liquefaction [1]. More recent work has focused upon the chemical reactions of coal models in supercritical water [2].

In summary of our experiments with coal [1], high conversions of Illinois No. 6 (River King Mine) bituminous coal were obtained in minireactor experiments at modest temperatures with little or no hydrogen-donor solvents.

The use of water in liquefaction has also been studied by others. When used in combination with carbon monoxide and a suitable catalyst, water was a source of hydrogen for the reduction of coal [3,4]. Liquefaction under carbon monoxide, without an organic solvent, has also been carried out with slurries composed of coal and either water or aqueous base [5,6]. In some cases, water served to carry dissolved metal salts used as homogeneous catalysts as well as acting as the liquefaction medium [7]. In comparison with conventional organic liquefaction solvents, water is quite effective when used in combination with H<sub>2</sub>S, in particular under synthesis gas rather than hydrogen [8]. Aqueous liquefaction using impregnated catalysts has also been combined with supercritical water distillation to separate the oil and asphaltene from the coal char residue [9]. The simple treatment of coal with supercritical water in the absence of hydrogen or catalysts renders a substantial portion of the treated coal extractable by tetrahydrofuran [10]. From these extraction studies, it is apparent that water is able to assist the diffusion and dispersion of liquefaction products and reactants.

In addition to these roles, water may directly participate as a reactant in the thermolytic chemistry of certain model compounds. In the presence of water, dibenzyl ether decomposes at 374°C by both pyrolytic and hydrolytic pathways [11]. The removal of nitrogen from heterocyclic compounds, such as isoquinoline, is accelerated in the presence of supercritical water [12]. Most recently, it was suggested

---

\* Author to whom correspondence should be addressed.

that in the presence of supercritical water the hydrolysis of coal models proceeds through a transition state that is more polar than the reactants [13].

Taken together, these studies indicate that under various conditions, supercritical water may act as a good liquefaction medium, dissolve or extract coal-derived liquid products, promote the cleavage of certain bonds likely to be found in coal, provide hydrogen through the water-gas shift reaction, and possibly assist the contacting of coal with catalysts or hydrogen.

For the past year our efforts have centered upon the study of two distinct coal model compound systems with water under liquefaction conditions. This research is intended to further evaluate the chemical role of water above its critical temperature in the conversion of coal to a liquefaction product.

## EXPERIMENTAL

Commercially available reagents were used without further purification. Bibenzyl (Aldrich), benzyl phenyl ether (TCI), and hydroquinone monobenzyl ether (Fluka) were analyzed for purity by gc/ms prior to use. All other models were synthesized from the commercially available substituted benzyl halides, with the exception of 2-bromo-p-toluic acetate which was synthesized from the reaction of diazomethane with 2-bromo-p-toluic acid. Reaction of the benzyl halides with triethylphosphite afforded the phosphonates which were in turn coupled via Wittig reaction with benzaldehyde or benzyl-ether-protected salicylaldehyde to form the substituted stilbenes and protected o-hydroxystilbenes respectively. Hydrogenation of the stilbenes over Pd/C afforded the desired products.

A five minireactor system [14] at the Pittsburgh Energy Technology Center was employed for all reactions with the bibenzyls. The bibenzyls (2.6 mmol) were reacted in the presence of 4.3 mL H<sub>2</sub>O and/or D<sub>2</sub>O solutions containing 2 mL n-pentanol as an internal standard per 93.4 mL H<sub>2</sub>O or 100 mL D<sub>2</sub>O. The reactors were purged with N<sub>2</sub> then submerged into a fluidized sand bath at 400 °C for 3 hours. The pressure of the reactants was not measured directly; using van der Waal's equation the partial pressure of water was estimated at 4290 psi. The density of the supercritical water was 0.10 g/mL. Once cooled, the reactors were washed several times with 5 mL dichloromethane. The resulting heterogeneous solutions were agitated for several days. Each organic layer was analyzed on DB1 capillary column using an HP #5790A gc and a HP #5970A MSD.

In the study of the benzyl phenyl ethers, 0.5 mmol of each model was reacted with 2.9 mL H<sub>2</sub>O or D<sub>2</sub>O (0.16 mmol) at 400 °C for forty minutes using a Parr # 4704 22 cc minireactor. The estimated pressure and water density in these reactions was 5900 psi and 0.13 g/cc. An internal standard was not employed in these studies and molecular oxygen was not excluded. Analysis was identical to that described above with the substitution of ether for CH<sub>2</sub>Cl<sub>2</sub>.

## DISCUSSION

In the first study, a Hammett series of substituted bibenzyls and o-hydroxy bibenzyls were synthesized via Wittig reaction with subsequent hydrogenation. The substituents synthesized were p-NH<sub>2</sub>, p-t-Bu, p-CH<sub>3</sub>, H, m-CF<sub>3</sub>, and p-CH<sub>3</sub>O<sub>2</sub>C.

Not surprisingly, thermolysis pathways dominated the observed products from these preliminary reactions of the substituted bibenzyls. Both the thermolysis products and recovered starting materials were observed to undergo deuterium exchange. The major products from all reactions with the bibenzyls and o-hydroxybibenzyls, along with the maximum number of deuterium incorporated into each, are compiled in Table 1.

With the simple bibenzyls, electron donating substituents were observed to enhance D-substitution into the recovered starting materials. D-exchange may be envisioned by either radical or ionic pathways as illustrated in Scheme 1. Ionic route B would be stabilized by electron donating groups, but alcohol products would be expected and these have not been observed. Ionic route C forms carbanion intermediates, hence electron withdrawing groups would be expected to stabilize the intermediates. Electrophilic aromatic substitution, illustrated via route A, would agree with the observed substituent effects, since electron donating groups would be expected to stabilize the intermediate arenium ions.

In the case of p-carboxylic acid methyl ester bibenzyl, demethylation and decarboxylation predominated with a deuterium substitution pattern suggestive of an ionic decarboxylation.

Comparison of the conversions of the o-hydroxy substituted bibenzyls in H<sub>2</sub>O and D<sub>2</sub>O suggested a primary isotope effect. This is an intriguing observation considering that thermolysis pathways again predominated.

The o-hydroxy bibenzyls exhibited more extensive deuterium exchange than with the simple bibenzyls, presumably due to the enhanced H(D)-atom transfer ability of the phenolic-H(D). The tautomerization pathway [15] contributed significantly to the product distribution with the o-hydroxy bibenzyls. The production of substituted ethylbenzenes also exhibited a

primary isotope effect suggesting that tautomerization is rate limiting.

2-Ethyl-4-substituted biphenyl ethers were also observed in some cases, presumably through the rearrangement of the respective substituted *o*-hydroxybibenzyls (Scheme 2.).

Cyclization of *p*-NH<sub>2</sub>-, *p*-CH<sub>3</sub>-, and *H*- *o*-hydroxy substituted bibenzyls to dibenz[b,f]dihydrooxepane was also observed. Two possible mechanisms for these transformations are illustrated in Scheme 3.

In our other preliminary study, benzyl phenyl ether (BPE) reactions pathways were complicated by the presence of molecular oxygen. For example, in addition to the thermolysis products phenol and toluene, autooxidation product benzaldehyde was also observed. Significant amounts of benzylalcohol and *o*-benzyl phenol were also produced. Both products can be explained through ionic reactions with water, although the former may also result from autooxidation.

Hydroquinone monobenzyl ether (HQMBE) also exhibited the expected thermolysis products hydroquinone and toluene, as well as the autooxidation product benzaldehyde. The tautomeric pathway was also important as evidenced by the significant production of benzylalcohol. The observed formation of catechol monobenzyl ether (CMBE) may also be simply explained by the recombination of phenoxy and benzoxy radicals, both requiring tautomerization for their generation. The deuterium substitution pattern of CMBE, however, suggests a fascinating mechanistic alternative. CMBE from reaction in D<sub>2</sub>O exhibited its parent ion at 203 *m/e*, an increase of three from unsubstituted CMBE. Recovered HQMBE exhibited its parent at 201 *m/e*, indicating only one deuterium substitution. If the methylene protons were responsible for the additional exchange in CMBE, similar D-substitution patterns would be expected for both HQMBE and CMBE.

Two successive nucleophilic aromatic substitutions of D<sub>2</sub>O with HQMBE would account for the observed substitution pattern. The first substitution would give resorcinol monobenzyl ether, followed by a more facile second to yield the thermodynamically preferred CMBE. This possibility is illustrated in Scheme 4.

The impact of these preliminary model compound studies toward an understanding of the organic chemical reactions of coal in supercritical water is striking. The observation that electron donating substituents favored D-exchange with the substituted bibenzyls supports our earlier suggestion [2] that electrophilic aromatic substitution by a proton for suitable aryl substituents is a possible alternative reaction pathway for coal in the presence of water. Even more dramatic is the possibility of nucleophilic aromatic substitution with water as suggested by the production and D-substitution pattern of CMBE. Such a reaction would be

consistent with the observed production of phenols during liquefaction.

The heterogeneous nature of coal requires that we view liquefaction as mechanistically complex. The results of this preliminary study suggest that the unique amphoteric character of water may present coal with reaction pathways unavailable under traditional liquefaction conditions.

### ACKNOWLEDGMENTS

The minireactor expertise of Henry Davis is gratefully recognized, as is the encouragement and advice of Brad Bockrath. Financial support from the DOE (DE-FG22-85PC81544) and Oak Ridge Associated Universities is acknowledged.

### REFERENCES

1. Blaustein, B.C.; Davis, H.M.; Friedman, S.; Illig, E.G.; Mikita, M.A. Am. Chem. Soc. Div. Fuel Chem. Preprints 1985, 30(2), 359.; Mikita, M.A. Bockrath, B.C.; Davis, H.M.; Friedman, S.; Illig, E.G. Energy Fuels 1988 (in press).
2. Mikita, M.A.; Fish, H.T. Am. Chem. Soc. Div. Fuel Chem. Preprints 1986, 31 (4), 56; Horiuchi, A.K. M.S. Thesis, University of Colorado at Denver, January, 1988; Fish, H.T. B.A. Honors Thesis, University of Colorado at Denver, December, 1987.
3. Appell, H.R.; Wender, I.; Miller, R.D. Chem. Ind. 1969, 1703.
4. Appell, H.R. Energy 1976, 1, 24.
5. Ross, D.S.; Blessing, J.E. Fuel 1978, 57, 379.
6. Ross, D.S.; Blessing, J.E.; Nguyen, Q.C.; Hum, G.P. Fuel 1984, 63, 1206.
7. Ross, D.S.; Nguyen, Q.C.; Hum, G.P. Fuel 1984, 63, 1211.
8. Stenberg, V.I.; Hei, R.D.; Sweeney, P.G.; Nowok, J. Am. Chem. Soc. Div. Fuel Chem. Preprints 1984, 29(5), 63.
9. Barton, P. Ind. Eng. Chem., Process Des. Dev. 1983, 22, 589.
10. Deshpande, G.V.; Holder, G.D.; Bishop, A.A.; Gopal, J.; Wender, I. Fuel 1984, 63, 956.
11. Townsend, S.H.; Klein, M.T. Fuel 1985, 64, 635.
12. Hoser, T.J.; Tiffany, D.M.; Li, Z.; McCarville, M.E.; Houghton, M.E. Fuel 1986, 65, 827.
13. Townsend, S.H.; Abraham, M.A.; Huppert, G.L.; Klein, M.T.; Paspek, S.C. Ind. Eng. Chem. Res. 1988, 27, 143.
14. Anderson, R. R.; Bockrath, B. C. Fuel 1984, 63, 329.
15. McMillan, D.F.; Orgier, W.C.; Ross, D.C. J. Org. Chem. 1981, 46, 3322.



Table 1. Major Products from the Reaction of Supercritical Water with

| products                         | OH               |                     | X-C <sub>6</sub> H <sub>4</sub> -CH <sub>2</sub> -CH <sub>2</sub> -C <sub>6</sub> H <sub>4</sub> -R |                     | X-C <sub>6</sub> H <sub>4</sub> -CH <sub>2</sub> -CH <sub>2</sub> -C <sub>6</sub> H <sub>4</sub> -R |                     | X-C <sub>6</sub> H <sub>4</sub> -CH <sub>2</sub> -CH <sub>2</sub> -C <sub>6</sub> H <sub>4</sub> -R |                        | starting materials    |                        | rearranged compound |    | epicis compound |    | high m. wt. compounds |    |       |
|----------------------------------|------------------|---------------------|---|---------------------|---|---------------------|---|------------------------|-----------------------|------------------------|---------------------|----|-----------------|----|-----------------------|----|-------|
|                                  | OH               | H                   | OH  | H                   | OH  | H                   | OH  | H                      | OH                    | H                      | OH                  | H  | OH              | H  | OH                    | H  |       |
| NH <sub>2</sub>                  | H <sub>2</sub> O | 0.22 <sup>(1)</sup> | -   | 0.16                | -   | 0.56                | -   | 0.062                  | -                     | 0.84                   | -                   | Y  | -               | OB | -                     | OB | -     |
|                                  | D <sub>2</sub> O | ND                  | ND  | ND                  | 0.21 <sup>3D</sup>  | ND                  | 0.12 <sup>6D</sup>  | ND                     | 1.44 <sup>5D</sup>    | -                      | ND                  | ND | ND              | OB | ND                    | OB | ND    |
| CH <sub>3</sub>                  | H <sub>2</sub> O | 0.12                | -   | 0.15                | -   | 0.27                | -   | 0.36                   | -                     | 0.80                   | -                   | OB | -               | OB | -                     | OB | -     |
|                                  | D <sub>2</sub> O | ND                  | ND  | ND                  | ND  | trace               | -   | 0.053 <sup>3D</sup>    | -                     | 1.85 <sup>6D</sup>     | -                   | DB | ND              | OB | ND                    | OB | -     |
| H                                | H <sub>2</sub> O | 0.009               | -   | 0.08                | -   | 0.10                | -   | 0.32                   | -                     | 1.01                   | -                   | OB | -               | OB | -                     | ND | -     |
|                                  | D <sub>2</sub> O | 0.062 <sup>3D</sup> | ND  | 0.026 <sup>4D</sup> | ND  | 0.23 <sup>6D</sup>  | 0.13 <sup>3D</sup>  | 0.15 <sup>3D</sup>     | 0.13 <sup>(2)</sup>   | 1.51 <sup>7D</sup>     | 2.39 <sup>3D</sup>  | OB | ND              | OB | OB                    | ND | trace |
| m-CF <sub>3</sub>                | H <sub>2</sub> O | ND                  | -   | 0.017               | -   | 0.014               | -   | 0.10                   | -                     | 1.14                   | -                   | OB | -               | ND | -                     | OB | -     |
|                                  | D <sub>2</sub> O | ND                  | ND  | ND                  | ND  | 0.069 <sup>6D</sup> | 0.16 <sup>2D</sup>  | 0.053 <sup>3D</sup>    | 0.064 <sup>2D</sup>   | 1.34 <sup>5D</sup>     | 1.83 <sup>2D</sup>  | OB | ND              | ND | ND                    | OB | OB    |
| CH <sub>3</sub> O <sub>2</sub> C | H <sub>2</sub> O | ND                  | -   | ND                  | -   | 0.13                | -   | 0.083 <sup>(-3D)</sup> | -                     | -                      | -                   | ND | -               | ND | -                     | OB | -     |
|                                  | D <sub>2</sub> O | ND                  | ND  | ND                  | ND  | 0.047 <sup>6D</sup> | 0.18 <sup>6D</sup>  | 0.056 <sup>5D</sup>    | 0.14 <sup>(-3D)</sup> | 0.021 <sup>(-3D)</sup> | 0.13 <sup>1D</sup>  | ND | ND              | ND | ND                    | OB | ND    |

(1) The numbers are the ratios of pentanol/product, measured by the area under the GC peaks. ND: not detected. number D: the number of possible deuteriums incorporated. OB: observed. (2) experimental value x 1/2



**Table 2. Products from the Reaction of Supercritical Water with Benzyl Phenyl Ether and Hydroquinone Monobenzyl Ether<sup>1</sup>**

From Benzyl Phenyl Ether

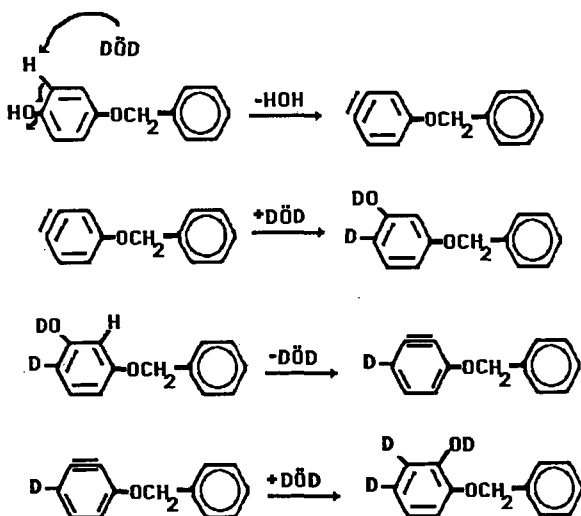
recovered BPE  
phenol  
benzaldehyde  
benzylalcohol  
o- or p- benzyl phenol  
toluene

From Hydroquinone Monobenzyl Ether

recovered HQMBE  
catechol monobenzyl ether  
benzylalcohol  
p-cresol  
benzaldehyde  
toluene

<sup>1</sup> Products are listed in the order of abundance as estimated from gc/ms. Quantitative experiments are in progress with these models.

**Scheme 4. Suggested Mechanism for the Formation of Catechol Monobenzyl Ether**



ADDITIVE EFFECTS OF SOLVENT REFINED COAL FRACTIONS AND  
NITROGEN-CONTAINING AROMATIC COMPOUNDS ON THE  
HYDROGENOLYSIS OF THE DIARYLMETHANE

Yoshio KAMIYA, Seiya KOYANAGI, and Shigeru FUTAMURA  
Department of Reaction Chemistry, Faculty of Engineering, The  
University of Tokyo, 7-3-1, Hongo, Bunkyo-ku, Tokyo, Japan 113

INTRODUCTION

The authors have already reported that solvent refined coal (SRC) promotes the hydrogenation of aromatic compounds in tetralin [1]. Further investigation has revealed that SRC not only donates its inherent hydrogen but mediates the hydrogen transfer from tetralin to the diarylmethane [2]. The structural analysis of SRC was monitored, and some imino linkages in SRC were suggested to be the possible moiety shuttling hydrogen.

This paper intended to clarify the action mechanism of SRC in hydrogen transfer reactions and presented the SRC-mimetic hydrogenolysis of the diarylmethane.

EXPERIMENTAL

Materials

The diarylmethanes were synthesized according to the method described in the previous paper [3]. The additives and the solvents were commercially purchased and purified if necessary by the conventional methods. The SRC's were prepared from Miike (C, 84.5%, H, 6.1%), Akabira (C, 83.4%, H, 6.2%), and Yallourn (C, 67.4%, H, 5.9%) coals as follows: each coal (20 g) was reacted in tetralin (60 ml) at 400 °C at 9.0 MPa of hydrogen for 30 min. The reaction mixtures were subjected to Soxhlet extraction for 15 h using tetrahydrofuran (THF) as solvent. The residues obtained in the reduced distillation (3 mmHg, at 250°C, for 1 h) of the THF extracts were used as SRC in the hydrogenolysis of the diarylmethane. Column chromatographic separation of SRC derived from Miike Coal, which would be designated only as SRC unless otherwise noted, was carried out by eluting ether-MeOH (98:2 v/v) (SRC-1, 54 wt%), THF (SRC-2, 38 wt%), and pyridine (SRC-3, 8 wt%). Table 1 shows the elemental analyses of the SRC's.

Hydrogenolysis of the diarylmethane

Prescribed amounts of a diarylmethane, a hydrogen donor solvent, and an additive were put into a 90 ml stainless, magnetically stirred autoclave. After being pressurized by 2.0 MPa of hydrogen, the autoclave was heated up to the reaction temperature and maintained during the prescribed period of time. After the reaction, the autoclave was cooled to room temperature by an electric fan.

Product analysis

The products were identified by GC-MS. Quantitative analysis of the products recovered with THF was carried out by GC. Structural change of SRC was monitored by means of <sup>1</sup>H- and <sup>13</sup>C-NMR, GPC, and elemental analysis.

## RESULTS AND DISCUSSION

### Solvent-dependent additive effect of SRC

As Table 2 shows, addition of SRC promotes the hydrogenolysis of di(1-naphthyl)methane. The additive effect does not seem to depend on SRC origin, reflecting their similar chemical compositions [4], but it is greatly affected by the hydrogen donatability of solvent. On addition of Yallourn or Akabira SRC (0.40 g), about a two-fold larger conversion of di(1-naphthyl)methane is obtained in tetralin than in 1-methylnaphthalene, respectively.

The additive effect of recovered SRC is also solvent dependent (Table 3). In tetralin, recovered SRC and raw SRC show the comparable additive effect and the similar conversion of tetralin is obtained. Under the reaction conditions, the rearrangement of tetralin to 1-methylindan also occurred and the molar ratio of 1-methylindan/naphthalene was 3.05 in the absence of SRC. This ratio decreased to 0.86-1.10 in the presence of SRC. These facts suggest that the initial transfer of  $\alpha$ -hydrogen in tetralin would occur more selectively in the presence of SRC since 1-methylindan is derived only from 2-tetralyl radical and isomerization of 1- and 2-tetralyl radicals is negligible [5]. Recovered SRC, which was partly dehydrogenated in the first reaction, showed the comparable promoting effect compared with raw SRC. This fact suggests that hydrogen shuttling could occur on the dehydrogenated moiety in the recovered SRC. On the other hand, in 1-methylnaphthalene, a modest conversion of 9-benzylphenanthrene is obtained in the presence or absence of recovered SRC, suggesting that almost no hydrogen transfer proceeds from 1-methylnaphthalene or decalin to dehydrogenated SRC.

Tables 4 and 5 show that the conversion of di(1-naphthyl)methane does not necessarily correlate with the amount of  $H_{\alpha}$  in the fractionated SRC. The weight ratio of hydrogen consumed in the hydrogenolysis of di(1-naphthyl)methane/ $H_{\alpha}$  lost from SRC falls on 1.8-5.7, which reinforces that some bondings in dehydrogenated SRC act as a hydrogen shuttler rather than a hydrogen donor as shown in Scheme 1.

### Structural analysis of SRC

Figure 1 shows the GPC profiles of the raw and recovered SRC's. Basically, similar molecular size distributions were obtained before and after the reactions for all the SRC's although the structures sensitive to light at 260 nm grew for SRC-3 after the reaction. These findings indicate that decomposition and condensation of SRC are negligible under the reaction conditions. Thus, the recovered SRC was analyzed by  $^{13}C$ -NMR in order to detect the chemical structures shuttling hydrogen in dehydrogenated SRC. Figure 2 shows the  $^{13}C$ -NMR spectrum of the recovered SRC soluble in THF. The carbon atoms at 139 and 154 ppm can be assigned to the azomethine carbons and the carbons at the ipso-positions in phenolics.

This finding urged us to investigate into the hydrogen shuttling

abilities of 3-ring azaaromatic compounds, which have been sparsely documented in the literature. They were also compared with the hydrogen shuttling abilities of some aromatic hydrocarbons.

#### Hydrogen shuttling effect of some azaaromatics

As Table 6 shows, the hydrogenolysis of 9-benzylphenanthrene is remarkably promoted on adding acridine or phenanthridine. However, 1- and 4-azaphenanthrenes are less effective additives.

These facts can be interpreted on the basis of the hydrogen accepting abilities of these hydrogen shuttlers. It has been reported in our previous paper [3] that the superdelocalizability gives a good measure to estimate the reactivity of the diarylmethane toward hydrogenolysis, and the quantum chemical data in Table 7 also indicate that phenanthridine and acridine are more hydrogen accepting than quinoline, 1-azaphenanthrene, and 4-azaphenanthrene (eqs. (1) and (5) in Fig. 3).

The other factor controlling the effectiveness of the shuttler is the hydrogen releasing ability of the hydroaromatic radical derived from the hydrogen transfer to the azaaromatic compound. If the hydroaromatic radical is more susceptible to further hydrogenation (eqs. (3) and (7)) rather than to hydrogen donation to 9-benzylphenanthrene (eqs. (2) and (6)), considerable amounts of hydrogen from tetralin is consumed in vain to afford the dihydro-derivatives of the shuttlers. The perhydro-derivatives of the azaaromatics are considered to show the lower hydrogen donatability than the hydroaromatic radicals. Direct and indirect overhydrogenation reactions of the shuttler such as disproportionation of these dihydro-derivatives formed in eqs. (3) and (7) are undesirable to promote the smooth hydrogen shuttling.

The azaaromatics used in this study showed the different reactivities toward hydrogenation of their own aromatic nuclei. In the tetralin-acridine system, 87% of acridine was converted to afford 9,10-dihydroacridine and 1,2,3,4-tetrahydroacridine in 18 and 60% selectivities, respectively. As for the tetralin-quinoline system, 52% of quinoline was converted to 1,2,3,4- and 5,6,7,8-tetrahydroquinolines in 69% combined selectivity. On the other hand, in the tetralin-phenanthridine system, the phenanthridine conversion was not more than 10% and 5,6-dihydrophenanthridine was formed in 60% selectivity. Therefore, there is no correlation between the 9-benzylphenanthrene conversion and the amounts of the perhydro-azaaromatics formed during the reactions.

These facts reveal that phenanthridine could act as an effective hydrogen shuttler since overhydrogenation of phenanthridine and adduction of phenanthridine derived compounds into the hydrogenolysates from 9-benzylphenanthrene occur only to a small extent, contrasting with the cases of quinoline-1,2,3,4-tetrahydroquinoline mixtures [6-8].

### CONCLUSION

We have shown that SRC and phenanthridine are effective hydrogen shuttlers. The effectiveness of phenanthridine can be ascribed to its facile hydrogen shuttling ability and higher stability under the reaction conditions.

### REFERENCES

1. Y. Kamiya, H. Ohta, A. Fukushima, M. Aizawa, and T. Mizuki, Proc., Int. Conf. on Coal Science, Pittsburgh, p. 195 (1983).
2. S. Koyanagi, S. Futamura, and Y. Kamiya, Proc., Conf. on Coal Science, Fukuoka, p. 206 (1987).
3. S. Futamura, S. Koyanagi, and Y. Kamiya, Fuel, in press.
4. Y. Kamiya, J. Fuel Soc. Jpn., 57, 12 (1978).
5. J. A. Franz and D. M. Camaioni, Fuel, 59, 803 (1980).
6. R. I. McNeil, D. C. Young, and D. C. Cronauer, Fuel, 62, 806 (1983).
7. J. W. Hellgeth, L. T. Taylor, and A. M. Squires, Proc., Int. Conf. on Coal Science, Pittsburgh, p. 172 (1983).
8. F. J. Derbyshire, G. A. Odoerfer, and D. D. Whitehurst, Fuel, 63, 56 (1984).

Table 1 Elemental Analyses of the Fractionated Miike SRC's.

|                    | SRC raw | SRC-1                | SRC-2     | SRC-3         |
|--------------------|---------|----------------------|-----------|---------------|
| Eluent<br>Weight % |         | Ether-Methanol<br>54 | THF<br>38 | Pyridine<br>8 |
| C                  | 86.9%   | 87.6 %               | 87.1%     | 78.3 %        |
| H                  | 5.8     | 5.9                  | 6.0       | 5.6           |
| N                  | 1.2     | 1.1                  | 1.1       | 1.7           |
| O(diff.)           | 5.9     | 5.4                  | 5.8       | 11.5          |
| Ash                | 0.23    |                      |           | 2.9           |
| H/C                | 0.80    | 0.81                 | 0.83      | 0.86          |

Table 2 Additive Effect of SRC on the Hydrogenolysis of Di(1-naphthyl)methane (DNM).

| SRC<br>(Amount/g) | Conv. of<br>DNM | Yield of<br>1-MN | Solvent<br>(Conv.) | Sel. of<br>1-MI |
|-------------------|-----------------|------------------|--------------------|-----------------|
| None              | 8%              | 6%               | Tet(8%)            | 47%             |
| Yallourn(0.1)     | 13              | 9                | Tet(8)             | 38              |
| Akabira (0.1)     | 12              | 9                | Tet(8)             | 40              |
| Yallourn(0.4)     | 38              | 19               | Tet(12)            | 26              |
| Akabira (0.4)     | 38              | 20               | Tet(12)            | 26              |
| Miike (0.4)       | 36              | 19               | Tet(16)            | 27              |
| None              | 5               |                  | 1-MN(0.3)          |                 |
| Yallourn(0.1)     | 9               |                  | 1-MN(3)            |                 |
| Akabira (0.1)     | 6               |                  | 1-MN(2)            |                 |
| Yallourn(0.4)     | 17              |                  | 1-MN(6)            |                 |
| Akabira (0.4)     | 20              |                  | 1-MN(7)            |                 |

DNM 7.5 mmol, solvent 75 mmol, 460°C, initial hydrogen pressure 2.0 MPa, 30 min.  
 Yallourn SRC (C, 83.3%, H, 6.0%), Akabira SRC (C, 86.2%, H, 6.3%), 1-MN = 1-Methylnaphthalene, Tet = Tetralin, 1-MI = 1-Methylindan.

Table 3 Additive Effect of the SRC's Derived from Miike Coal on the Hydrogenolysis of 9-Benzylphenanthrene (9-BP).

| Solvent  | Additive      | Conv. of<br>9-BP | Selectivities of |      |     | Conv.<br>of Solv. | Select. of |     |
|----------|---------------|------------------|------------------|------|-----|-------------------|------------|-----|
|          |               |                  | Tol              | Phen | DHP |                   | MI         | NpH |
| Tetralin | none          | 19%              | 71%              | 70%  | 13% | 13%               | 61%        | 20% |
| Tetralin | raw SRC       | 52               | 83               | 88   | 11  | 20                | 38         | 44  |
| Tetralin | recovered SRC | 42               | 86               | 75   | 11  | 18                | 44         | 40  |
| Decalin  | none          | 17               | -                | 75   | Nd  | 7                 |            |     |
| Decalin  | raw SRC       | 35               | -                | 90   | 3   | 7                 |            |     |
| Decalin  | recovered SRC | 20               | -                | 77   | Nd  | 7                 |            |     |

9-BP 7.5 mmol, solvent 75 mmol, SRC 0.4 g, 430°C, initial hydrogen pressure 2.0 MPa, 5 h.

Tol = Toluene, Phen = Phenanthrene, DHP = 9,10-Dihydrophenanthrene, MI = 1-Methylindan, NpH = Naphthalene. Nd = Not detected.

Table 4 Additive Effect of the Fractionated SRC's Derived from Miike Coal on the Hydrogenolysis of Di(1-naphthyl)methane.

| Additive<br>SRC | Conv.<br>of DNM | Yield<br>of 1-MN | Conv.<br>of Tet | Select.<br>of MI |
|-----------------|-----------------|------------------|-----------------|------------------|
| none            | 8%              | 6%               | 8%              | 47%              |
| SRC raw         | 36              | 19               | 16              | 27               |
| SRC-1           | 49              | 33               | 16              | 26               |
| SRC-2           | 41              | 19               | 17              | 26               |
| SRC-3           | 30              | 25               | 10              | 26               |

DNM 7.5 mmol, tetralin 75 mmol, SRC 0.4 g, 460°C, initial hydrogen pressure 2.0 MPa, 30 min.

Table 5 Amounts of Hydrogens Bonded to  $\alpha$ -Position on the Aromatic Ring in 0.4g of the SRC Derived from Miike Coal.

|         | H $\alpha$ /mg in<br>Original SRC<br>A | H $\alpha$ /mg in<br>Recovered SRC<br>B | Consumed<br>H $\alpha$ /mg<br>A - B | Amounts of Hydrogen<br>Needed in the<br>Hydrogenolysis<br>of DNM/mg |
|---------|--|---|-------------------------------------|---|
| SRC raw | 7.83                                   | 4.83                                    | 3.00                                | 5.40  |
| SRC-1   | 7.83                                   | 4.92                                    | 2.91                                | 6.15  |
| SRC-2   | 5.92                                   | 4.74                                    | 1.18                                | 4.95  |
| SRC-3   | 3.60                                   | 3.02                                    | 0.58                                | 3.30  |

Table 6 Hydrogen-shuttling effect of the azaaromatics in the hydrogenolysis of 9-benzylphenanthrene (9-BP).

| Additive (mmol)        | Conv. of 9-BP(mol%) | Selectivities(mol%) |      |     | Tetralin conv. (mol%) | Select.(mol%) |     |
|------------------------|---------------------|---------------------|------|-----|-----------------------|---------------|-----|
|                        |                     | Tol                 | Phen | DHP |                       | 1-MI          | NpH |
| None                   | 19                  | 71                  | 70   | 11  | 13                    | 61            | 20  |
| Quinoline (7.5)        | 22                  | 76                  | 73   | 9   | 19                    | 47            | 36  |
| 1-Azaphenanthrene(7.5) | 23                  | 71                  | a)   | 8   | 18                    | 50            | 27  |
| 4-Azaphenanthrene(7.5) | 23                  | 69                  | 72   | 7   | 17                    | 52            | 28  |
| Phenanthridine (3.3)   | 25                  | 74                  | 74   | 9   | 20                    | 47            | 34  |
| Phenanthridine (7.5)   | 33                  | 65                  | 73   | 7   | 23                    | 43            | 39  |
| Phenanthridine (15.0)  | 36                  | 72                  | 76   | 8   | 26                    | 33            | 44  |
| Phenanthridine (22.5)  | 37                  | 70                  | 75   | 8   | 28                    | 38            | 43  |
| Acridine (7.5)         | 40                  | 76                  | 79   | b)  | 25                    | 37            | 53  |

9-BP 7.5 mmol, tetralin 75 mmol, reaction temperature 430°C, initial hydrogen pressure 2.0 MPa, reaction time 5 h.

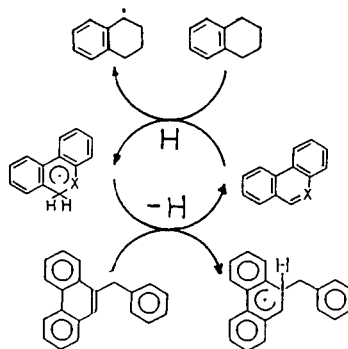
a) Not calculated owing to the inseparability of phenanthrene and the perhydro-derivatives of 1-azaphenanthrene.

b) Not calculated owing to the inseparability of DHP and the tetra- and octahydroacridines.

Table 7 Superdelocalizability values (Sr(R))<sup>a)</sup> of some azaaromatics.

| Aromatic compounds   | Sr(R) (position) |
|----------------------|------------------|
| Quinoline            | 1.0527 (4-)      |
|                      | 1.0059 (5-)      |
| Phenanthridine       | 0.9905 (8-)      |
|                      | 1.1045 (6-)      |
|                      | 0.9993 (7-)      |
| 1-Azaphenanthrene    | 0.9936 (5-)      |
|                      | 1.0214 (4-)      |
| 4-Azaphenanthrene    | 1.0009 (5-)      |
|                      | 1.0151 (5-)      |
|                      | 0.9926 (6-)      |
| Acridine             | 1.4732 (9-)      |
|                      | 1.2738 (10-)     |
|                      | 1.0564 (4-)      |
| 9-Benzylphenanthrene | 0.9803 (9-)      |

a) Superdelocalizability values toward radical reactions, which were calculated according to the Simple Hückel Theory.



Scheme 1 Hydrogen Shuttling Cycle.

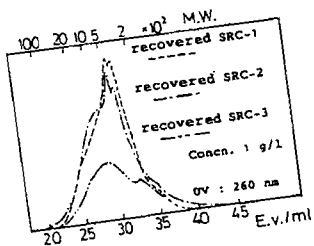
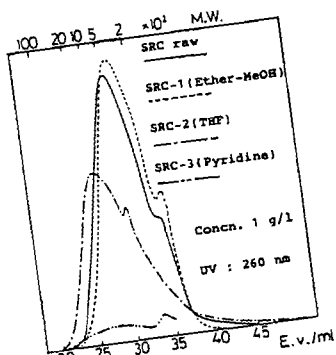


Fig. 1 GPC Profiles of the SRC's.

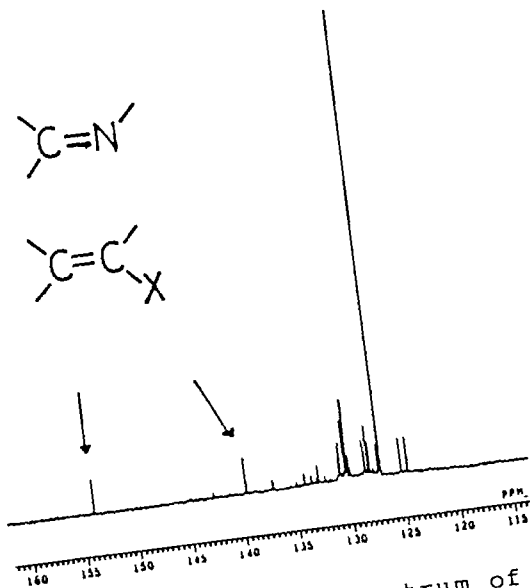
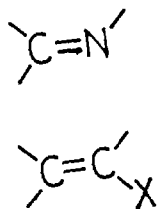
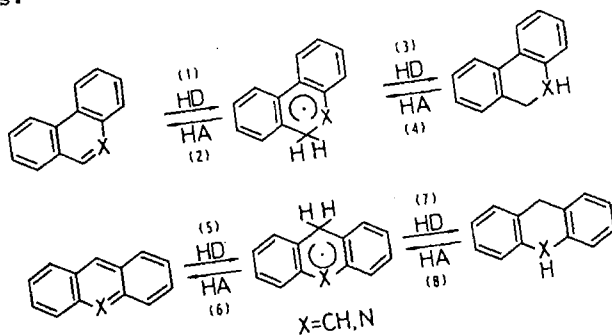


Fig. 2  $^{13}\text{C}$ -NMR Spectrum of the Recovered SRC Soluble in  $\text{THF-d}_8$ .



HD=Hydrogen donor  
HA=Hydrogen acceptor

Fig. 3 Hydrogen Transfer Processes where the 3-ring Aromatic Compounds and Their Dihydro-derivatives are Involved.